UNIVERSITY OF BRASILIA

FACULTY OF TECHNOLOGY

DEPARTMENT OF ENVIRONMENTAL AND CIVIL ENGINEERING

BEHAVIOR OF PILED RAFT SYSTEMS FOUNDED ON SOFT CONSOLIDATING SOILS VIA NUMERICAL METHODOLOGIES

ANDREA JULIANA ALARCÓN POSSE

SUPERVISOR: RENATO PINTO DA CUNHA, Ph.D.

CO-SUPERVISOR: JUAN FÉLIX RODRÍGUEZ, Dr.

DOCTORAL THESIS IN GEOTECHNICS

BRASILIA / DF: 12/08/2022

UNIVERSITY OF BRASILIA
FACULTY OF TECHNOLOGY
DEPARTMENT OF ENVIRONMENTAL AND CIVIL ENGINEERING

BEHAVIOR OF PILED RAFT SYSTEMS FOUNDED ON SOFT CONSOLIDATING SOILS VIA NUMERICAL METHODOLOGIES

ANDREA JULIANA ALARCÓN POSSE

A THESIS SUBMITTED TO CIVIL AND ENVIRONMENTAL ENGINEERING DEPARTMENT OF THE FACULTY OF TECHNOLOGY, UNIVERSITY OF BRASÍLIA AS REQUIREMENT FOR DOCTORAL DEGREE IN GEOTECHNICAL ENGINEERING.

EXAMINATION BOARD:

_____
Renato Pinto da Cunha, Ph.D. (FT/UnB)
(ADVISOR)

_____
Juan Félix Rodríguez, Dr. (FT/UnB)
(CO-ADVISOR)

_____
Gabriel Auvinet Guichard, Dr. (UNAM)
(EXTERNAL EXAMINER)

_____
Juan Carlos Ruge, DSc. (UnB)
(EXTERNAL EXAMINER)

_____
Manoel Porfírio Cordão Neto, DSc. (FT/UnB)
(INTERNAL EXAMINER)

DATE: BRASILIA/DF, 12 08 2022.

FICHA CATALOGRÁFICA

REFERÊNCIA BIBLIOGRÁFICA

ALARCÓN, J. (2022). Behavior Of Piled Raft Systems Founded on Soft Consolidating Soils Via Numerical Methodologies. Doctoral Thesis, Publication G.TD-177/2022, Department of Environmental and Civil Engineering, University of Brasilia, Brasilia, DF, 191 p.

CESSÃO DE DIREITOS

_____
Andrea Juliana Alarcón Posse
SQN 206, Bloco D, Apto. 605.
CEP: 70844-040, Asa Norte, Brasília, DF - Brasil.
Julianaalarcon2@hotmail.com

*"*No matter ***how much it hurts,*** how dark it gets*,*

or how hard you fall, you are NEVER out of the fight"

Marcus Luttrell

ABSTRACT

In this work, a 3D numerical model was developed using a software based on the Finite Element Method, and the results obtained in a geotechnical centrifuge model of a piled raft system founded on soil subjected to regional subsidence. The numerical model was calibrated for an initial configuration of nine piles distributed in the center of the raft. Soil parameters were obtained, calibrated and validated for the Hardening Soil Model based on laboratory results of triaxial and consolidation tests. In addition, other laboratory tests were carried out in a centrifuge that allowed obtaining the resistance parameters of the foundation studied.

 The developed numerical model reproduced satisfactorily soil and foundation consolidation displacements due, not only to the structural service load but also to the pore pressure drawdown. For load distribution on piles and raft, the model reproduces with good agreement the foundation behavior only for the structural service load, for pore pressure drawdown some adjustments on the embedded piles elements shaft and base resistance had to be done. The developed model allowed to identify the most sensitive parameters for this type of simulation, to define the types and stages of analysis that had the best fit for the physical model, and to obtain additional results to those measured in the physical model, e.g., the axial load distribution developed along the piles and therefore the magnitude of the negative skin friction, that is an important load that should be considered for the structural safety review of piled foundations subjected to these complex conditions.

This model was used to carry out a parametric analysis that allowed evaluating the influence of geometric characteristics such as the spacing, length and slenderness of the piles in the piled raft systems. With the assessment of these results, some graphs are presented to estimate the negative skin friction from these characteristics.

TABLE OF CONTENTS

FIGURES

TABLES

LIST OF SYMBOLS, NOMENCLATURE AND ABBREVIATIONS

A_p	Area of the pile base
A_L	Pile lateral area
A_{LM}	Smallest area of the raft
ABAQUS	Finite element modeling Software Abaqus
A_G	Pile group area
A_R	Raft area
c	Cohesion
c_a	Adhesion pile-soil
cm	Centimeter
C	Centered in the raft
C	Load cell
CC	Cam Clay yield surface
CR	Reduction factor
Cc	Compression Index
Cs	Recompression index
C_p	Tip load capacity
C_f	Shaft load capacity
CSL	Critical state line
CID	Drained consolidated triaxial tests
C_v	Vertical consolidation coefficient
D	Pile diameter
d	Project pile diameter
e	Void ratio
e_{init}	Initial void ratio
E_i	Initial stiffness
E_1	Young's modulus in a first axial direction
E_2	Young's modulus in a second axial direction
E_{50}	Confining stress-dependent stiffness modulus for the primary load
E_{ur}	Stress-dependent stiffness modulus for unloading and reloading
E_{50}^{ref}	Reference secant stiffness from drained triaxial test
E_{oed}^{ref}	Reference tangent stiffness for oedometer primary loading
E_{ur}^{ref}	Reference unloading/reloading stiffness
Er	Strain gauge in the raft
Es	Strain gauge in the soil
FEM	Finite Element Method
FDM	Finite difference method
FF	Filling Factor
FOPAE	*Fondo para Atención y Prevención de Emergencias*
F_R	Resistance factor
f	Flexiforce load cell
f	Average pile-soil lateral adherence
f^c	*cap* compression hardening yield function
f_s	Shear hardening yield function
Gs	Specific gravity

H	Model profile thickness
HSM	Hardening Soil Model
HP	*Horse power*
K_0	Lateral earth pressure coefficient
K_o^{nc}	Coefficient of earth pressure at rest (NC state)
kg	Kilogram
kN	Kilo Newton
k	Permeability
kPa	Kilo Pascal
L	Pile length
LE	Elastic models
LL	Liquid limit
LVDT	Linear variable differential transformer
M	Tangent of the critical state line
m	Exponential power
m	Metro
mm	Millimeter
MC	Mohr-Coulomb
MCC	Modified Cam Clay
MPa	Mega Pascal
N	Newton
N	Number of times Earth's gravity is scaled in geotechnical centrifuge models
NF	Negative friction
NP	Neutral point
N_c	Bearing capacity factors
N_p	Number of piles
OCR	Over Consolidation Ratio
P	Pile perimeter
p_{ref}	Stress of reference
PLAXIS	Finite element method Software to numerical modeling
POP	Pre-overburden pressure
PP	Honeywell piezometer
PI	Plastic index
PL	Plastic limit
P_p	Pre-consolidation stress
p_v	Effective vertical stress
P_{su}	Load capacity by lateral friction
p	Stress variant
q	Stress variant
$\tilde{q}$	Special stress measurement for deviatoric stresses
q_a	Asymptote of the shear strength
q_f	Ultimate deviatoric stress at failure
Q_{adm}	Load applied on the system
Q_t	Total load capacity
Q_w	Foundation system's workable load capacity
R_f	Failure ratio
s	Spacing between piles
SF	Safety factor
SLS	Serviceability limit state

t	Time
T	Distributed on the raft
t_0	Centrifugal modeling start time
t_A	Time to scale the model in Stage 1
t_B	Stage 1 stop time
t_C	Time to scale the model in Stage 2
t_D	Loading start time in Stage 2
t_E	Maximum load application time in Stage 2
t_F	Stage 2 stop time
t_G	Time to scale the model in Stage 3
t_H	Loading start time in Stage 3
t_J	Maximum load application time in Stage 3
t_K	Stage 3 stop time
u_x	Displacements in x direction
u_y	Displacements in y direction
u_z	Displacements in z direction
Uz	Degree of consolidation
ULS	Ultimate limit state
z	Depth
Z_0	Neutral point depth
δ_{Ytotal}	Total vertical displacement
δ_{Ysub}	Superficial subsidence induced by drawdown pore pressure
δ_{Yeff}	Vertical effective displacements
ε_1^p	Plastic axial strain
ε_v^p	Plastic volumetric strain
φ	Friction angle
γ^p	Plastic shear strain
κ	Cam-Clay swelling index
λ	Cam-Clay compression index
σ'_1	Confining stress in the triaxial test
σ'_3	Confining stress in the triaxial test
σ_v	Vertical stress due to the weight of soil
σ'_v	Effective vertical stress
υ_{ur}	Unloading/reloading Poisson´s ratio

CHAPTER 1

1.1   Introduction

The quick growth of the world population in recent years has generated an intense urban expansion, which led to rapid increase of high buildings in order to find a solution for the lack of space in some cities.

As well discussed by Rodríguez (2016), many of those cities are developing on soft soils: Shanghai, Bangkok, Mumbai, Kuala Lumpur, Jakarta, Singapore, Bogota, Mexico, etc., and so it is necessary to understand the behavior of these foundation systems with the soil conditions prevailing in situ. The development of these cities imposes an increase in the need for water supply, which leads to the use of groundwater through the alteration of aquifers. Consequently, phenomena related to the water table drawdown process occur, which change working conditions of foundations presenting damages as those reported by Bareño & Rodríguez (1999).

Countries like Mexico or Colombia, as well as many others, have developed research on the use of piled raft systems as a foundation in low and middle rise buildings (up to seven levels). (Rodríguez, 2016). In Brazil, especially in the Federal District, the solution with piled raft systems has the potential to be widely applied as an economic alternative to deep foundation projects for middle-class homes or low-cost, supported on collapsible porous clay or soft organic deposits.

A considerable number of structures, especially high buildings are founded on piled raft (Poulos, 2001). The primary difference between this foundation with respect to others lies in the fact that the loads are absorbed by both raft and piles, considering thus a safety factor appropriate for each case. The improved workability for piled raft occurs when only the raft, as a foundation, has the bearing capacity of the system, however, the total and differential settlement exceed tolerable limits, thus is recommended the use of raft and piles together as the two basic project criteria will be met: sufficient load-bearing capacity and tolerable settlements.

Compared with traditional piles foundations (pile group), where the load of the superstructure is transferred to the soil only by piles, piled raft type foundations reflect a more sophisticated

calculation approach, which is economically justified from a construction point of view (Cordeiro, 2007). Many field studies have been done worldwide on individual piles arranged in a soil that is consolidated by the reduction of the pore pressure, but only some of them work as floating piles or friction piles (Rodríguez, 2010).

Also, numerous authors, such as Chow et al. (1996), Pooroohasb et al. (1996), Briaud (1997), Comodromos & Bareka (2005), El-Mossallamy et al. (2013), Rodríguez & Auvinet (2015), Rodríguez et al. (2015), Huang et al. (2015), Rodríguez et al. (2015), Auvinet & Rodríguez (2017), among others, used numerical tools to evaluate the negative friction developed in the shaft of piles working on soft soils subjected to different loading conditions, groundwater abatement and other situations. Eventually, everyone concluded that these tools are ideal for analysis and quantification of negative friction and analysis of the behavior of the piles subjected to these axial forces, providing accurate results, and greatly reducing the time of problem assessment.

1.2   Motivation

According to Auvinet & Rodríguez (2017) cited by Melo, worldwide, a substantial number of field and laboratory studies related to the development of negative friction in piles individual have been carried out, but limited research has been performed with three-dimensional models or have used simplified models and constitutive models that require basic parameters that do not give an optimum response of the system's behavior.

To design piled raft with efficiency and economy it is necessary to know how the structural loads are transferred to the supporting soil by foundation elements, and, in addition, to understand the factors that affect the differential and total settlements under working conditions. It is necessary to advance in the understanding and evaluation of the influence of consolidation and regional subsidence on piled raft systems in soft soils. In this way, this work seeks to propose a 3D model, that represents the experimental work done by Rodríguez (2016), using The Finite Element Method (FEM). This model aims to allow the assessment of the aforementioned factors' magnitude, which would result very useful for designing and optimizing foundation systems.

1.3   Objectives

The main objective of this research is to analyze and understand the behavior of piled raft systems founded on soft soils undergoing a consolidation process by using numerical tools to simulate the subsidence problem.

To achieve this goal, the following tasks and secondary objectives need to be attended:

- To calibrate a 3D numerical model using the finite element method representing the behavior of a piled raft foundation system founded on a soft consolidating soil that reproduces soil and foundation structure displacements due to not only to consolidation caused by load, but also to the drawdown of the water pore pressure (regional subsidence).
- To assess the bearing capacity and settlements (elastic, consolidation) of the elements of the system during the loading stage, also observing the load transfer and load mechanisms to be developed along the process.
- To evaluate some fundamental aspects of the problem such as the dragload forces to be developed along the piles, given the possible occurrence of negative friction, or the partial/total contact loss between the raft and the underneath soil.
- To estimate the influence of the effects of external geometrical factors on the results, such as the pile configuration, different spacings, and raft thicknesses, besides of the slenderness of the pile foundations and their diameters.
- To assess the piled raft behavior not only in terms of the initial load-related consolidation but also in terms of load-related consolidation plus water pore pressure drawdown.
- To propose graphs for piled raft foundation designs related to systems in consolidating soils. Such specifications may be useful for preliminary projects where an initial input, based on design charts either in quantitative or qualitative terms is required (rational design based on geometrical variables and conditions that eventually lead to a "better" geotechnical performance).
- To determine reduction factors for the shaft resistance that allow proposing a practical design tool for obtaining the negative friction magnitude on piles located in the center, border, and corner of the raft.

1.4   Methodology

By way of explanation, Figure 1.1 can be seen as a general description of the followed methodology for this work. For the development of the research, seven stages were carried out:

- In Stage 1 the problem and objectives that had to be fulfilled were defined

- In Stage 2. a literature review was prepared to improve the understanding of the main concepts of the piled raft foundation system, negative skin friction, regional subsidence, and numerical modeling that allowed to assess the purpose of the present research. It was important to review the previous works that had been done and to assess the missing information in order to contribute to different research on the topic chosen.

- In Stages 3 and 4 already looking for results, it was proposed a geotechnical profile with the information from the previous experimental research done by Rodríguez (2016). The constitutive models were chosen and validated. It was founding out limitations and lack of parameters needed for proper calibration of the numerical model.

- In Stage 5 was carried out and experimental work (load pile centrifuge test and triaxial and consolidation tests), and pile test to collect information needed to calculate the parameters for the Hardening Soil Model (model chosen to simulate the soil).

- In Stage 6 a new numerical model was proposed and calibrated with the parameters obtained from the experimental work.

- In Stage 7 were presented and discussed the results of a parametric analysis carried out. All results were analyzed and compared between them. In this step, the influence of the parameters was determined.

- In Stage 8 final conclusions and design recommendations were presented.
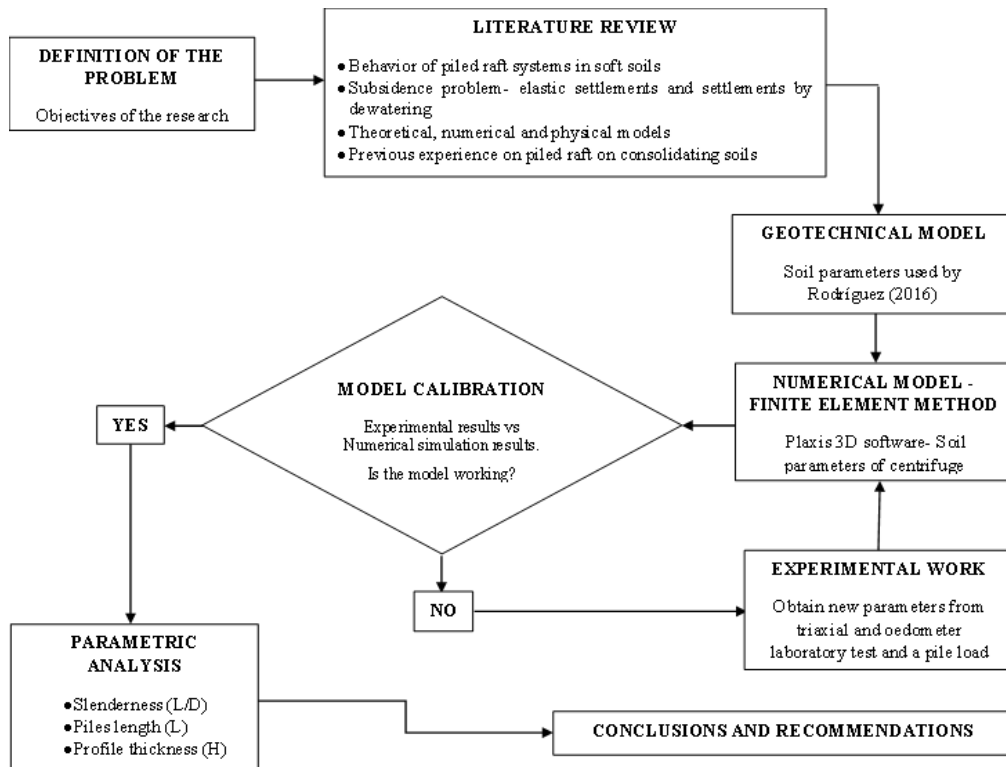
Figure 1.1 . Methodology

1.5   Thesis structure

The thesis is structured in five chapters as follows:

In Chapter 1 an introduction to the research is presented, the problem that motivated it, the objectives and the methodology followed. In addition, the general structure and content of the thesis are presented.

In Chapter 2 a literature review is carried out on the topics and works already done related to the present research to understand its purpose.

In Chapter 3 are presented the results of the constitutive models' validations, the experimental work carried out, and the calibration of the numerical model.

In Chapter 4 are presented and discussed the results of the parametric analysis varying geometric parameters on the 3d model that was carried out.

In Chapter 5 conclusions and recommendations for future research are presented.

CHAPTER 2

2. LITERATURE REVIEW

Main concepts of piled raft foundation system, negative skin friction, regional subsidence, and numerical modeling that allow understanding the purpose of the present research are presented in this chapter. The considerations are related to advances in the use of this foundation system in soft soils, and how the consolidation processes have been placed as a research topic.

2.1 Piled raft system

The foundation is considered the most critical part of an engineering project since it works as an interface between the load-carrying components and the ground. It is also defined as the part of an engineered system that transmits to and into the underlying soil or rock the loads supported by the foundation and its self-weight (Bowles, 1998).

In general, foundations may be classified based on where (depth) the load is carried by the ground, in two categories: shallow and deep foundations. Shallow foundation's main characteristic is that the distribution of the received load occurs horizontally. Spread footings, combined footings, or mats belong to this category. On the contrary, deep foundations distribute the load vertically rather than horizontally. Some examples of this type are caissons, piers, and piles (end-bearing, or floating).

A foundation is economical when the bearing capacity criteria and settlements are satisfied optimally, having some cases in which it is cheaper to control settlements than to suppress them. For those cases, a combination of shallow and deep foundations is used, i.e., piled raft foundation, which has been proved to be cost-effective and reduces settlements.

Piled raft foundations are increasingly being recognized and widely employed as an adequate foundation not only for high-rise buildings but in general for engineering constructions in all types of soils, especially soft soils, which is the main topic of this work. It is defined as a geotechnical composite structure that combines the bearing effect of both foundation elements

raft and piles by considering interactions between the structural components and the surrounding soil. Janda et al. (2009) also defined piled raft as a foundation system in which both structural components (piles and raft) interact with each other and with the surrounding soil to sustain vertical, horizontal or moment loads coming from supported superstructures. According to Alnuaim (2018), those components interact complexly with each other and with the surrounding soil (pile-soil, raft-soil, and pile-raft) to bear vertical, horizontal, and moment loads coming from the superstructure.

The combination and load sharing behavior of rafts and piles have been studied since the fifties by researchers like Zeevaert (1957a), Burland (1967), and Hooper (1973). In recent decades and with the advance of technology, many papers have been presented in order to understand the pile raft systems' behavior. In general, they agree with the concept that pile raft system design considers piles as an element to reduce settlements and not to load-bearing, as shown in Figure 2.1. It is noted in this figure that the introduction of a small number of piles is enough to reduce the raft intensity on the soil.
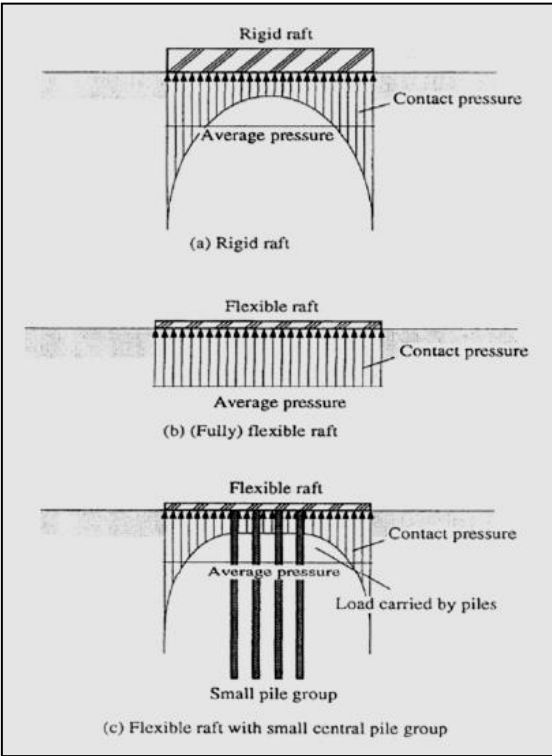
Figure 2.1. General concept of piled raft system. Poulos (2001)

For the system, the piles provide sufficient stiffness controlling the maximum and differential settlements at the serviceability load. In contrast, the raft provides additional capacity at the

ultimate load (Alnuiam et al., 2013). The correct arrangement of these piles below the raft is an optimization exercise of the project, searching to obtain optimal values of number, length, and configuration to keep the system within external and internal stresses admissible, according to Cunha et al. (Cunha et al., 2001).

The piled raft foundation system offers some advantages in terms of serviceability and efficiency of the components. One of those advantages is that piled raft when compared to pile group design, requires fewer piles to comply with the same capacity and settlement requirements. Besides, as mentioned by (Poulos et al., 2011), if any of the piles in the foundation becomes defective, the raft allows redistribution of the load from the damaged pile to other piles. Moreover, the pressure applied from the raft to the subsoil may increase the lateral stress between the underlying piles and the soil, which in turn increases the pile load-carrying capacity (Katzenbach et al., 1998).

If the structural components are analyzed separately, according to Chan (2006), for piles the analysis constitutes a complex interaction problem pile- structure, since the group's behavior is influenced by several factors including installation method (with displacement or soil replacement), the predominant form of loads transfer (floating or end-bearing pile), nature of the foundation soil, geometry of the group configuration and rigidity. When analyzing the raft, settlements are the main issue to assess. Poulos (2001) mentions that when the load applied to the semi-flexible raft is well distributed, settlements in the center are larger than at the edges. These settlements, total or differential, when excessive, can compromise the functionality or even the stability of the structure. This can be limited by "piling" the raft. Consequently, piles in piled raft foundation can be used for two reasons: To reduce total settlement in a rigid raft and to reduce total and differential settlement in a flexible raft (El-Mossannamy et al., 2006; Horikoshi & Randolph, 1996; Russo, 1998; Viggiani et al., 2014).

According to Chow (2007), in piled raft system, it is necessary to understand the load transfer mechanism from the raft to the piles and soil to determine (i) raft behavior including settlements, moments, and load percentage that this element takes, and (ii) the behavior of piles which includes displacement and load distribution along these.

In the piled raft system, piles are responsible for initially absorbing most of the load imposed on the foundation, as well as reducing absolute or differential settlements. The pile cap, on the other hand, also supports part of the load foundation, which is a function of geometry, number

of piles, raft flexibility, piles spacing, soil type, deformation stage, etc. The raft also tends to improve the performance of the piles due to the increased lateral confinement thereof. In general, the pile's resistant load must be enough to absorb 50 to 70% of the average tension applied to a rigid raft (Cunha et al., 2001).

Other authors (Poulos, 1993; Durán, 2003; Rodríguez, 2016) have mentioned load proportions assumed by the piles by up to 20%, with the raft supporting 80% of the total load under load conditions without changes in soil water conditions. Rodríguez et al. (2020) used in their analysis a graph presented by Mandolini et al. (2013) (Figure 2.2), where the variation of the load assumed by the raft was established as a function of the Filling Factor (FF). The FF establishes that the behavior of a piled raft system is influenced by the relative response of the pile group and the raft, as presented in Equation (2.1).

$$FF = \frac{A_G/A_R}{s/d} \qquad (2.1)$$

where: A_G: pile group area, defined by Sanctis et al. (2002), Equation (2.2).

$$A_G = \left[\left(\sqrt{N_p} - 1\right)s\right]^2 \qquad (2.2)$$

A_R: raft area; s: spacing between piles; d: pile diameter and N_p: number of piles in the group.

9
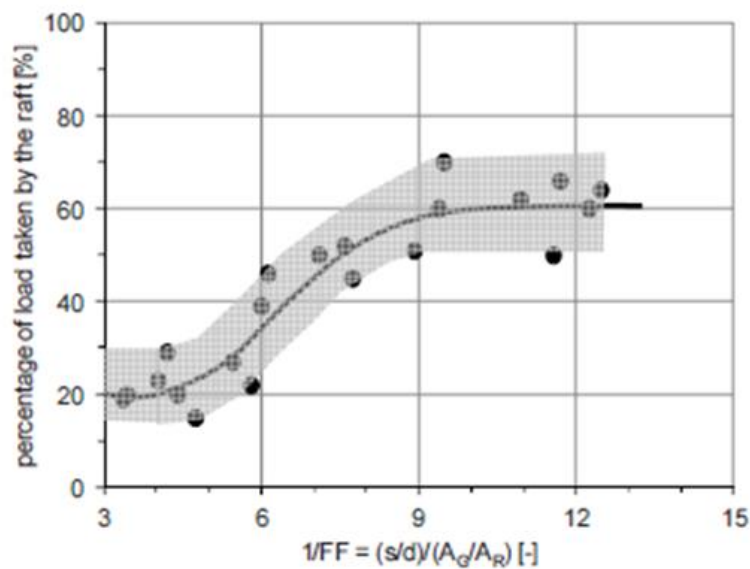
Figure 2.2. Percentage of load taken by the raft: experimental data collected by Mandolini et al. 2013.

2.2   Analysis methods of piled raft systems

The three-dimensional foundation system design includes complicated interactions between the elements that constitute them and the use of complex numerical models that represent in a reasonable way the field conditions can give an approximate solution. According to Balakumar (2008) and Chow (2007), many authors have developed analytical methodologies for piled raft systems. Van Impe (2001) and O'Neill et al. (1996). presented complete reports on piled raft systems, another contribution of piled raft modeling was also presented by El-Mossallamy & Franke (1997). Furthermore, the concept of work or piled raft systems behavior has been described by authors such as Zeevaert (1957b), Davis & Poulos (1972), Hooper (1973), Burland et al. (1986), Randolph (1994a), Sommer et al. (1985), Price & Wardle (1986), Franke et al. (1994), Katzenbach et al., (1998), Reul (2002) and many others.

One-dimensional to three-dimensional models have been developed for the analysis of this type of foundation (Chow, 2007). The analysis methods can be grouped into:

- Analytical Methods: These methods, although not proposed exactly for raft systems, were modified to determine its behavior as a combination or by itself. The use of these methods for the analysis of rafts has been investigated in a lot of research Zhemochkin & Sinitsyn (1962), Brown (1969a, 1969b). Although, those only referred to geometrical shapes and using homogeneous soils. Later, computational development led researchers to adopt alternative methods of numerical modeling to solve the same problem. Theories of equivalent piles and rafts were included in this category, and methods that include stiffness matrix were included in the simplified numerical methods (Rodríguez, 2016).

- Numerical methods: The rapid development of computers and high-speed processors encouraged researchers to develop various numerical methods to study the load-settlement response and load distribution on piled raft systems elements. Within this group are the Boundary element method and the Finite element method. According to Balakumar (2008), numerical methods have been worked by Brown & Wiesner (1975), Wiesner & Brown (1980), Poulos (1991, 1994), Clancy & Randolph (1993), Hain &

Lee (1978), O'Neill et al. (1977), Chow (1986, 1987), Randolph & Wroth (1978), and others that will be listed ahead in this research work.

2.3   Design philosophies for piled rafts

According to Mandolini et al. (2013), cited by Rodríguez (2016), Piled raft systems can be designed to provide safety in limited states, namely: to ensure load-bearing capacity and control settlements; ensure only load capacity or only control settlements.

In the traditional design of pile groups project, the number of piles is calculated by dividing the total load by individual pile load-bearing capacity, seeking to ensure a minimum safety factor ("medium") for all piles. When analyzing the influence of group stiffness, still within the traditional conception, are generally found higher loads in peripheral piles, which in many designs leads to an increased number of piles to ensure a minimum safety factor (SF) in all piles (Sales, 2002).

Sanctis et al. (2002) presented two classifications for piled raft systems, which represent the design philosophies considered by Randolph (1994b):

- "*Small piled raft*": the main reason to add piles is to increase the safety factor (usual rafts with widths between 5 and 15m);

- "*Large piled raft*": the raft has the capacity to support the load with a reasonable safety margin applied, plus the piles are used to reduce total and differential settlements. In this case, the raft width is greater than the pile's length.

However, considering that the mechanical response of a pile group with a pile cap in the head is different from that of a piled raft, Poulos (2001) presented three design philosophies for piled raft:

- In the "*conventional approach*", where piles are considered as the primary load-carrying structural members, the raft's bearing contribution to the system increases the ultimate load capacity of the foundation.

- In "*Creep piling*", piles work on approximately 70-80% of single pile's ultimate axial load capacity, a point where the creep behavior on the pile starts. Therefore, the required numbers of piles are determined by targeting the transmitting stress to be lower than its pre-consolidation pressure.

- "*Differential settlement control*" is an approach in which the piles are used mainly to reduce differential and overall settlements rather than to improve the bearing performance of the foundation system.

2.4   Negative skin friction on piles

In soft soils, the load capacity of the piles used as foundations depends mainly on the lateral friction component, which depends on the interaction between the pile and soil. According to Poulos & Davis (1980), the load capacity per shaft can be determined with Equation (2.3).

$$P_{su} = \int_0^l P(c_a + K_0 \sigma_v \tan \phi) dz \qquad (2.3)$$

Where P_{su} is the load capacity by lateral friction, P is the perimeter of the pile, L is the length of pile, c_a is the adhesion pile-soil, K_0 is the coefficient of lateral earth pressure, σ_v vertical stress due to the weight of soil and ϕ is the friction angle.

Usually, to develop the friction capacity by the shaft, only a small displacement is necessary, however, to develop the end bearing capacity, a displacement between 10 to 15% of the pile length is required. Positive friction in the pile shaft is developed when the pile moves concerning the surrounding soil. On the other hand, it has been long recognized that when the pile is founded on soil undergoing consolidation, a downward force is induced in the pile because of the downward movement of the soil relative to it. This downdrag effect is commonly named "negative friction" (Poulos and Davis, 1980). More explicitly, the negative friction is developed when the soil settlement is higher than the vertical movement of the pile shaft.

Negative friction can occur in soils subjected to regional subsidence, settlements of compressible layers, settlements of collapsible soils by wetting, settlements associated with

liquefaction, or water pore pressure drawdown, among other causes. Measurements of the downdrag force induced by negative friction revealed that it can be sufficiently large to exceed the design load and can generate excessive settlements in the pile (Bjerrum et al., 1969).

Piles with negative friction transfer most of the load structure to the surrounding soil through the perimeter friction. According to Auvinet & Rodríguez (2017), piles can be used as a complement to a raft to reduce settlements or to support the total weight of the structure ensuring stability to the foundation. In any of these cases, it is generated a complex interaction between soil, piles, and structure since the soil is submitted to a double consolidation process: firstly, due to load transferred by the structure, and second, to variations in pore pressure for pumping water or refill of soil voids. The foundation design in piles with negative friction can be based on the evaluation of stresses developed at the base and along the pile perimeter, strains, and the forces developed inside it. Negative skin friction is common to develop in the upper part of the pile and positive friction on its bottom, having a point where there is no displacement between soil and pile called the "neutral point" (Neto, 1981).

Different conclusions related to this "neutral point" and where it is located have been taken from diverse researchers. Bozozuk (1972) suggests that the depth of this point only depends on the length of the pile embedded in the soil layer. According to Okabe (1977), the negative friction and the depth of the neutral point increase with increasing stiffness of the layer closest to the tip. For Fellenius (1984), the highest axial load on the pile occurs at the neutral point, and it is located below the midpoint of the piles. Other authors such as Prakash & Sharma (1990), based on experimental tests, suggested that the neutral point is located at 0.75 of the pile length. Poorooshasb et al. (1996) notice that this neutral axis is not very influenced by the overload, however, it is influenced by the stiff layers close to the pile tip. From laboratory tests, Leung (2009) observed that the neutral plane, of single piles subject to simultaneous negative skin friction and axial load, shifts gradually downwards along the pile and finally stabilizes at about 12 m below the original ground surface. This observation is contrary to that observed for the case of a pile subject to negative skin friction only in which the elevation of the neutral point rapidly reaches its final position of around 90% of the pile length. Figure 2.3 shows the loads developed on a friction pile subjected to negative friction.
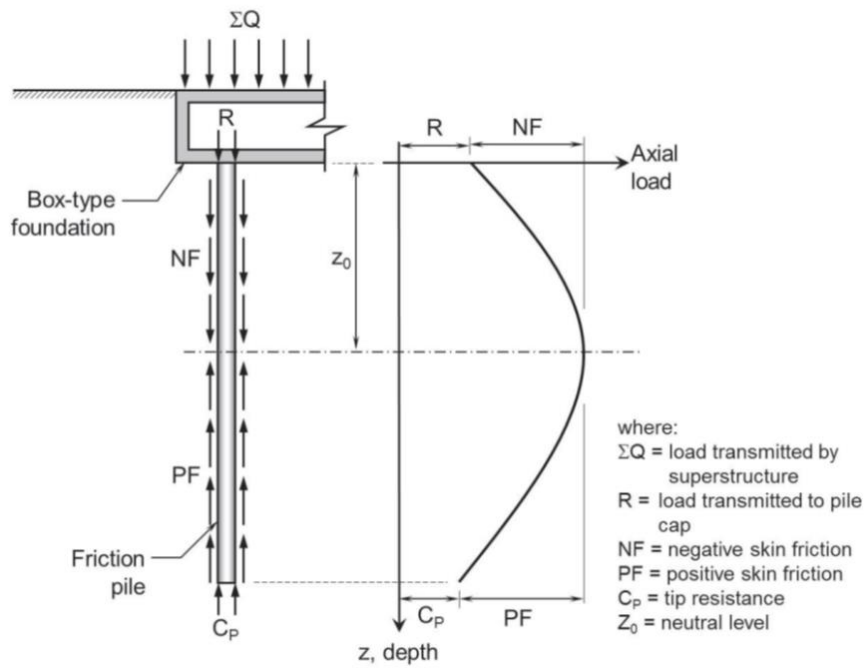
Figure 2.3. Loads developed on a friction pile subjected to negative friction due to pore pressure drawdown. Auvinet & Rodríguez (2017)

Regarding piles group with a block or rigid raft, Santos Neto (1981) noticed that a different load on the piles is expected due to their position in the group because negative friction is given by the weight of the soil volume that is transferred to the pile. Consequently, the internal piles will receive a lower overload than the external ones due to having the areas of minor influences, as shown in Figure 2.4. Also, Lee (1993) stated that negative friction at an individual pile in the group is smaller than in an isolated pile due to the interaction effects.
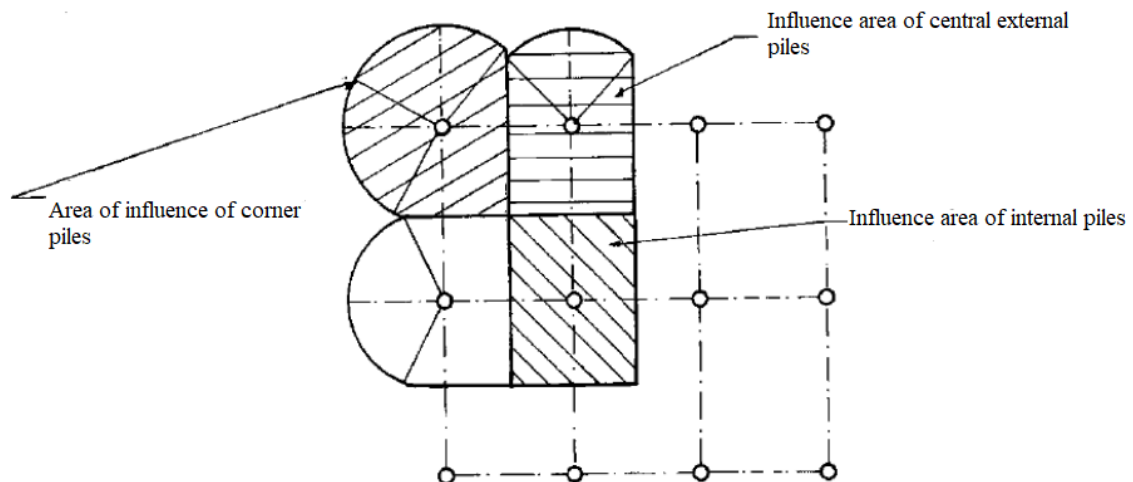
Figure 2.4. Areas in a group of piles with a slab or rigid raft. Adapted from Santos Neto (1981)

14

In order to understand better the development of negative friction in pile groups, some authors, such as Plomp & Mierlo (1948), Endo et al. (1969), Auvinet & Hanell (1981), Keenan & Bozozuk (1985), Little (1994) and Dai et al. (2012), among others, developed field studies regarding the subject matter. In addition to these, Whitaker (1957), Shibata et al. (1982), Leung et al. (2004), and Huang et al. (2014) carried out laboratory research on the topic as well.

As mentioned by Auvinet & Rodríguez (2017), due to the complexity of the problem and the considerably high number of parameters involved, few analytical methods have been developed for the analysis and design of friction pile foundations subjected to external loads and soil consolidation due to variations in piezometric conditions. Most of them are simplifications aiming at evaluating the magnitude of negative skin friction.

Some analytical models for the analysis and design of friction piles foundations have been proposed by some authors like Zeevaert (1957a, 1962, 1983), Reséndiz & Auvinet (1975), Auvinet & Díaz-Mora (1981), Briaud et al. (1991), Jeong et al. (1997), Alberro & Hernández (2000), Rodríguez (2011) and Auvinet & Rodríguez (2000, 2017).

In recent decades, the use of numerical models has been increasing and they offer new possibilities for the analysis of foundations subjected to negative skin friction (Jeong et al. (1997); Jeong et al. (2004); Auvinet & Rodríguez (2001, 2002, 2017); Lee & Ng (2004); Comodromos & Bareka (2005); Rodríguez (2011); Rodríguez et al. (2015); Melo (2018)). These models allow a detailed evaluation of the magnitude of the developed stresses at the pile's tips and shafts, as well as the consequent deformations (Auvinet & Rodríguez, 2017).
.

2.5   Regional subsidence problem

The presence of subsidence in various regions of the world shows how serious the impact of the phenomenon can be and is also a wake-up call to continue the study of its behavior, at least to mitigate the detrimental effects. It is there, where the academic contribution is valuable when discussing the issue and showing its importance. According to Yang et al. (2018), subsidence is a phenomenon of gradual ground settlement associated with subsurface fluid extraction, underground mining, or engineering construction. It is also associated with properties changes in-depth due to: the existence of soluble materials, superficial mechanical erosion processes, plastic flow, compaction, and tectonic subsidence (Hewitt, 2011).

The first time the subsidence was linked to water extraction was in 1908 by Fuller (1908). Terzaghi's work in 1925, permitted regional subsidence to be quantified for the first time with the one-dimensional consolidation equation derivative. Since then, the interest to study the mechanisms and effects of the subsidence associated with drops of the piezometric head has increased substantially. By the year 1969, such was the interest in the subject, that the First International Symposium on Land Subsidence was held in the city of Tokyo, Japan (Garzón, 2011).

The ground subsidence, resulting from the exploitation of groundwater, is a complex phenomenon due to the lack of temporal and spatial uniformity involved in the extraction processes (Figure 2.5). Also, included the complexity regarding the materials that undergo this phenomenon, whose mechanical parameters exhibit anisotropy dependence on time and stress history, coupled with the lack of knowledge of mechanical properties and flow net.

As previously stated, many cities are developing on soft soils, such as Shanghai, Bangkok, Kuala Lumpur, Jakarta, Singapore, Bogotá, and Mexico City, among others (Rodríguez et al., 2020). Since groundwater exploitation is increasingly intense and most often occurs in urbanized and/or industrial areas, the effects of the settlements associated with the descent of the water table extend into large areas affecting the infrastructure.
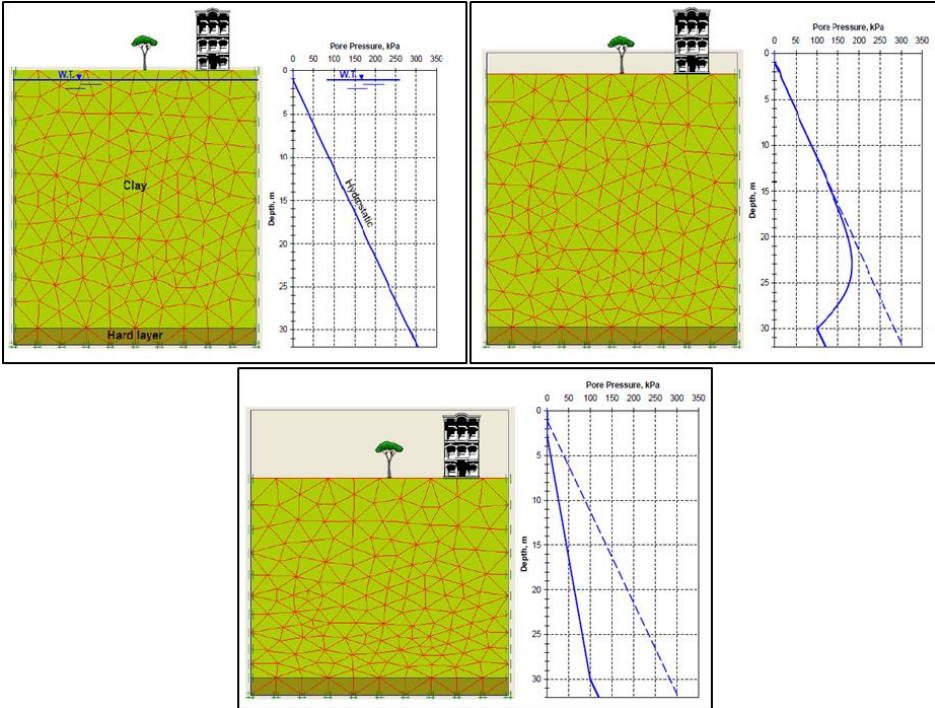
Figure 2.5. Regional subsidence phenomenon. Pore pressure vs. depth (Rodríguez-Rebolledo, 2011)

16

According to Lobo – Guerrero (1992), the use of groundwater in Bogotá dates from colonial times. Since there are a lot of wells drilled, severe problems of overexploitation in many parts appeared. The potentiometric level of groundwater of some basins is decreasing at rates between 3 and 5 m / year due to an extraction higher than natural recharge, being this the main factor influencing consolidation and settlements of superficial layers. The "*Fondo para Atención y Prevención de Emergencias*" (FOPAE) 2010, conducted observational studies that evidenced subsidence processes that can be seen in vertical displacements of lightweight structures (platforms and access stairs). In some cases, settlements in these zones have reached 90 cm, according to Bareño & Rodríguez (1999).

As mentioned by Rodríguez et al. (2015), since the end of the 19th century, Mexico City Lake Zone has suffered regional subsidence. Historical data records showed that the city has settlements up to 10 m according to the reference of the Metropolitan Cathedral, with high variation rates of height up to 7 cm/year (Figure 2.6). Also, in Southeast Asia, for more than 30 years, the City of Bangkok had suffered severe subsidence caused by excessive pumping of water from aquifers. Likewise, more than 50 cities in China have faced land subsidence issues, and of these, Beijing has been among the most severely affected since the 1950s (Zhu et al., 2015). In general, uneven ground surface settlement has been reported to cause damage to urban infrastructures, such as wall cracks and pipeline ruptures, leading to economic prejudices.

Figure 2.6. Settlements in Mexico City. (Rodríguez, 2011)

2.6   Piled raft systems in soft soils with consolidation

Poulos (1993) presented some situations where it is not recommended to use piled raft systems, including soil profiles with soft clays or loose sands near the surface, or those which have compressible, collapsible, or expansive soils. However, some other authors have shown that piled raft system may be employed in different types of soil if it is properly designed.

In the case of clays, Cunha et al. (2004) showed that piled raft systems could be used in tropical clays, for example, in some areas of the Brazilian Mid-west regions, with proper behavior of load and settlements, to reduce the costs of foundations. As regards the inclusion of subsidence phenomena in the analysis of piled raft systems in soft soils, most references register research on groups of piles with different conditions of the top cap block, field studies, or analysis of individual piles, focused on negative friction. Table 2.1 presents some of the research works carried out.

Table 2.1. Piled raft systems research works carried out

REFERENCES	RESEARCH	REMARKS
Ng et al. (1976)	Estimated the negative friction piles working by tip.	An analytical method based on elastic theory
Okabe (1977)	Reported the dragload measurements of a group of piles undergoing subsidence processes in the soil and overload.	Field study that led to finding that, compared with isolated piles; the piles within the group have reduced dragload.
The Canadian Geotechnical Society (1978)	Determine the magnitude of dragload.	Empirical method.
Inoue (1979)	Established the variation of the dragload and its time dependence; the relationship between the negative friction and settlements; the relationship between friction and tension around the piles; the influence of settlement speed and soil properties at the location of the neutral axis and, finally, shows a practical procedure to determine the dragload.	Field study of pile groups.
Shibata et al. (1982)	Analyzed piles covered with bitumen and without cover concluding that, applying the bitumen, the negative friction decreases, however, the pile load bearing capacity is lower. They also presented a methodology to determine the group effect on negative friction for piles without coverage.	Scale model 1g.
Kuwabara & Poulos (1989)	Evaluated the dragload on a group of piles.	Method proposed as an extension of the methodology presented by Poulos and Davis (1980) to assess the negative friction in isolated piles.

REFERENCES	RESEARCH	REMARKS
Thaher & Jessberger (1991)	Evaluated the effect of the number, diameter, and length of piles in a piled raft that undergoes an axial load.	Experimental model in geotechnical centrifuge (50g)
Chan (2006)	Mentioned that Little in 1994 concluded that piles working for tip experience higher dragload than floating piles. In both cases, the central piles have higher dragload, compared with piles at the edges.	Real scale field study of piles groups.
Ergun & Sonmez (1995)	Noted that the spacing influences the magnitude of the negative friction and the settlement in the interior of the piles (if compared with the soil settlement outside area of influence) is indicative of the effect of the group.	Studied on a 1g model of driven piles working by tip.
Horikoshi & Randolph (1996)	Analyzed: the effect of the number of piles, the pressure on the raft; settlements; and the percentage load on the piles.	Experimental study in Geotechnical centrifuge (100 g).
Katzenbach et al. (1998)	Analyzed the soil-pile interaction and its influence on the settlements, load distribution and piles distribution through the numerical model of the Geotechnical Institute of the Technical University of Darmstadt.	Drucker Prager model was used for the soil.
Reul (2000)	With the use of three-dimensional analysis in a Finite Element Model, engaging the pore pressure and stresses, presented a three-dimensional analysis of piled raft behavior systems and the effect of load consolidation.	Abaqus software was used
Chow et al. (2001)	Analyzed raft and piles both using minimum potencial energy. By representing the deformation of the piles and raft using finite series, concluded that the method was very efficient for the analysis of a piled raft with a large number of piles.	Presented a. variational approach for the analysis of piled raft foundations
Reul (2002)	Performs uncoupled analysis in short and long-term of drained and undrained parameters of piled raft behavior system, subjected to axial load.	Abaqus software was used
Lee et al. (2002)	Analyzed the behavior of soil-piles interface.	Abaqus software was used.
Durán (2003)	Analyzes the behavior of piled raft systems in soft soils of Bogota. Concluded that piled raft systems are better prepared than raft without piles or long piles working by lateral friction to support the secondary compression processes and subsidence generated by dewatering process.	Stated that the regional subsidence produces excessive settlements in the superficial foundations like raft, besides producing negative friction at the top of long piles, reducing the safety factor of the foundation
Lee & Ng (2004)	Simulated piles groups in soils with consolidation without raft and drained conditions.	Abaqus software was used
Sanctis & Mandolini (2006)	The study had a three-dimensional parametric analysis to determine the coefficients to be applied to each of the capabilities to determine the total capacity.	Presented an analytical method to determine the system's load capacity, as a result of the sum of the individual capacities of the components.
Shen et al. (2006)	Analyze the behavior of single piles and pile groups supported on a rigid layer (working for tip), with presence of negative friction due to overload at soil surface, concluding that the piles dragload within the group it was similar to that obtained for single piles.	Experimental study in Geotechnical centrifuge (80 g).

REFERENCES	RESEARCH	REMARKS
Bajad & Sahu (2008)	Reported results concluding that load distribution and settlements are more influenced parameters by the length piles. Also, some methodologies, such as Poulos & Davis (1980), allow evaluating the relationship between piles number and the average settlement, providing a quick method of evaluation of the project.	Experimental study (1g)
Small & Liu (2008)	Presented a 3D numerical study (Finite Element) including was carried out to estimate the rate of consolidation of piled rafts, and to calculate the magnitude of differential deflections and the associated moments that develop in the raft with time.	The soil was treated as a poroelastic material and modelled by three-dimensional finite elements in the region of interest, but infinite consolidation elements were used to model the lateral boundaries of the region.
Lee et al. (2010)	Presented a three-dimensional model of piled raft systems behavior subjected to vertical load in soft clay. The authors analyzed the load distribution in the system, the influence of spacing and soil-pile-raft interaction presenting an analytical solution to assess the safety factor for a given settlement and how this could be used for a preliminary design.	Modeled in Abaqus software
Cui et al. (2010)	Reported the importance of considering the behavior dependent on time in the analysis of foundations in soils due to consolidation and the use of numerical methods to study the effect of time on piled raft system. Also point out that, few studies have been developed to analyze the time dependent behavior of the three-dimensional systems structure - pile - raft - soil, because of which normally does not represent the variation of pore pressure in the soil.	Constitutive model based on Mohr Coulomb´s yield criterion was used. The numerical analyses were conducted in ABAQUS software
Roy et al. (2011)	Presented a methodology for piled raft system design in consolidating soils, analyzing soil response and materials with linear behavior laws.	The methodology has been proposed to determine the time required to establish piles load transfer to the raft, separately evaluating the bearing capacity of piles and raft.
El-Mossallamy (2011)	Using the 3D PLAXIS, examined the behavior of piled raft systems, including linear behavior of the soil, the development of rupture surfaces along the pile shaft and the raft stiffness.	The water table is considered mostly above the clay surface. The subsidence was not evaluated.
Cho et al. (2012)	Investigated the piled raft response systems considering interface elements between piles and soil using ABAQUS.	The Mohr-Coulomb Model was used to simulate the soil. Consolidation effects in the model were neglected. After comparing load-settlement curves of uniform loading and point loading, was concluded that an effect of loading type could be negligible. The emphasis of the work was on quantifying the reduction of the average and differential settlements in soft and stiff clay soils.
Tran et al. (2012)	Two centrifugal model tests were conducted to evaluate the effect of ground subsidence on load sharing among piles and raft and settlement of raft and piled raft foundations. As a conclusion,	Used two conditions consisting of undrained (without groundwater pumping) and drained (with

REFERENCES	RESEARCH	REMARKS
	the distribution of the load on the piles is the most important factor for estimating the settlement of the foundations noting that few studies have focused on the response of foundations, when subjected to ground subsidence processes.	groundwater pumping) conditions were considered.
Tran et al. (2012)	Three-dimensional model used in PLAXIS to analyze the effect of subsidence and spacing in the load bearing capacity of piled raft systems and load distribution along the piles.	The Mohr-Coulomb model was used to model the soft clay. Also, drained conditions for the material type was selected for the soil when simulating ground water pumping condition.
Elwakil & Azzam (2015)	This research sheds some light on the philosophy of using piles as settlement reducers for raft foundations and the behavior of piled raft embedded into sand. Small scale model tests are performed. The effects of pile length and alignment on the attained ultimate load are experimentally investigated.	Do not take into account the subsidence
Watcharasawe et al. (2015)	Focused on the investigation of influencing factors on the behavior of piled raft foundation in Bangkok subsoil. This research performed the consolidation analysis of piled raft foundation systems for low and high-rise buildings with basement levels in clay soil, using coupled three-dimensional (3D) mechanical and hydraulic numerical model.	Not focused specifically on simulate regional subsidence.
Rodríguez (2016, 2020)	Experimental analysis of piled raft systems on consolidating soft soils	Experimental study in Geotechnical centrifuge (70 g).
Sinha & Hanna (2017)	A 3D FEM of a piled raft foundation was developed to simulate the case of a piled raft foundation. The model accounts for pile-to-pile, raft-to-pile, pile-to-soil, and raft-to-soil interactions. The model was used to examine the effect of the key parameters governing the performance of this foundation during loading and, accordingly, the load shared by the piles and the raft.	- Used Drunker Prager constitutive law - Used Software Abaqus. Also, mechanical properties of the soil were modified to examine its influence on the model
Banerjee et al. (2016)	Parametric Study and Centrifuge-Test Verification for Amplification and Bending Moment of Clay–Pile System Subject to Earthquakes. Seismic effects on fixed-head, end-bearing piles installed through soft clay were examined.	The numerical analyses were conducted using ABAQUS with a hypoelastic constitutive model for the clay.
Goh & Zhang (2017)	3D finite-element simulations were carried out to examine the response of pile-raft-soil systems under seismic excitation representative of far-field events. The numerical procedure was first validated by a series of seismic centrifuge tests performed on pile-raft systems embedded in soft clays and was subsequently extended to study the influence of various factors on the computed raft acceleration and maximum bending moment near the pile head.	The numerical analyses were conducted in ABAQUS software. Not focusing on regional subsidence.
Zhang & Liu (2017)	Investigated the pile bending moment and raft acceleration response under seismic excitation of a pile raft system embedded in soft kaolin clay.	Experimental study in Geotechnical centrifuge (50 g).

REFERENCES	RESEARCH	REMARKS
Mali & Singh (2018)	A large piled raft was simulated numerically through a 3-D finite element on clay soil modeling. The objective was to investigate the effect of pile spacing, length, diameter, and raft-soil stiffness ratio on the settlement, load-sharing, bending moments, and shear force behavior.	• The soil was modeled with MC constitutive model. • The water table was considered at ground level. • It focused on the influence of Raft soil Stiffness ratio on the settlement.
Khanmohammadi & Fakharian (2018)	Presented a numerical investigation of piled-raft foundations performance on soft clay with focusing on a case study. A 3D FEM numerical model is developed using ABAQUS. The model was calibrated by comparing physical and numerical modeling results of other researchers. The results indicate that choosing the proper combination of length and spacing for piles can lead to acceptable differential and total settlements.	• The soil was modeled with MC constitutive model. • Consolidation effects were neglected. • Although the profile is mainly clay. It has one layer with sand properties. • It focused on pile length and spacing.
Luo et al. (2018)	Presented and validated a practical analysis method for piled raft in clay, against the results from the existing numerical simulations and field measurements. A parametric study was performed to investigate the variation of the normalized settlement of the piled raft, including the effects of soil condition, pile dimensions and soil-pile adhesion.	Boundary element method was used.
Gu et al. (2020)	The piled-raft foundation in soft clay ground for high-speed trains has suffered serious settlement due to cyclic train loading in recent years. In this research, firstly, a ground treatment technique was proposed to reduce permanent train-induced deformation. Permeation grouting was injected into the bearing strata of group piles with constant pressure. Then numerical simulations based on sophisticated constitutive model and soil–water coupled finite element-finite difference (FE)-(FD) compound arithmetic, were carried out to explore the mitigation effect of the proposed technique.	• Constitutive model of CM (Cyclic Mobility)
Rincon et al. (2021)	The research is based on the implementation of reduced-scale models in a geotechnical centrifuge; the influence of the separation and number of piles on the deformation or settlement of the system is analysed. It is shown that, normally, groups of piles with greater separation control settlement more effectively. However, the settlements are greater when the soil is subjected to the weight of the structure in addition to a process of depletion of the pore pressure, because the settlement depends on the distribution of the piles, which is described using the Filling Factor (FF).	• Experimental study in Geotechnical centrifuge
Watcharasawe et al. (2021)	Presented the monitoring results and their interpretation on load sharing of the pile foundation during the construction of a high-rise (124 m in height) building in Bangkok, in soft clayey ground.	• The soil was modeled with MC constitutive model.

As shown in Table 2.1, research on piled raft systems has focused on the development of analytical methodologies, experimental models, and numerical analyzes that provide a better understanding of the behavior of this type of foundation.

Authors such as Ng et al. (1976) proposed an analytical methodology based on the theory of elasticity to estimate the value of the negative friction in piles that work by tip. Other authors such as Sanctis & Mandolini (2006) presented a new methodology to estimate the piled raft load capacity systems considering the load capacities of each component. The authors performed a parametric analysis in three dimensions to estimate values of dimensionless coefficients that, when applied to the components of the system, allowed evaluating the bearing capacity of the foundation.

In the experimental field, in situ and laboratory tests have been carried out that allow quantitative measurement of the variables that influence the behavior of piled raft. For example, Okabe (1977) measured in the field the dragload of a group of piles subjected to a process of regional subsidence. Other authors such as Thaher & Jessberger (1991) Horikoshi & Randolph (1996) Shen et al. (2006) Rodríguez (2016, 2020) and Zhang & Liu (2017) carried out laboratory tests in a centrifuge at different accelerations of gravity to simulate the behavior of the piled raft considering the soil-structure interaction and regional subsidence phenomena.

Finally, numerical studies have been developed in recent decades with the aim of understanding the behavior of each of the components of the piled raft. Authors such as Katzenbach et al. (1998), Cui et al. (2010), Cho et al. (2012), Tran et al. (2012), Sinha & Hanna (2017), Mali & Singh (2018), Khanmohammadi & Fakharian (2018), Xie & Chi, S. (2020) used different constitutive models developed in the theory of elastoplasticity to represent the behavior of the soil and thus analyze its interaction in different scenarios with this type of foundation.

2.7 Numerical modeling of foundations

The development of computer technology and high-speed processor provides greater and quicker numerical methods in geotechnical engineering (Patil et al., 2013). The numerical modeling tools allow the geotechnical engineer to simulate complex structures (in terms of geometry and behavior). Besides, they allow solving problems that cannot be solved analytically in an approximate way.

Some advantages of solving problems using numerical tools are reduction of analysis time, accurate results, simulation realistic analysis of complex problems, savings compared to experimental tests, and producing excellent results for projects that need reliability and security. Compared to the simplified methods, numerical models in a continuous medium consider the entire configuration of soil mass, system elements, and the interfaces between the various components. Such modeling leads to the calculation of displacements, strains, and stresses for each element and allows considering the hydro-mechanical coupling when consolidation problems appear (Briançon et al., 2011).

Brown P.T (1969b) introduces the numerical method in geotechnical engineering of a circular raft on an elastic layer of finite depth. Hooper (1973) was the first user of the finite element method (FEM) for understanding the complex interaction of piled raft foundations. This method is one of the most used in continuum mechanics and is the one used as a numerical tool for this work.

2.7.1 Finite element method (FEM)

FEM is a tool for solving problems in continuum mechanics that use constitutive models to describe the behavior of a material. It also allows simulating the behavior of the medium discretized in terms of strains and stresses under the load effect (Briançon et al., 2011). The result obtained by this method produces an approximate solution whose accuracy depends on:

- Constitutive laws model of materials and interfaces;
- Discretization, resulting in a mesh pattern that should be thinner where the stress field variations are larger;
- Type of adopted elements (number of nodes) and interpolation laws incorporated into each element.
- Use of interfaces between structural elements and the ground to allow integration of soil interaction/structure;
- Boundary conditions.
- Quality and accuracy of the data used

2.7.2 Constitutive models

A constitutive model can be understood as a set of mathematical equations that describes the relationship between stresses and strains produced within a material as a function of a determined number of parameters that depend on its mechanical properties. To model the stress-strain behavior of soils, these models are to be used with finite element and/or finite difference calculations of soil structures interaction problems under conditions, which can be a plain strain, axisymmetric, and/or three dimensional (Lade, 2005). There is a variety of constitutive models that can be used to represent soft soil behavior, for the present work were used the Modified Cam Clay (MCC) and Hardening Soil Model (HSM) are presented below

2.7.2.1 Modified Cam Clay (MCC)

The elastoplastic Cam-Clay (CC) model is based on critical state theory, a concept that was published by Roscoe et al. (1958). It was developed to simulate the behavior of normally consolidated or slightly over-consolidated clayey soils. Professor John Burland (1967) was responsible for the modification to the original model, which was revised again by Roscoe & Burland (1968). The difference between the two models is shown in Figure 2.7, CC yield surface is a logarithmic curve, while the MCC yield surface plots as an elliptical curve.
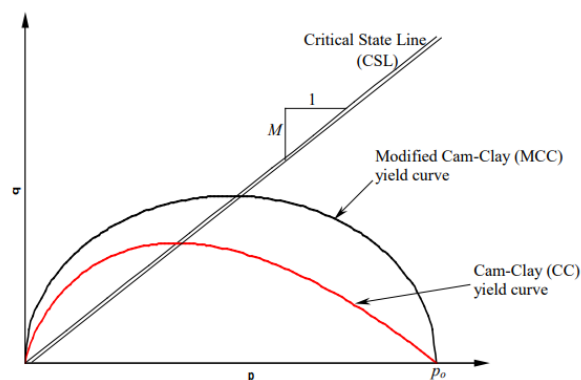
Figure 2.7. Cam-Clay and Modified Cam-Clay yield surfaces. The parameter *M* is the slope of the Critical State Line.

The critical state theory includes the following concepts: a) critical state; b) void ratio and mean effective stress dependence; c) permanent strain; d) rupture criterion. The critical state is defined as one in which there is no volume or stress variation (Schofield & Wroth, 1968). The

fundamental concept of critical state theory is the State Boundary Surface, which is defined in the three-dimensional space formed by the stress invariants (p and q) and void ratio (e). The upper curved edge of this surface, called the Critical State Line, is the locus of the points where there is no volume change, which means that rupture has occurred. The pre-consolidation stress (p_p) controls the size of the ellipse yield surface. The parameter M determines the shape of the yield surface (height of the ellipse). The State Boundary Surface for the Modified Cam-Clay model is shown in Figure 2.8 The MCC is based on five parameters:

- ν_{ur}: Poisson´s Ratio
- κ: Cam-Clay swelling index
- λ: Cam-Clay compression index
- M: Tangent of the critical state line
- e_{init}: Initial void ratio

The model has some limitations that need to be addressed. Although the constitutive model is able to model softening, in the finite elements, there are convergence problems to simulate such behavior. It may allow for unrealistically high shear stress for an overconsolidated stress state where the stress path crosses the critical state line. Also, since the model assumes an associated flow rule, unrealistic (very high) values of K_0 are obtained in the normally consolidated range.
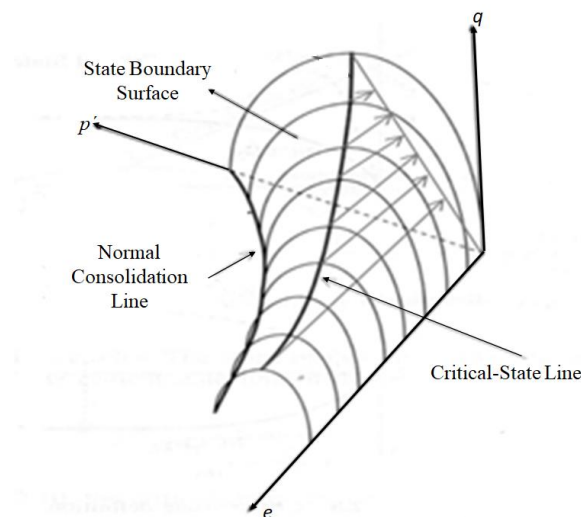
Figure 2.8. State Boundary Surface and Critical-State Line

2.7.2.2 Hardening Soil Model (HSM)

The HSM is an isotropic hardening double surface plasticity model that gives more accurate displacement patterns for working load conditions (Schanz et al.,1999). This model considers both theories of the non-linear elasticity and the plasticity, representing a significant advance in comparison with the basic linear elastic models (LE) and the elastic-perfectly plastic model of Mohr-Coulomb (MC). This model is available in the Plaxis software and was implemented by the program initially as an extension of the MC model (Nordal, 1999). Although the results obtained with this model are closer to "reality", it requires a higher number of input parameters that demand more work to be obtained. HSM basic characteristics are:

HSM basic characteristics are:

- Total strains are calculated using a stress-dependent stiffness according to a power law. (Input parameter m)
- Shear hardening: plastic straining due to primary deviatoric loading. (Input parameter E_{50}^{ref})
- Compression hardening: plastic straining due to primary compression. (Input parameter E_{oed}^{ref})
- Failure according to MC failure criterion. (Input parameters c', φ' and ψ)
- Stiffness is defined by loading and unloading/reloading conditions. (Input parameters E_{ur}^{ref} and v_{ur})
- Non-associated flow rule assumed for shear hardening
- Associated flow rule assumed for compression hardening

Table 2.2 presents the parameters for the HSM.

Table 2.2. Hardening soil model input parameters.

Parameter	Description
φ'	Internal friction angle (°)
c'	Cohesion (kN/m²)
R_f	Failure ratio
ψ	Dilatancy angle (°)
E_{50}^{ref}	Reference secant stiffness from drained triaxial test (kN/m²)
E_{oed}^{ref}	Reference tangent stiffness for oedometer primary loading (kN/m²)
E_{ur}^{ref}	Reference unloading/reloading stiffness (kN/m²)
m	Exponential power
v_{ur}	Unloading/reloading Poisson´s Ratio
K_o^{nc}	Coefficient of earth pressure at rest (NC state)
Ko	Coefficient of earth pressure at rest
OCR	Over Consolidation Ratio
p_{ref}	Stress of reference, usually 100 kPa

For the case of drained triaxial test, Figure 2.9 shows the hyperbolic relationship between the vertical strain, ε_1, and the deviatoric stress, q, in primary loading formulated first by Kondner (1963) and then used by Duncan & Chang (1970).
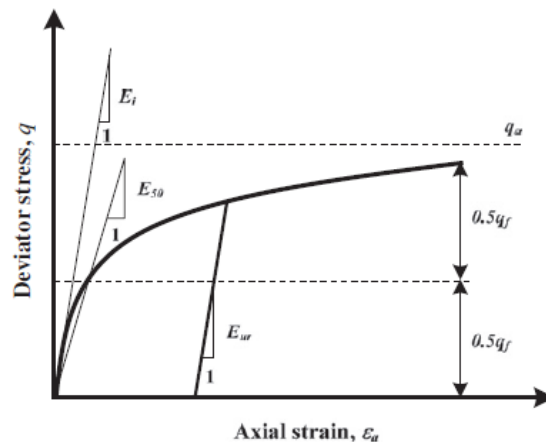
Figure 2.9. Hyperbolic stress-strain relationship in primary loading for a standard drained triaxial test (Schanz et al., 1999).

As formulation of this relationship, we have:

$$\varepsilon_1 = \frac{1}{E_i}\frac{q}{1-\frac{q}{q_a}} \quad , \text{for } q < q_f \tag{2.4}$$

where q_a is the asymptote of the shear strength:

$$q_a = \frac{q_f}{R_f} \tag{2.5}$$

where R_f is the failure ratio (0.9 by default in the Plaxis), and q_f is the ultimate deviatoric stress at failure, derived by the MC criterion:

$$q_f = \frac{2\sin\phi'}{1-\sin\phi'}(\sigma'_3 + c'\cot\phi') \tag{2.6}$$

where c' and φ' are the effective shear strength parameters, σ'_3 is the confining stress in the triaxial test (Plaxis considers this parameter as negative in compression),

The initial stiffness E_i is related to E_{50} by:

$$E_i = \frac{2E_{50}}{2-R_f} \tag{2.7}$$

where E_{50} is the confining stress-dependent stiffness modulus for the primary load, defined as:

$$E_{50} = E_{50}^{ref}\left(\frac{c'\cos\phi' + \sigma'_3\sin\phi'}{c'\cos\phi' + p^{ref}\sin\phi'}\right)^m \tag{2.8}$$

where E_{50}^{ref} is the reference secant stiffness modulus for the drained triaxial test, p_{ref} is the reference isotropic stress considered by default as 100 kPa in the Plaxis, and m is the exponent that gives the amount of stress dependency. According to Brinkgreve et al. (2018), to simulate a logarithmic compression behavior, m should be taken equal to 1.0 for soft clays. Also as mentioned by Obrzud & Truty (2018) and Brinkgreve et al. (2018), Janbu (1963) reported values of m equal to 0.5 for Norwegian sands and silts. Values between 0.38 and 0.84 for soft lacustrine clays were also provided by Kempfert (2006), and Soos von (2001) reported a range of m values from 0.5-1 for different soil types.

The stress-dependent stiffness modulus for unloading and reloading stress paths is defined as:

$$E_{ur} = E_{ur}^{ref} \left(\frac{c' \cos \phi' + \sigma'_3 \sin \phi'}{c' \cos \phi' + p^{ref} \sin \phi'} \right)^m \qquad (2.9)$$

where E_{ur}^{ref} is the reference stiffness modulus for unloading and reloading conditions, it can be considered by default in Plaxis as $3E_{50}^{ref}$

As presented in Figure 2.10, the elastic region in the HSM is limited by the shear and compression hardening yield function.
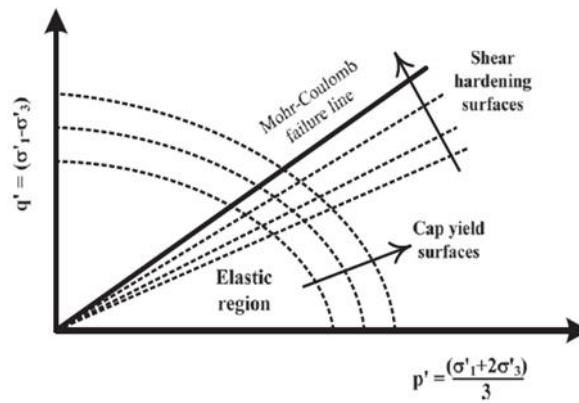
Figure 2.10. Shear hardening and cap yield surfaces in the HSM (Schanz et al., 1999).

The shear hardening yield function (f_s) is defined as:

$$f_s = \bar{f} - \gamma^p \qquad (2.10)$$

where $\bar{f}$ is:

$$\bar{f} = \frac{2}{E_i} \frac{q}{1 - \dfrac{q}{q_a}} - \frac{2q}{E_{ur}} \qquad (2.11)$$

and the plastic shear strain(γ^p) is calculated as:

$$\gamma^p = 2\varepsilon_1^p - \varepsilon_v^p \approx 2\varepsilon_1^p \qquad (2.12)$$

where ε_1^p is the plastic axial strain and ε_v^p is the plastic volumetric strain.

The *cap* compression hardening yield function (f^c) is given by:

$$f^c = \frac{\tilde{q}^2}{\alpha^2} + p^2 - p_p^2 \tag{2.13}$$

where p is the isotropic stress, p_p is the pre-consolidation isotropic stress, α is an auxiliary parameter of the model related to K_0^{nc}, and $\tilde{q}$ is the special stress measurement for deviatoric stresses:

$$\tilde{q} = \sigma'_1 + (\delta - 1)\sigma'_2 - \delta\sigma'_3 \tag{2.14}$$

Where

$$\delta = \frac{3 + \sin \phi'}{3 - \sin \phi'} \tag{2.15}$$

Should be mention that for triaxial compression ($\sigma'_2 = \sigma'_3$), $\tilde{q} = \sigma'_1 - \sigma'_3$, and for triaxial extension ($\sigma'_1 = \sigma'_2$), $\tilde{q} = \delta(\sigma'_2 - \sigma'_3)$.

The volumetric plastic strains in isotropic compression (ε_v^{pc}) are given by:

$$\varepsilon_v^{pc} = \frac{\beta}{1 - m}\left(\frac{p_p}{p^{ref}}\right)^{1-m} \tag{2.16}$$

where β is an auxiliary parameter of the model related to the reference tangent stiffness modulus for oedometric loading E_{oed}^{ref} ($E_{50}^{ref} = 1{,}25 E_{oed}^{ref}$ by default in Plaxis). The axial stress-dependent stiffness modulus (E_{oed}) for primary oedometric loading (σ'_1) is obtained as follows:

$$E_{oed} = E_{oed}^{ref}\left(\frac{c' \cos \phi' + \sigma'_1 \sin \phi'}{c' \cos \phi' + p^{ref} \sin \phi'}\right)^m \tag{2.17}$$

The two flow surfaces are presented in Figure 2.11, shear hardening and compression hardening, or "Cap" surface in the principal stress space. Being incorporated of this last surface,

and the phenomenon of dilatancy in the constitutive matrix, the significant advantages of the HSM in comparison to the hyperbolic elastic model of Duncan & Chang ((DUNCAN; CHANG, 1970)).
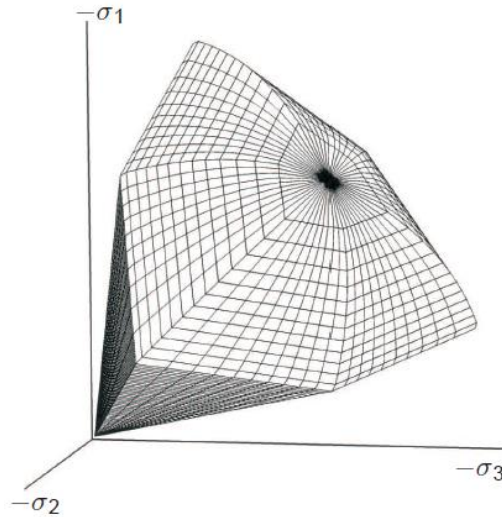
Figure 2.11. Representation of total yield contour of the HSM in principal stress space for cohesionless soil. (Brinkgreve et al., 2017)

The HSM, like the rest of the models, is not perfect, and one of its disadvantages is that the number of parameters used is high, and many of them are obtained from approximations through semi-empirical graphs. Also, not all parameter combination works showing the internal limitations of the model. It also does not consider soil anisotropy, neither the plastic flow.

2.7.3 Plaxis software

The PLAXIS software was chosen as the tool for this research. The main reason is that it can model the problem of subsidence that we are working with and is the software available at the University of Brasilia. PLAXIS is a two-dimensional and three-dimensional finite element software specifically for the analysis of deformations and stability of geotechnical works. It began to be developed in 1987 by the Technical University of Delft (Holland), and it is regularly updated. It was elaborated with the purpose of constituting a practical numerical tool for the use of geotechnical engineers who are not necessarily specialists in numerical procedures. This development philosophy of the software resulted in a quite handy user-engineer interaction since the pre-and post-processing routines are easy to manipulate (Brinkgreve et al., 2017).

2.7.3.1 3D plate elements

Plates are structural area elements used to model thin structures in the ground with a significant flexural rigidity that does not allow plastification only linear elastic behavior. Regarding meshing, the Plaxis 3D Scientific Manual (2018) described these elements as composed of 6-node triangular (Figure 2.12). Plate elements cannot sustain torsional moments; then, they have only five degrees of freedom per node, i.e., one axial displacement (u_x), two transverse displacements (u_y and u_z), and two rotations (φ_y and φ_z).
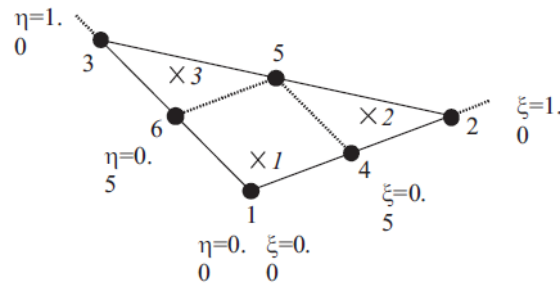
Figure 2.12. Local numbering and positioning of nodes (•) and integration points (X) of a 6-node plate triangle. (Brinkgreve et al., 2018)

The material behavior in plate elements is defined by the following parameters:

- E_1: Young's modulus in a first axial direction
- E_2: Young's modulus in a second axial direction
- G_{12}: In-plane shear modulus
- G_{13}: Out of plane shear modulus related to shear deformation over the first direction
- G_{23}: Out of plane shear modulus related to shear deformation over the second direction
- v_{12}: Poisson's ratio ($v_{12}<\sqrt{(E1/E2)}$)

2.7.3.2 Embedded beams (Embedded piles)

An embedded beam element is defined in the Plaxis Reference Manual as a structural object with special interface elements providing the interaction between the beam and the surrounding soil. The interaction may be involving skin resistance as well as base resistance, which are

determined by the relative displacement between soil and pile. Those special interface elements are different from the ones used in walls or volume piles. Therefore, at the beam element nodes, virtual nodes are created in the soil volume element from the element shape functions. Figure 2.13 illustrated how the beam crosses a 10-node tetrahedral element at any place with any arbitrary orientation (Plaxis Scientific Manual, 2018).
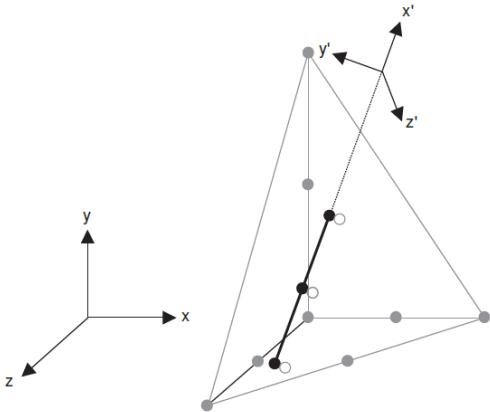
Figure 2.13. Illustration of the embedded beam element denoted by the solid line. The blank grey circles denoted the virtual nodes of the soil element. (Brinkgreve et al., 2018)

The embedded element does not occupy volume. Although, it behaves almost like a volume pile since a particular volume around the pile (elastic zone) is assumed in which plastic soil behavior is excluded (Figure 2.14). The size of this zone is based on an equivalent pile diameter inputted in the material data set.
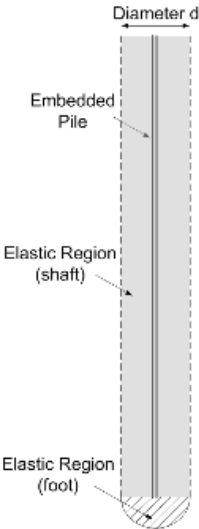
Figure 2.14. Elastic region around embedded pile (Dao, 2011)

Regarding beam element elastic behavior is defined by:

- *A*: Beam cross-section area
- *E*: Young's modulus in the axial direction
- I_2: Moment of inertia against bending around the second axis
- I_3: Moment of inertia against bending around the third axis

According to the Plaxis Material Models Manual, the interaction of the skin pile with the soil is described as linear elastic and is defined by the parameter T_{max} (Maximum traction allowed at the skin of the embedded beam which can vary along the pile). On the other hand, the interaction of the pile with the soil at the foot of the pile is described by a linear elastic perfectly plastic interface element. The strength of the base is described by the parameter F_{max} (Maximum force allowed at the foot of the embedded beam). Table 2.3 shows the parameters required to use the embedded piles.

Table 2.3. Embedded pile required parameters

Parameter	Description
Predefined pile type	Massive circular pile/ Massive tube/ Massive square pile
Diameter	Diameter (m)
E'	Young's modulus (kN/m^2)
γ	Unit weight (kN/m^3)
Axial skin resistance	Linear / Multi-linear / Layer dependent
$T_{top,max}$	Maximum traction allowed at the pile top (kN/m)
$T_{bot,max}$	Maximum traction allowed at the pile bottom (kN/m)
F_{max}	Base resistance (kN)

The embedded pile is used as a simplification of the volume pile (created by volume elements) and has some advantages. According to Dao (2011), the most important of them is that the mesh refinement is lower, reducing the time for numerical calculations. It is because when creating the embedded pile, no corresponding geometry points are created, so it does not give influence on the mesh. Also, an embedded pile can directly provide the force results of in output, which

can't be obtained from the volume pile because it is assigned with soil material. On the other hand, an embedded pile may be applied effectively in modeling the piles in which the installation process results in low disturbance since the installation effects of the pile are not considered.

2.7.3.3 Volume elements (Volume piles)

The soil volume in the Plaxis program is modeled by 10-node tetrahedral elements and has three degrees of freedom per node (u_x, u_y, u_z) (Figure 2.15). The volume piles are composed of this type of element in which the interaction with surrounding soil is modeled using interface elements. Their properties of them are assigned in the material data set for soil but with concrete properties. According to Dao (2011), and as mentioned in the previous item, the volume pile cannot give results of force like in the embedded pile due to being created as a volume element with soil material. Another disadvantage of these elements' use is that the computational time increases considerably due to the need for the mesh to be finer and the extra elements generated.
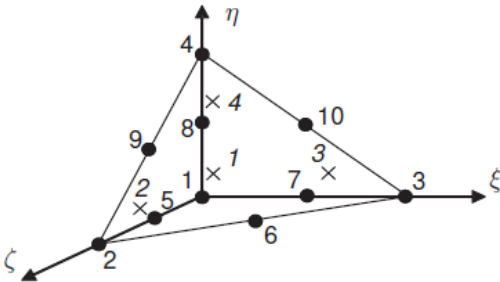
Figure 2.15. Local numbering and positioning of nodes (•) and integration points (X) of a 10-node tetrahedral element (Brinkgreve *et al.*, 2018).

2.7.3.4 Interface elements

Interfaces are joint elements to be added to plates or geogrids to allow proper modeling of soil-structure interaction (Plaxis Reference Manual, 2018). To describe the behavior of these elements, an elastic-plastic model is used. Interface elements are composed of 12-node interface elements, which consist of pairs of nodes instead of single nodes as used in the plate elements. Each node has three translational degrees of freedom (u_x, u_y, u_z). Also, each interface has assigned a 'virtual interface thickness,' which is defined as an imaginary dimension used to

determine the material properties of the element. The higher the value for this property, the more elastic deformations are generated. Plaxis gives a default value of 0,1.

The most important parameter is R_{inter} (the strength reduction factor), which defined the strength of the element. According to the manual previously cited, in the absence of information, this parameter value should be of the order of 0.6. Also, mention that for real soil-structure interaction, the interface is weaker and more flexible than the surrounding soil, which means that the value should be less than 1.

2.8   Centrifuge modeling

Centrifuge model testing represents a valuable tool available to the geotechnical engineer since it enables the study and analysis of design problems by using geotechnical materials (Taylor, 1995). This physical modeling technique provides data for investigating deformation and failure mechanisms and for validating analytical and numerical methods (Ng, 2014). It tries to predict the behavior that will occur in a prototype, reproducing the conditions in a model, which usually corresponds to a reduced version of the prototype. The two events should be similar, and that similarity needs to be related by appropriate scaling laws (Table 2.4) (Taylor, 1995).

Table 2.4. Scaling laws in the geotechnical centrifuge

Parameter	Unit	Scale Factor
Acceleration	L/T^2	N
Density	M	1
Tensions	M/LT^2	1
Deformations	-	1
Velocity	L/T	1
Length	L	1/N
Time (static event)	T	$1/N^2$
Time (dynamic event)	T	1/N
Displacement	L	1/N
Unit weight	M/L^2T^2	N
Flow speed	L/T	N
Temperature	°	1

Authors such as Tang et al. (2012) and Cui et al. (2010) presented regional subsidence studies caused by engineering environmental effects of high-rise building groups with different plot ratio. Regarding modeling regional subsidence due to groundwater exploitation, Sun et al. (2008) developed a drainage system to simulate the water pumping during the centrifuge tests. Additionally, Cheng et al. (2011) carried on centrifuge model tests to evaluate the influence of this phenomenon on a high-speed railway bridge. Wang et al. (2013) studied stratified and rebound settlement due to dewatering in a Shanghai subway station based on centrifugal model tests. Zhang et al. (2017) carried out seismic centrifuge model tests to study the behavior of pile groups in soft kaolin clay. On the other hand, various research have been done works using piled rafts on centrifuges like Thaher & Jessberger (1991), Horikoshi & Randolph (1996), Bajad & Sahu (2008), Goh & Zhang (2017) among others. Tran et al. (2012) and Rodríguez et al. (2020) focused specifically on the behavior of the piled raft under the effects of regional subsidence, assessing not only settlements but also load distribution.

2.9   Experimental research by Rodríguez (2016)

To develop and reach the main objective of this thesis, the experimental work done by Rodríguez (2016) in the geotechnical centrifuge, will be used as a base to validate the 3D numerical model. The research focused on the evaluation of the behavior of piled raft systems in soft soils along the consolidation process. This consolidation process was generated either by the structural load or by the drawdown of the pore-pressures in depth. The decrease in the pore pressure value was associated by the referenced author, with the subsidence process induced by the extraction of water from deep permeable layers (Figure 2.16).
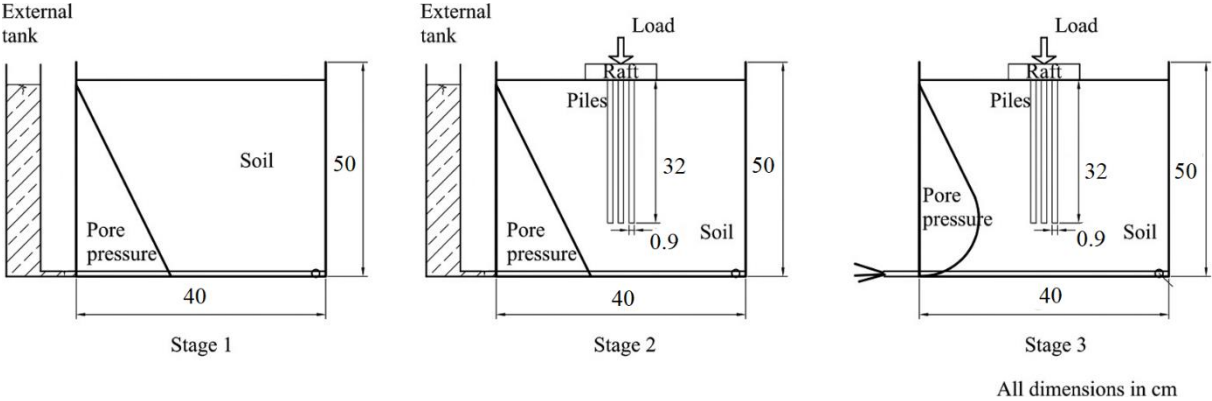
Figure 2.16. Representation of pore pressure conditions at testing stages. Adapted from Rodríguez, 2020.

The soil profile presented in Figure 2.17 was the one used for the test. This profile is composed of three layers of kaolin divided by two sand layers that work as a filter and a bottom layer as drainage.
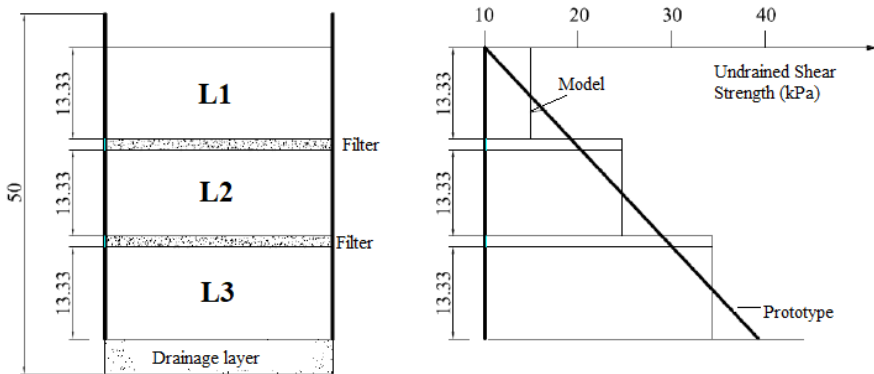
Figure 2.17. Measurements in cm of the layer distribution and Soil undrained shear strength profile. Adapted from Rodríguez (2016).

Kaolin was the material chosen for the models. It can be described as a clayey material that allows the manufacture of soils in the laboratory, guaranteeing homogeneity, linearity in the stress profile, and cohesion of the sample. Characterization, granulometric analysis by sedimentation tests, consolidation tests, and three Consolidated Undrained Triaxial Compression tests (CU) were carried out by Rodríguez (2016), to get the soil parameters. Figure 2.18 shows the consolidation curves and some triaxial results. The summary of the soil parameters is presented in Table 2.5.
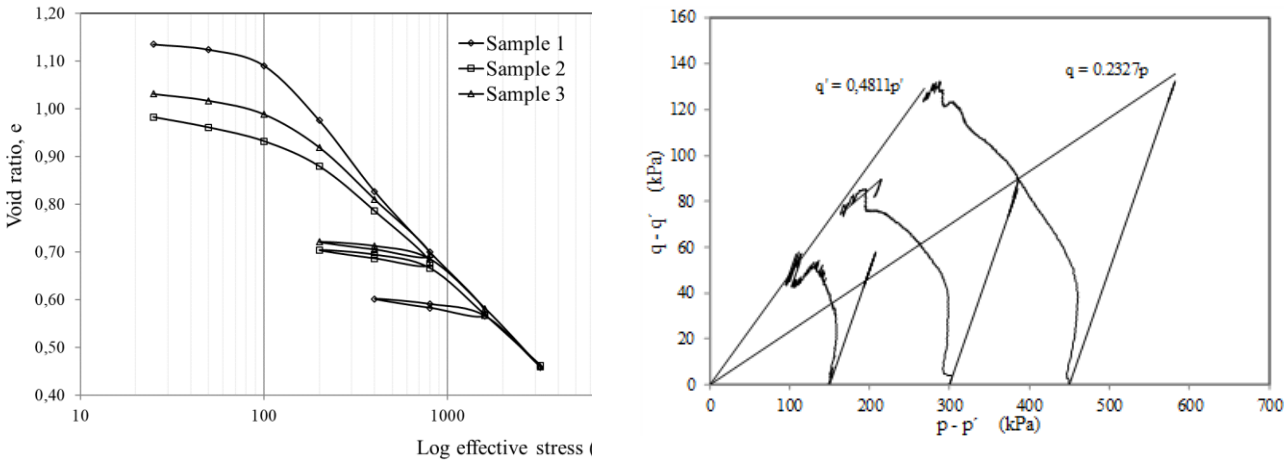
Figure 2.18. Kaolin consolidation test and Triaxial test results (CU). Rodríguez (2016)

Table 2.5. Kaolin parameters presented by Rodríguez (2016)

Parameter		
Specific gravity	Gs	2.68
Liquid limit	LL (%)	54
Plasticity index	PI (%)	33
Plastic limit	PL (%)	21
Slope of compression line	λ	0.16**
Slope of recompression line	κ	0.04**
Compression Index	Cc	0.37
Recompression index	Cs	0.09
Vertical consolidation coefficient	*Cv (m^2/s) x 10^{-6}	0.49-0.62

*Cv to vertical stress of 100 kPa ** Estimated. $\quad \lambda = \dfrac{Cc}{Ln10} \qquad \kappa \cong \dfrac{Cs}{Ln10}$

This author has adopted two different scales 70 g and 200 g in his experiments, so to assess the behavior of the piled raft in clays, with some constant characteristics and other variables. For instance, the following parameters were considered as variables to evaluate their influence on the system: pile spacing and quantity and geometry distribution on the system. Nevertheless, in the present research, only the 70 g scale models were adopted since they have proved to be more consistent and allowed better experimental results. Table 2.6 summarizes the piled raft elements' dimensions and their equivalent for the prototype.

Table 2.6. Elements dimensions of the Piled Raft for models with a scale factor of 70g.

		MODEL
	Material	Aluminum
	Thickness	13 mm
Raft	Young's modulus	70000 MPa
	Width	200 mm
	Length	200 mm
	Material	Aluminum
	Diameter	9 mm
Piles	Young's modulus	70000 MPa
	Length	320 mm

The piled raft configuration and geometry proposed for the experimental centrifuge tests are depicted in Figure 2.19. Due to different factors not all the models could be made. Thus, the models that were carried out are presented in Table 2.7.
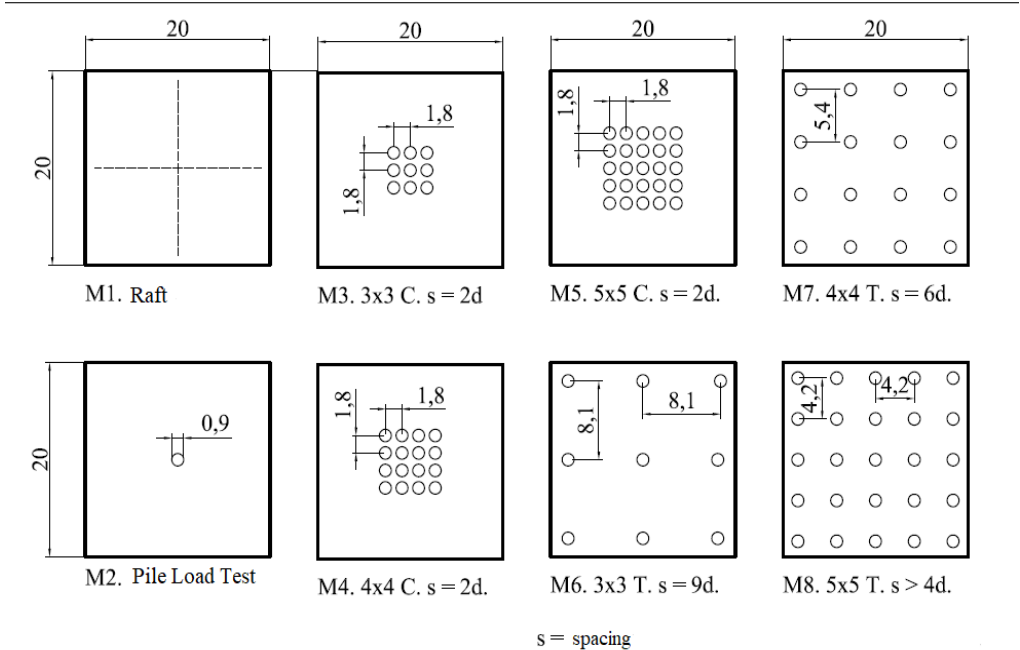
Figure 2.19. Geometric configuration of the proposed models in scale 1/70 (Measurements are in cm). Adapted from Rodríguez (2016).

Table 2.7. Proposed models on scale 1/70. Adapted from Rodríguez (2016)

Model Name	Raft dimensions (cm)	Raft thickness (cm)	Piles diameter (cm)	Piles length (cm)	Configuration	Spacing (cm)	Number of piles
M1	20 x 20	1,3			-		0
M2	-	-	0,9	32,0	1		
M3	20 x 20	1,3	0,9	32,0	3 x 3 C	1,8	9
M4	20 x 20	1,3	0,9	32,0	4 x 4 C	1,8	16
M6	20 x 20	1,3	0,9	32,0	3 x 3 T	8,1	9

C: Distribute in the raft center. T: Distribute in all the raft area.

Significant results were obtained regarding the piled raft behavior. Figure 2.20 shows some of the soil and raft displacement data obtained from the models and the ones that were used for the present work. Regarding strain gauges instrumentation, when data were processed, it was observed that several instruments did not show variation in the measured values, and in others, the data was inconsistent. Due to this and as a limitation, it was not possible to assess the load

generated along the pile shaft, which is important data when working with soft soils undergoing regional subsidence.
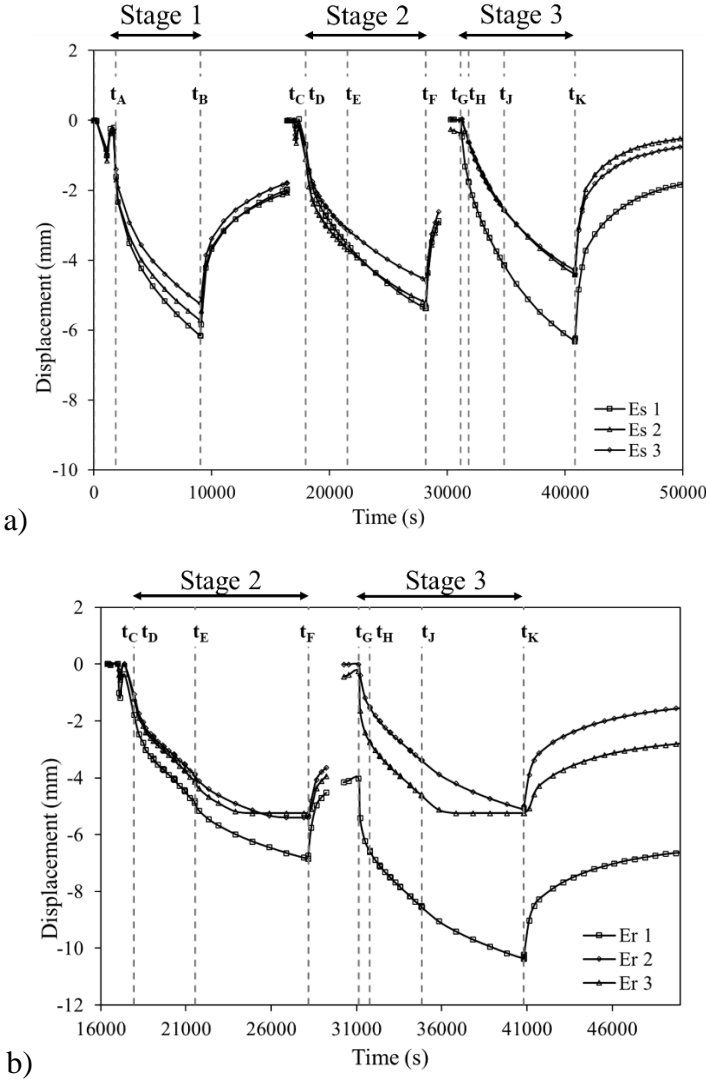
Figure 2.20. a) Soil displacement data. and b) Piled raft displacement data. Adapted for Rodríguez (2016).

2.10 Chapter summary

In this chapter, the main characteristics of piled raft systems and their possibility of use in soft soils were presented, and for some authors, these systems can be widely used because they have greater load capacity and lower differential settlements.

The regional subsidence problem was described, which can be generated by the water pore pressure drawdown of soil due to pumping processes. As a result of this phenomenon, it can be

developed negative friction in the piles of the systems affecting their behavior. Negative friction is associated with drag loads generated by the downdrag force. The presence of negative friction and dragload forces generates a change in the distribution of the load through the friction along the piles.

Different studies have been conducted to understand the behavior of individual piles used in soft soil with consolidation processes by loading or by pore pressure abatement, most of them, associated with piles that work by tip capacity.

For the piled raft systems founded on soft soils and subjected only to loading, most of the studies were theoretical, and have been focused on the analysis of the influence of negative friction on the system response (settlements, raft load, load distribution along the shaft piles and distribution of the load between piles and raft).

A substantial number of field and laboratory studies related to the development of negative friction in piles individual has been carried out, but few research have work with three-dimensional models or have used simplified models and constitutive models that requires basic parameters that do not give an optimum response of the system's behavior. Some of these studies were presented in Table 2.1.

There is a need to work with models that are more complete and use complex constitutive models that better represent the behavior of these soft soils that suffer from regional subsidence. For this reason, the work that will be presented uses a more complex constitutive model that allows assessing strength and deformability parameters of soft soils with greater precision. In addition, considering the influence of pore pressure variation and negative friction on the soil-piled raft behavior, it will be possible to propose new methodologies or tools to optimize foundation projects built on this type of soil.

The aim is to use the data to complement or propose analysis methodologies or tools that will allow to project more efficiently and fast foundation systems when built-in soft soils with the mentioned conditions.

CHAPTER 3

3. RESULTS: NUMERICAL MODELING AND EXPERIMENTAL WORK

As shown in Figure 3.1, the results will be divided and presented into three major parts. A proposed numerical model validated the experimental results obtained by Rodríguez (2016) in the geotechnical centrifuge. The CCM and HSM methods were used to calibrate and refine all numerical analyses that simulated centrifuge results. Although the MCC was validated, it was observed that Rodriguez's laboratory test samples were not manufactured with the same soil stress level (consolidation) as used in the physical model of the centrifuge. Because there was insufficient information to calculate the parameters for the HSM, it was decided to conduct laboratory tests to provide the precise parameters required. Finally, the mechanical parameters of the HSM were calibrated from the experimental test of this research in order to numerically reproduce the behavior of a pile raft foundation system.
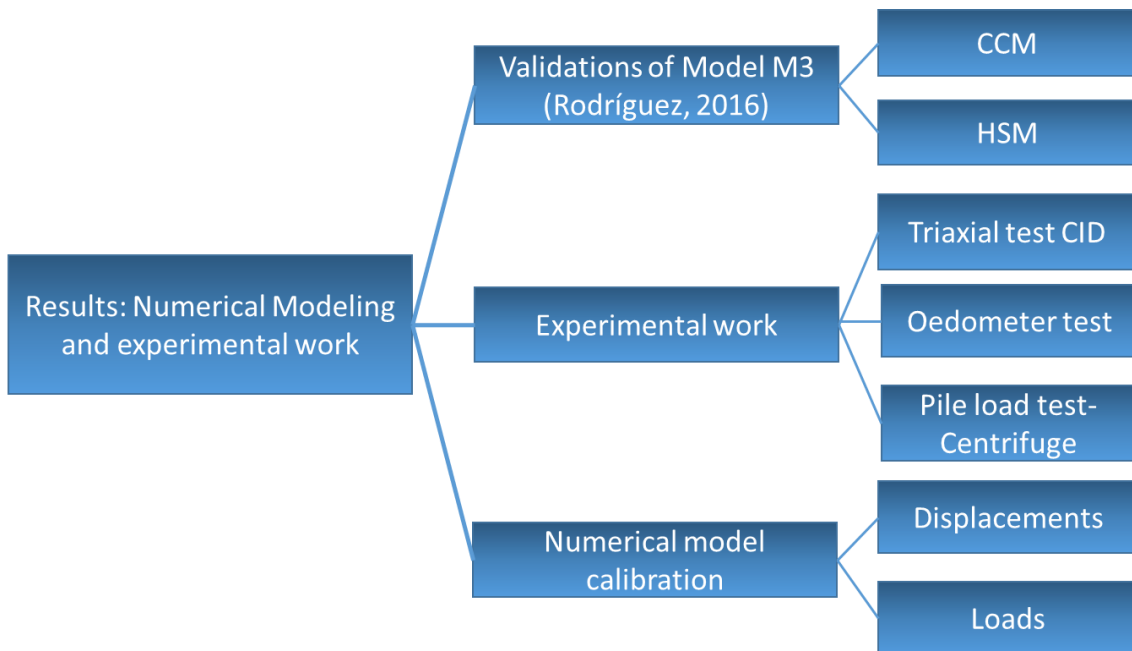
Figure 3.1. Results: Numerical Modeling and experimental work outline

3.1   Validations of Rodríguez (2016) experimental model M3

A numerical model using FEM is proposed to identify the most sensitive parameters for this type of simulation, and to define the types and stages of analysis that had the best fit to the

physical model, and finally to obtain additional results to those measured in it. The numerical modeling is carried out by the FEM using the PLAXIS 3D software, which is widely used for geotechnical analysis.

The geometric configuration of the M3 model was chosen not only because it has fewer structural elements, but also because its data shows the best behavior among the other configurations. M3 model had a piled raft and nine piles arranged in the center, with a spacing of two diameters between them, i.e., an easier configuration to simulate numerically. The model and soil body measurements are also presented in (Figure 3.2 and Figure 3.3)
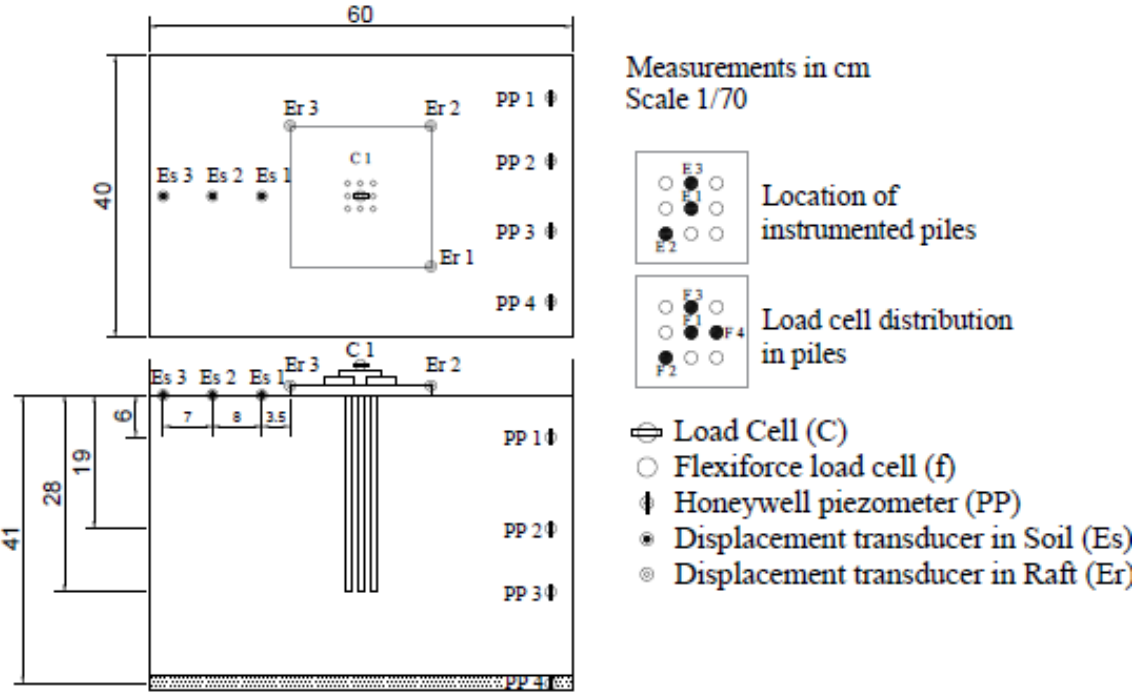
Figure 3.2. Instrumentation distribution of the reduced scale model M3. Adapted after Rodríguez (2016).

Figure 3.3. Assembly and instrumentation details of M3 model. (Rodríguez, 2016)

3.1.1 Constitutive model validation for soft soil simulation

The constitutive model choice and validation of its parameters consisted of comparing experimental results from Rodríguez (2016) to numerically simulated data. This data was gathered by analyzing the problem with PLAXIS software using triaxial and oedometer test results.

A *SoilTest* tool has been developed in PLAXIS to allow the simulation of different laboratory tests based on a single point algorithm, i.e., without the need to create a complete final model (PLAXIS Reference Manual, 2018). *SoilTest* works with the inputted soil parameters obtained from an investigation site to compare with the behavior as defined by the soil model chosen. Using this tool and with the data of the CU triaxial compression tests presented in Figure 2.18, it was possible to compare and validate the results for both constitutive models previously stated choosing the one that represented better the behavior of the soil. Following, the MCC and HSM used for the soil simulation will be presented.

3.1.1.1 Modified Cam-clay model

At first, the MCC model was chosen because it accurately represents the behavior of soft soils with few initial parameters. From the laboratory tests (Figure 2.18), the MCC parameters presented in Table 3.1 were calculated. The results obtained from the simulation are shown in Figure 3.4.

46

Table 3.1. Input parameters of the Modify Cam Clay model.

Parameter	Description	M5-7
ν	Poisson's ratio	0.3
λ	Cam Clay compression index	0.147
κ	Cam Clay swelling index	0.036
M	Tangent of the critical state line	0.96
ϕ' (°)	Friction angle	24
e_{init}	Initial void ratio	0.96
Initial Conditions		
POP	Pre-overburden pressure	0
OCR	Over consolidation ratio	1
K^0	Coefficient of lateral earth pressure	0.73
e_0	Initial void ratio	0.96

The stress paths for different confining pressure values (σ_3 = 150, 300, and 450 kPa) are shown in Figure 3.4(a), and it is well predicted by the MCC. The experimental results were presented by dotted lines and the numerical by continuous lines. In terms of the deviator stress plotted in Figure 3.4(b) and pore pressures in (Figure 3.4(c), it can be observed that the results show the same behavioral path. Nevertheless, for confining pressure of 300 kPa and 450 kPa, the numerical values showed small differences, being the simulated pore pressures lower than those from the tests. On the other hand, the FEM results for deviator stresses were higher than the laboratory measures. The oedometer test was also simulated with good agreements, as shown in Figure 3.4(d).

Although the MCC was validated, it was observed that the laboratory test samples mentioned above were not fabricated with the same stress level of the soil (consolidation) as adopted in the physical model of the centrifuge, thus hampering the assessment of the correct numerical simulation input parameters. By evaluating the physical model, it was found that the soil was in an over-consolidated condition and not normally consolidated, as observed in the characterization tests of the material. Due to this fact, it was decided to use the HSM noticing the limitations of the MCC to represent these materials' behavior in PLAXIS.
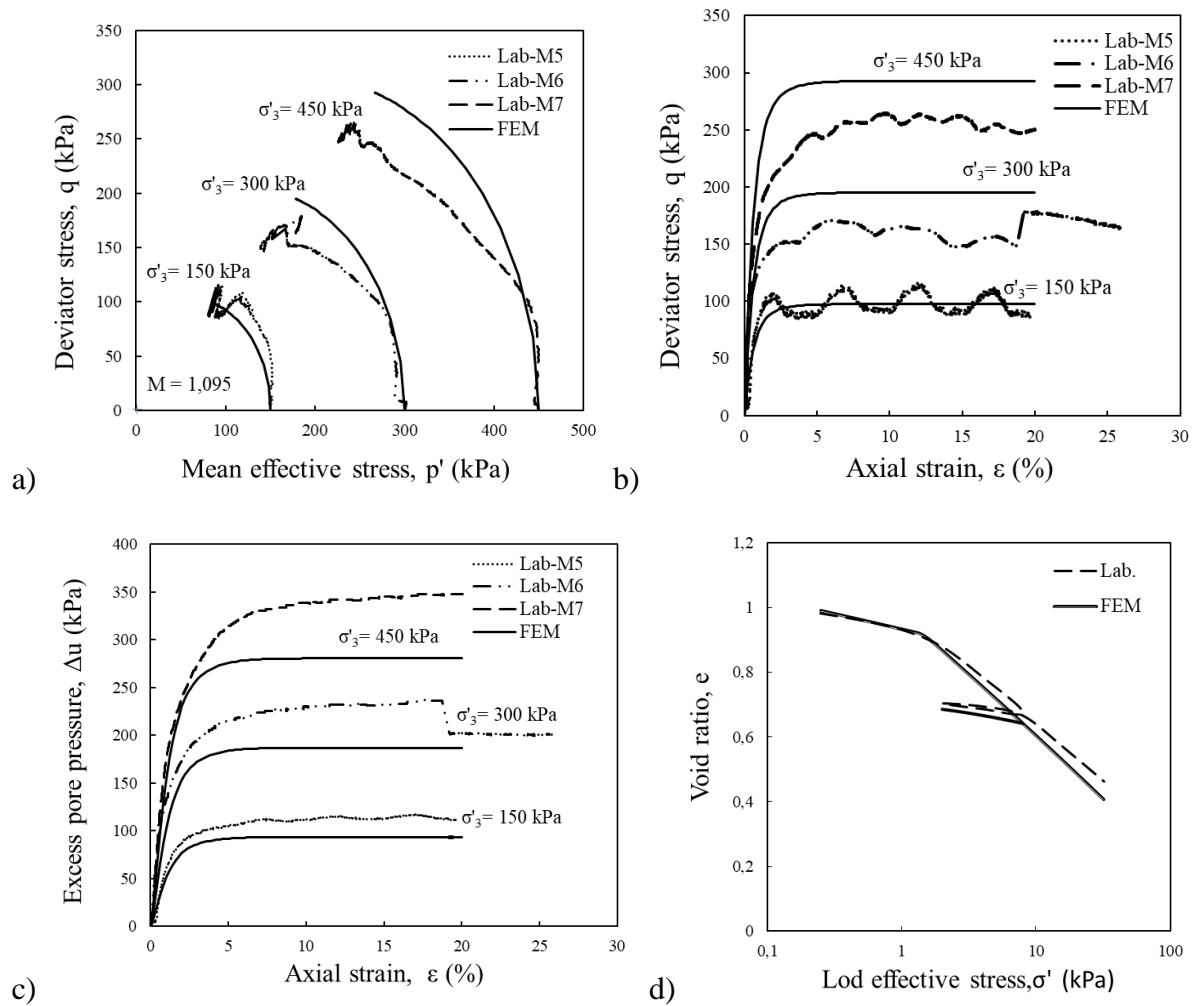
Figure 3.4. CU test results and their simulations from the MCC (a)Deviator stress vs Mean effective stress (b)Excess pore pressure vs axial strain(c) Deviator stress vs axial strain and (d)Void ratio vs Log effective stress.

3.1.1.2 Hardening soil model

Among the constitutive models available in the PLAXIS software is the HSM, which was introduced by the program initially as an extension of the Mohr-Coulomb, and it has an additional cap that allows considering the pre-consolidation pressure. For its formulation, it was considered suitable to numerically model the experimental test. However, HSM requires a high number of input parameters that are obtained from triaxial, consolidation, and direct shear tests. Many of them are obtained from approximations through semi-empirical graphs.

Having no extra experimental information to calculate these parameters, it was conducted an extensive literature review to get theoretical parameters of a soil with similar characteristics to those of the test material that presented a phenomenon of regional subsidence. Soils like those of Shanghai, Singapore, Jakarta, and Bangkok are an example of this condition. Surarak et al. (2012) analyzed a set of experimental data on Bangkok subsoils from oedometer and triaxial tests to determine the stiffness and strength parameters for HSM. Two sets of parameters for soft and stiff Bangkok clays were also numerically calibrated against undrained and drained triaxial results using PLAXIS finite element software. Based on their results, the parameters of the HSM were assumed to develop the numerical model at the beginning (Table 3.2).

Table 3.2. HSM input parameters based on CID and Oedometer testing results of soft Bangkok clay. (Surarak et al.2012)

Type of soil	c' (kPa)	Φ (°)	Ψ (deg)	E^{ref}_{50} (kPa)	E^{ref}_{ur} (kPa)	E^{ref}_{odo} (kPa)	K_0^{nc}	R_f	m	ν_{ur}
Overconsolidated Clay	11.5	28	0	9500	30000	12000	0.74	0.9	1	0.2
Lightly overconsolidated Clay	1	27	0	800	8000	850	0.5	0.9	1	0.2

3.1.2 Prototype

Next it will be presented the characteristics of the prototype, like soil profile, structural components, and mesh used to simulate the real situation that was experimentally modeled with the centrifuge in the laboratory developed by Rodríguez (2016).

3.1.2.1 Soil profile

At first, it was assumed the soil profile presented by Rodríguez (2016). The soil fabrication process allowed to obtain a profile with the presence of a top layer of up to 4.7m of clay with OCR values higher than 5 and undrained shear strength values very close to the theoretical values proposed by Rodríguez (2016) (Figure 2.17). Bowles (1997) considers that OCR values below 2 correspond to clays with low pre-consolidation. Thus, with the data and the results obtained from the tests, an initial (tentative) geotechnical model of the soil used in the research could be established, as summarized in Table 3.3.

Table 3.3. Summary of the geotechnical profile for the soil used in the models given by Rodríguez (2016)

z (m)	Material	OCR	Su (kPa)	Parameters
0.0 – 4.7	Heavily Overconsolidated Clay	8.9 – 2.2	11 – 16.4	w = 34.0 %; γ_T = 18.6 kN/m³; LL= 60 %; PL= 40%, Cc = -0.373; Cr = -0.099.
4.7 – 28.0	Lightly overconsolidated Clay	2.2 – 1.34	16.4 – 43.0	

z: Depth; OCR: Overconsolidation ratio; Su: Undrained shear strength; w = Moisture content; γ_T = Density; LL= Liquid limit; PL= Plasticity limit; Cc = Compression index; Cr = Recompression index.

As the stress state has a significant variation throughout the depth, for the numerical simulation, the soil profile was divided into several layers using the over consolidation ratio (OCR) values as a criterion. Besides being an indicator of the stress state, the OCR is one of the input parameters of the HSM. Also, the ground-water table was considered at 3.5m deep regarding the surface, as proposed by Rodríguez (2016). A stiffer layer is formed on the surface when the water level dropped in the fabrication process. The parameters adopted for this layer were the ones calibrated for stiff clay by Surarak et al. (2012). The geotechnical parameters from the different soil layers needed for the numerical simulations are presented in Table 3.4.

Table 3.4. Geotechnical parameters of the soil profile

Layer	Z m	γ kN/m³	σ'_0 kPa	σ kPa	σ_P kPa	c' kPa	f °	k_0	k_0^{nc}	E_{50}^{ref} MPa	E_{ur}^{ref} MPa	E_{oed}^{ref} MPa	m	v	OCR
SL1	0 - 3.5	18.67	28	28	170	11.5	28	1.24	0.50	9.5	30	12	1	0.2	6.07
SL2	3.5 - 6	18.67	74	84	170	1	27	0.8	0.74	0.8	8	0.85	1	0.2	2.3
SL3	6 - 15	18.67	126	196	191	1	27	0.66	0.74	0.8	8	0.85	1	0.2	1.52
SL4	15 - 23	18.67	204	364	382	1	27	0.73	0.74	0.8	8	0.85	1	0.2	1.87
SL5	23-28	18.67	256	476	382	1	27	0.65	0.74	0.8	8	0.85	1	0.2	1.49

The initial condition of the soil is determined according to parameters obtained from the samples taken from the models fabricated by Rodríguez (2016). With the density data, it was

possible to establish an approximate stress profile in the soil, as shown in Figure 3.5. To obtain the effective stress profile, the ground-water table was considered as proposed by the cited author. The vertical stress applied in the fabrication of the soil can be considered as the pre-consolidation stress of the material, as presented by Thaher & Jessberger (1991) and Tran et al. (2012).
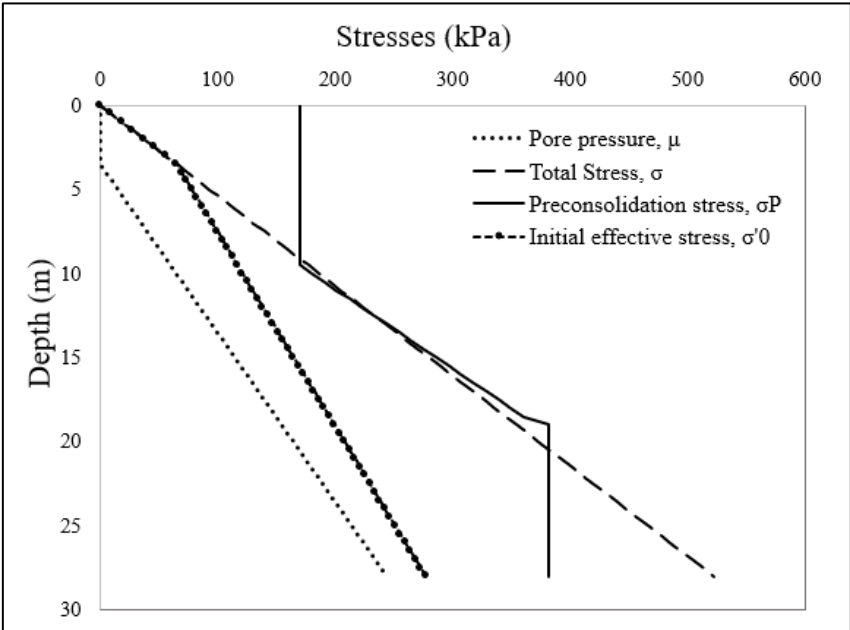
Figure 3.5. Prototype stress profile.

3.1.2.2 Structural components

To model the structural components, such as concrete piles and raft, the linear elastic constitutive model was assumed. Regarding the element type used for the design of the piled raft foundation, the plate type element for the raft and the embedded beams type for the piles were used. Plates are structural objects used to model structures in the ground with a significant flexural rigidity that does not allow plastification only linear elastic behavior (item 2.7.3.1). As an embedded beam element, it is defined in PLAXIS Manual as a structural object with special interface elements providing the interaction between the beam and the surrounding soil (item 2.7.3.2). The interaction involves skin resistance as well as base resistance, which is determined by the relative displacement between soil and pile. This element type was chosen instead of the volume elements as with them, a mesh with fewer finite elements is generated, which reduces the time of analysis. A validation between these two elements type was carried out by Melo

51

(2018), which corroborates the likeness of the results obtained in the simulations using both elements, as shown in Figure 3.6.
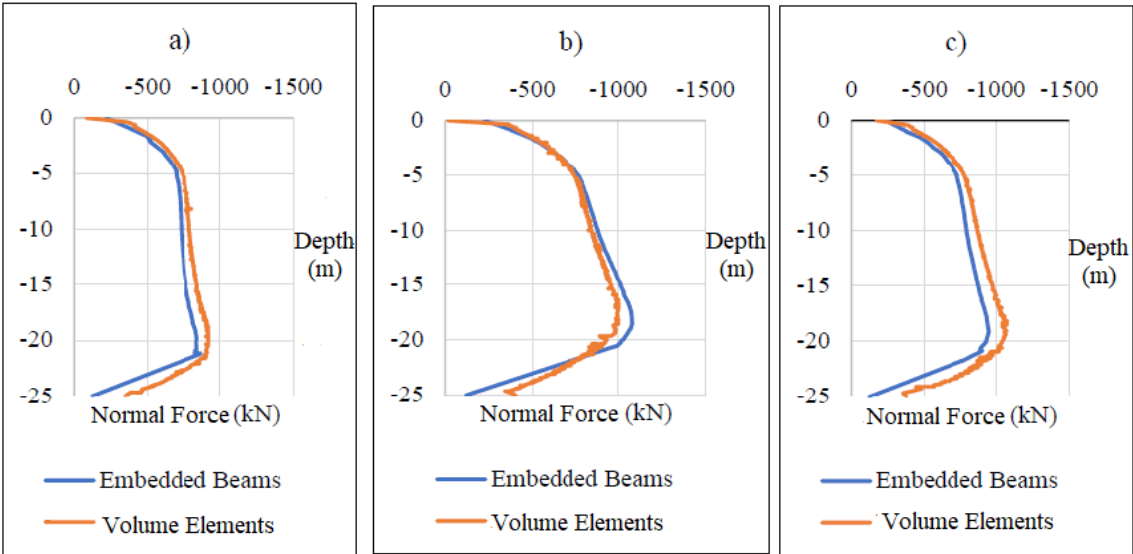
Figure 3.6. Calibration of the piles load capacity in moderate drawdown pore pressure, ELS, using a shaft load capacity of 200 kN / m, for the piles of a) center, b) edge, and c) corner. Adapted from Melo (2018).

For the proposed model in this work, the geometry of the piled raft and the soil body boundary conditions are presented in Figure 3.7 and Figure 3.8. Properties are listed in Table 3.5
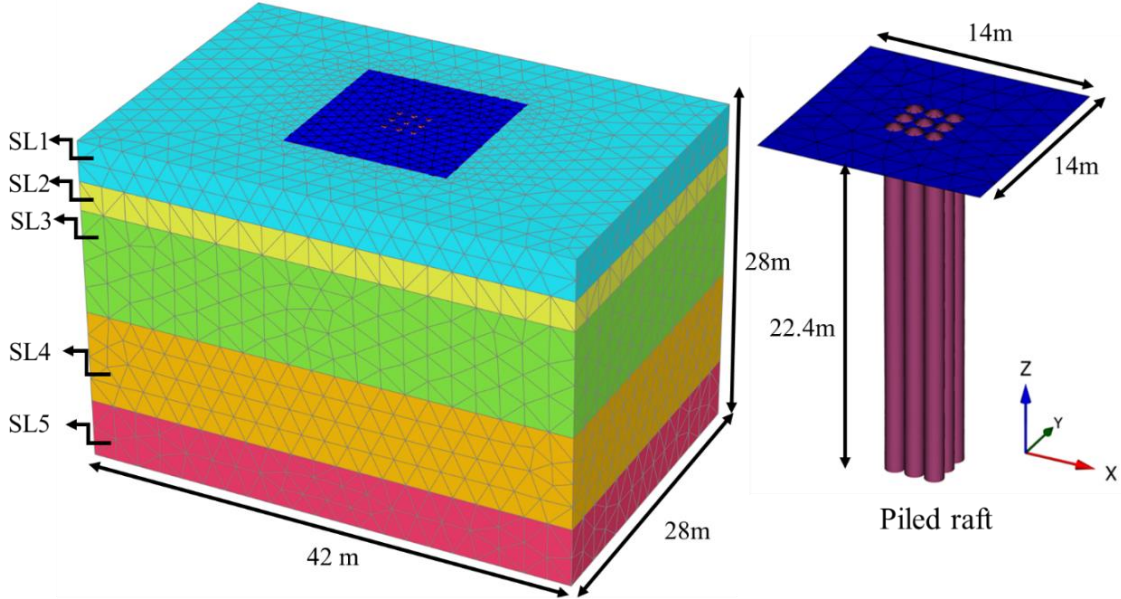
Figure 3.7. Geometry and mesh of the 3D model developed in PLAXIS.
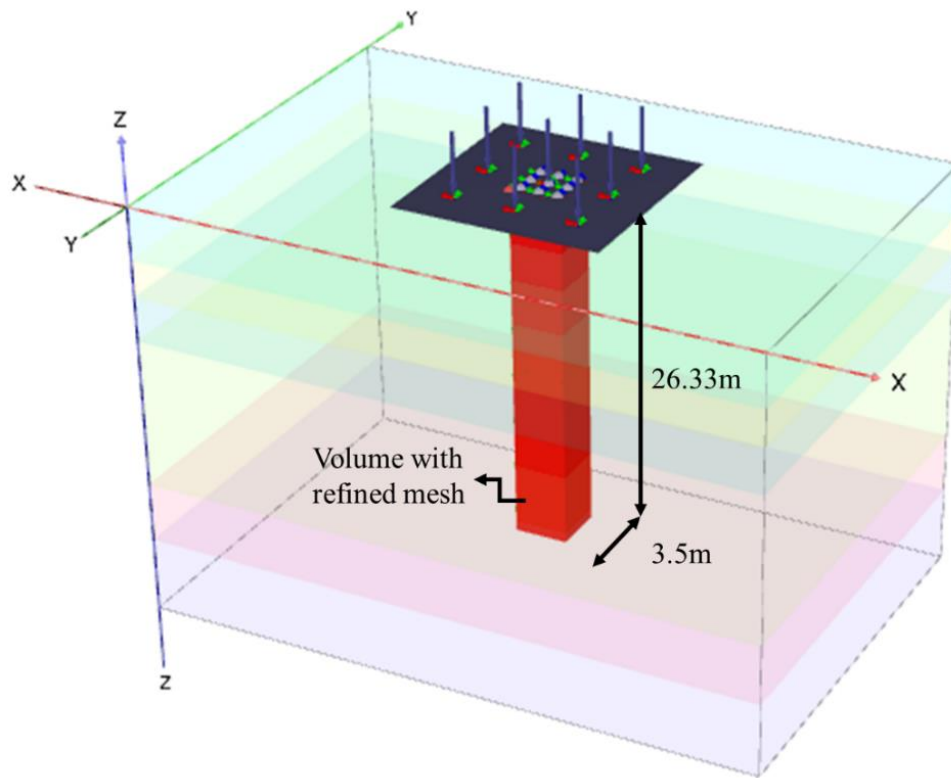
Figure 3.8. Volume around the piles with a refined mesh.

Table 3.5. Main properties of prototype structural components

Element	Parameter	
Plate (Raft)	Unit weight	25 kN/m^3
	Thickness	1.147 m
	Young's modulus	35000 MPa
	Width	14 m
	Length	14 m
Embedded beams (Piles)	Unit weight	25 kN/m^3
	Diameter	0.63 m
	Young's modulus	30000 MPa
	Length	22.4 m
	Axial skin Resistance	57 kN/m
	Base Resistance	345 kN

3.1.2.3 Mesh and boundary conditions

Once the geometry is defined, it is necessary to generate the mesh that is a composition of the finite elements in which the geometry was divided to perform the calculation. The mesh that is going to be used should be sufficiently fine to obtain accurate numerical results, although, as is widely known, very fine meshes will lead to excessive calculation times. The mesh calculation considers the soil stratigraphy as well as all structural objects, loads, and boundary conditions. Table 3.6 describes the type of FEM elements used in the numerical model.

Table 3.6. Types of FEM elements used in the numerical model

Type of Element	Number of Nodes	Description
Soil elements	10	10-node tetrahedral
Embedded beams	3	3-node line elements compatible with the 3-node edges of a soil element
Interface elements	12	Elements used to simulate soil-interaction behavior
Plate	6	Used to simulate the behavior of plates.

Initially, it is necessary to evaluate the influence of the number of mesh elements with a sensibility study of the discretization. For this analysis, it was run the first phase of the model with three generated meshes. Each mesh had element distribution between very fine, fine, and medium, which are options presented by PLAXIS. The number of elements and nodes used for each simulation are summarized in Table 3.7. Two nodes A and B were chosen to compare the results of the displacements and so determine which would be the most optimal to use. After being compared the results presented in Table 3.7, it was decided to employed the fine mesh, showing fairly approximate results between them and using a shorter computational time than the very fine mesh.

Table 3.7. Comparison between three different types of mesh, description, and displacements of the two nodes chosen.

	Number of Elements	Number of Nodes	Displacements Node A	Displacements Node B
Very Fine	74391	105488	-3.73	-6.37
Fine	33462	48182	-3.74	-6.29
Medium	13212	19546	-3.63	-6.11
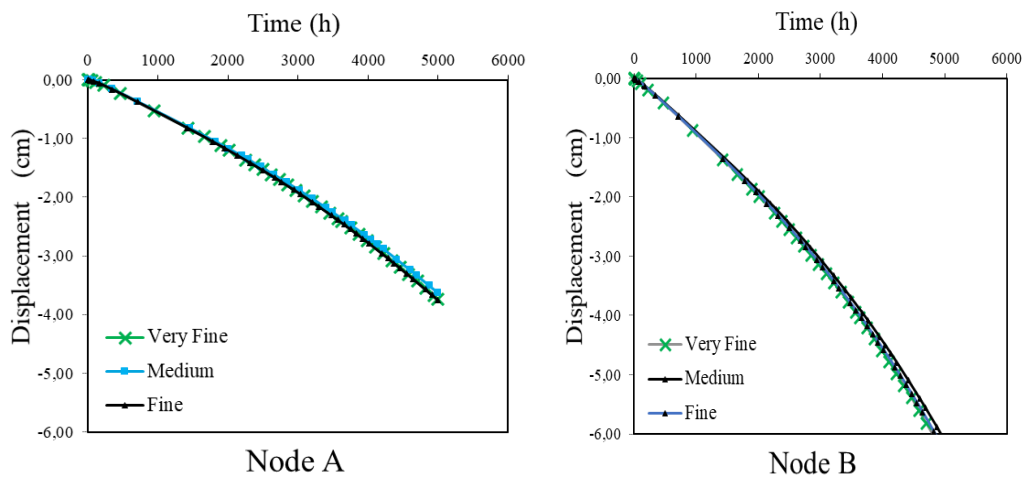
Figure 3.9. Displacement vs. Time in two nodes of the mesh.

Regarding boundary conditions, the same measurements were taken as the soil container used in the centrifuge in the prototype scale. Once the model gets calibrated can be analyzed the influence of these boundary conditions on the results. The horizontal movements in the four boundaries were fixed as well as the vertical displacement at the inferior boundary. Regarding water boundary conditions, the water flow exit was just restricted in the inferior boundary in the phases before the drawdown pore pressure phase.

3.1.3 Stages of analyses

A graphic representation of the centrifuge test stages and their conditions are presented in Figure 3.10, where the time intervals are also specified. The model was analyzed in terms of effective stresses, with drained parameters and initial drained conditions. According to Rodríguez (2011), this analysis type allows obtaining stresses, strains, and displacements before, during, and after the consolidation process.
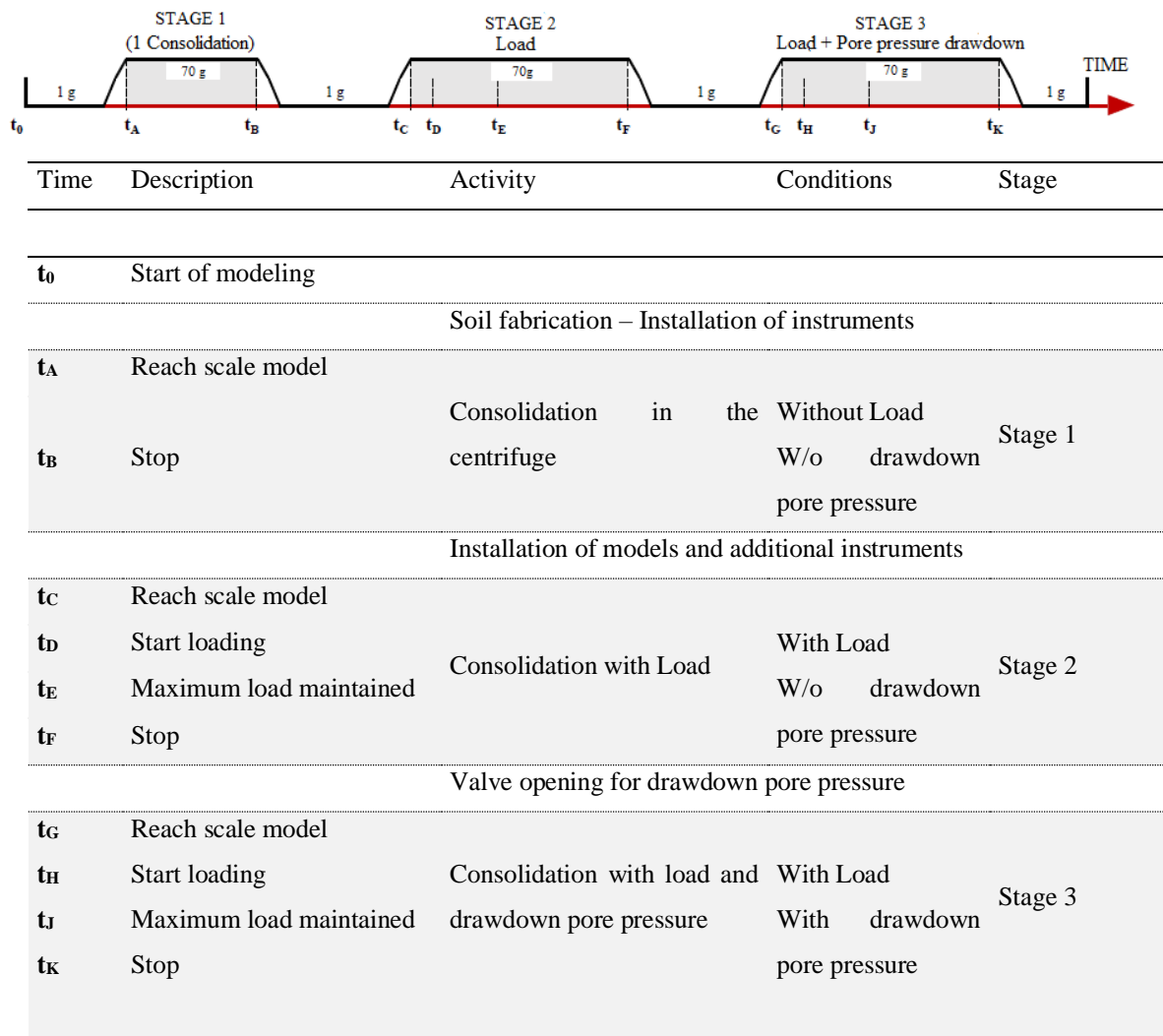
Figure 3.10. Description of the test carried out in the centrifuge and the pore pressure condition in the three stages. Adapted from Rodríguez (2016).

To simulate the centrifuge test, the calculation phases considered are described below:

- *Initial Phase*: corresponds to the stage 1 of Figure 3.10. Here, the initial stress of the soil is generated. This stress state is usually characterized by an initial vertical effective stress. In PLAXIS, initial stresses may be generated by using the K_0 procedure which is a special calculation method to define these stresses, considering the loading history of the soil (PLAXIS, 2018).

- *Phase 1, construction and loading:* in this phase was simulated the construction of the piled raft and the application of the load along the foundation surface in accordance with the Rodríguez (2016) experimental test. A consolidation calculation was used to analyze the

56

development of pore pressure as a function of time. As it is possible to apply load in this analysis, 38,25 kPa were applied in 5000 hours corresponding to the interval time from t_C-t_E of the centrifuge test, Figure 3.10.

- *Phase 2, consolidation:* in this phase, the same analysis was used as in the previous one to represent the interval time from t_E-t_F (Figure 3.10) in which the load has reached its maximum value and is maintained for 8914 hours. Phase 1 and Phase 2 correspond to stage 2 of Figure 3.10.

- *Phases 3 to 6, pore water pressure drawdown:* these phases correspond to the Stage 3 explained in Figure 3.10 in which the drawdown of the pore pressure is generated. Table 3.8 summarizes each of these phases that correspond to a degree of consolidation to be reached in a certain period.

Table 3.8. Description of the phases that simulated the drawdown pore pressure.

Phase	Consolidation degree (%)	Time (hr)
3	20	795.3
4	40	2270
5	60	3813
6	88	6118

3.1.4 Comparison with laboratory results (validation)

In order to calibrate the numerical model, the data of the centrifuge test was used in the comparison. As instrumentation was installed three strain gauges on the soil, three more on the raft, four piezometers, a load cell on the actuator type air spring, and miniature load cells on four of the installed piles. The distribution of the instrumentation was already shown in Figure 3.2. The called Stage 1 in the laboratory test was not modeled since its purpose is the same as the initial phase generated by the software.

3.1.4.1 Phase 1-2, construction and loading (Stage 2)

As was explained in Figure 2.17 and in order to reduce the time of fabrication and flight of the models in the centrifuge, sand layers between two filter papers were used to divide the kaolin layers. In addition to these layers, non-woven geotextile (NT 2000 PAVCO reference) was used as a coating on the container walls to guarantee the continuity of water flow both in the consolidation process in the fabrication and in the flight of the models.

In the numerical model, the profile summarized in Table 3.4 was used, where sand layers were not used because of their small thickness and to be working just as a filter. Due to this reason, it was necessary to find an equivalent coefficient of permeability (k) in order to simulate the drainage required or used in the centrifuge model. The coefficient was calculated with Equation 3.4.1-1 (Matheron, 1967), which allowed an equivalent hydraulic conductivity in a stratified soil with vertical water flow as the one used in the centrifuge container. As the permeability influences the rate of settlement of saturated soil under load, the coefficient of permeability value was modified to get a displacement of both, soil and raft, close to the one registered in the laboratory test.

$$k_{min} = \frac{\sum_{i=1}^{n} di}{\sum_{i=1}^{n} \left(\frac{di}{ki}\right)}$$

(3.4.1-1)

where d: Layer thickness

Since the result obtained with the calculated k_1 did not represent well the laboratory test, different coefficients were used in the numerical simulations in order to obtain a suitable value to give the best fit results (Table 3.9). Figure 3.11 and Figure 3.12 show the results obtained for each of the coefficients. The value chosen was k_3 equal to $2{,}81 \times 10^{-4}$ m/h, which showed not only a good approximation with soil displacement results but also a reasonably good displacement for the foundation system.

Table 3.9. Values of k coefficient used in the numerical simulations.

Coefficient of permeability equivalent, k	(m/h)
k_1	8.07×10^{-6}
k_2	5.2×10^{-5}
k_3	2.81×10^{-4}
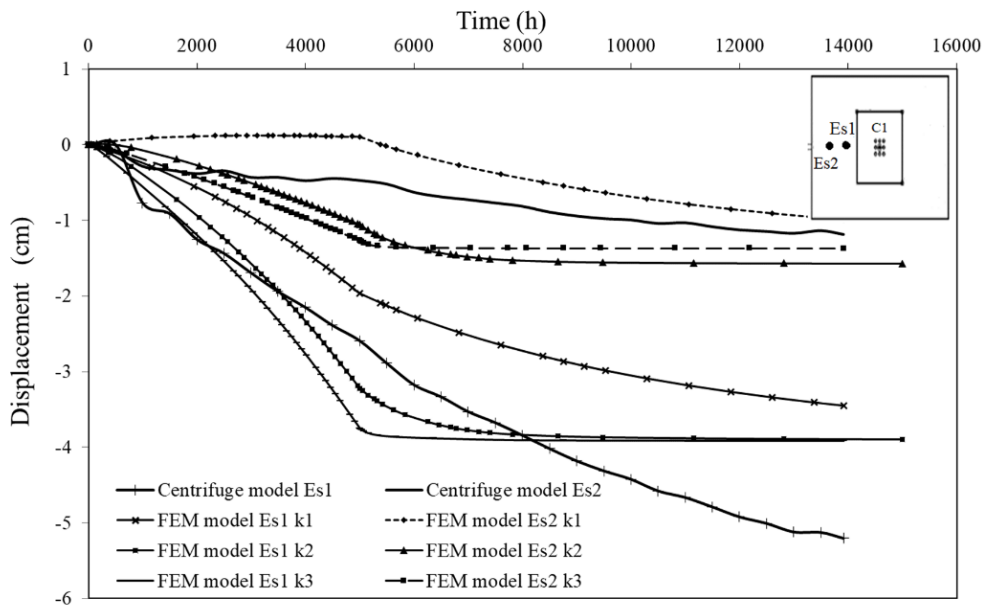
Figure 3.11. Displacements *vs* time curves obtained at point Es1 and Es2 by centrifuge and FEM models for different *k* during Phase 1-2.
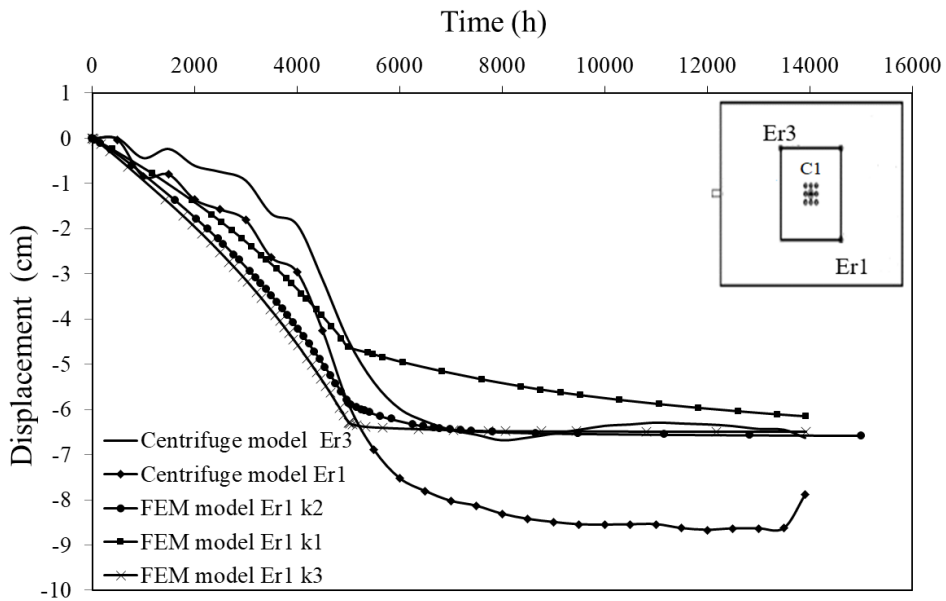
Figure 3.12. Displacements *vs* time curves obtained at point Er1 by centrifuge and FEM models for different *k* during Phase 1-2.

3.1.4.2 Pore pressure drawdown-phase 3-6 (Stage 3)

The piezometer data obtained was measured very close to the filter layers which could not be used to input the exact drawdown of the pore pressure in the numerical model. In the last stage

59

of the centrifuge test, a drawdown pore-pressure was induced, and the soil was brought to an 88% degree of consolidation. To simulate this stage, it was necessary to calculate the curves that show the variation of the degree of consolidation (Uz) with depth (z), called isochrones. At a given time the degree of consolidation at any depth z is defined as:

$$Uz = \frac{excess\ pore\ water\ pressure\ disspated}{initial\ excess\ pore\ water\ pressure} = \frac{\Delta\sigma'}{u0} \tag{3.1}$$

where $\Delta\sigma'$ is the increase of effective stress at a depth z due to consolidation and u_0.

$$u_{i,n+1} = \lambda u_{i-1,n} + (1-2\lambda)u_{i,n} + \lambda u_{i+1,n} \tag{3.2}$$

$$\lambda = C_v \frac{\Delta t}{(\Delta z)^2} \tag{3.3}$$

where Cv: Vertical consolidation coefficient.

The third stage was divided into four parts in the numerical model, where the pore pressures were imposed in order to reach the 20, 40,60, and 88% of degree of consolidation. Using the finite difference method (FDM), and the Equation (3.2), the isochrones presented in Figure 3.13 were obtained.
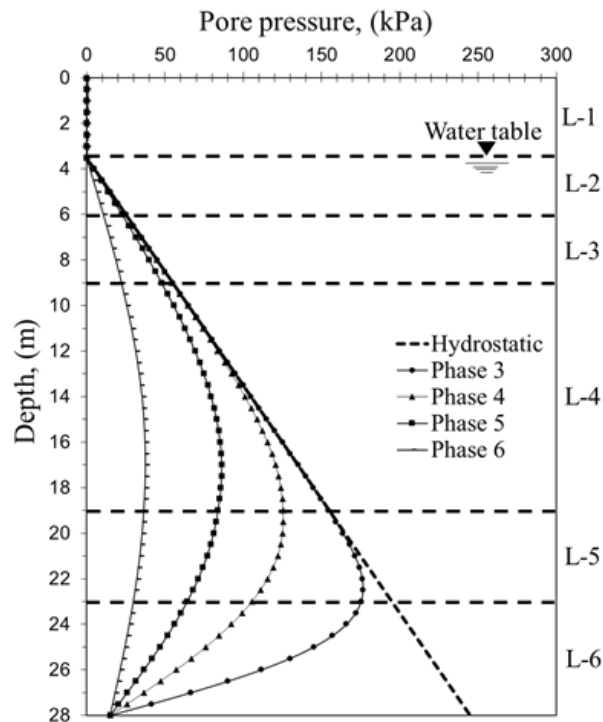
Figure 3.13. Pore water pressure conditions.

3.1.4.3 Comparison of displacements

Once the numerical model was completed, all the centrifuge test was compared. Figure 3.14 shows the displacements of two points on the soil Es1 and Es2 concerning time. In the first stage of the test, the path of both points in the prototype is very close to the ones of the laboratory. For the drawdown pore pressure phase, the results move away slightly although the behavior is the same. The displacements on the foundation system in the model were measured in three corners of the raft, which results are plotted in Figure 3.15. When comparing the model and the FEM, it was observed that the two paths are reasonably close.
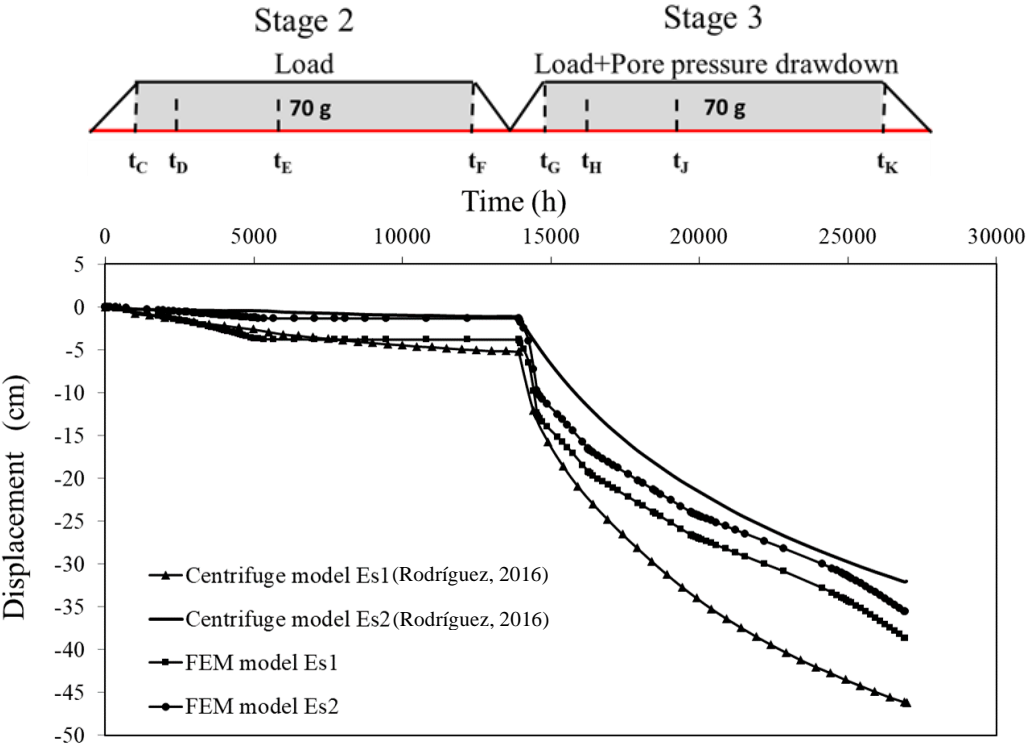
Figure 3.14. Displacements *vs* time curves obtained at point Es1 and Es2 by centrifuge and FEM models.
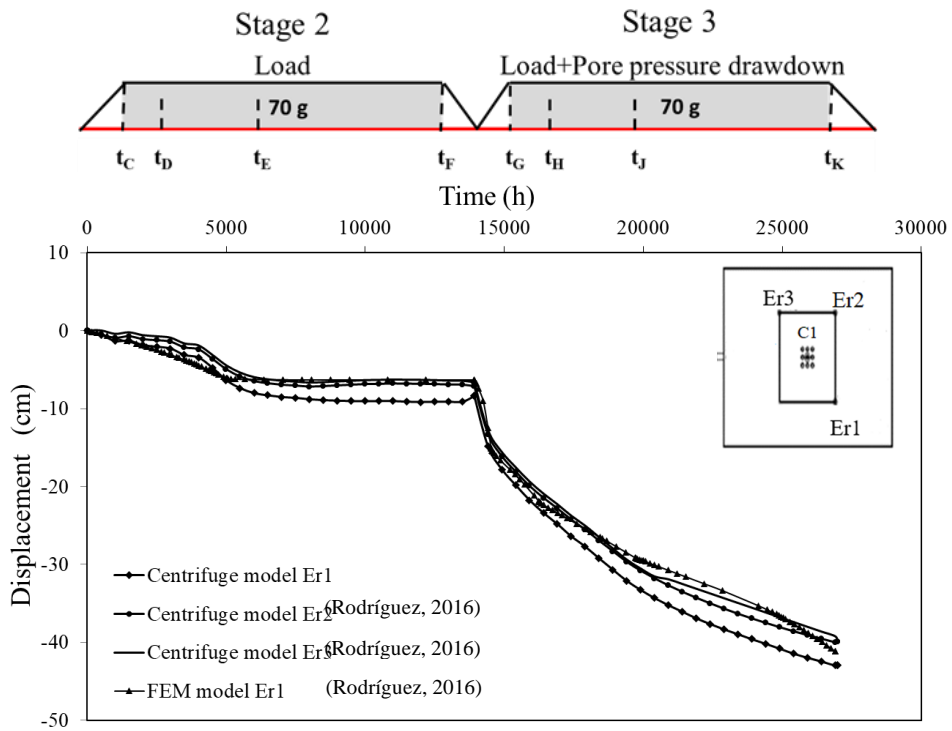
Figure 3.15. Displacements *vs* time curves obtained at point Er1 by centrifuge and FEM models.

Figure 3.16a shows how the piled raft settled more than the soil surrounding it in phase 2 where the load was applied. This difference between the foundation system and the surrounded soil is smaller at the end of phase 6 since it represented the regional subsidence where both suffer large displacements (Figure 3.16b). Already, with the similar results presented of soil and foundation, and the accurate representation of the phenomenon, the model is considered "calibrated" for the centrifuge tests carried out in the laboratory.
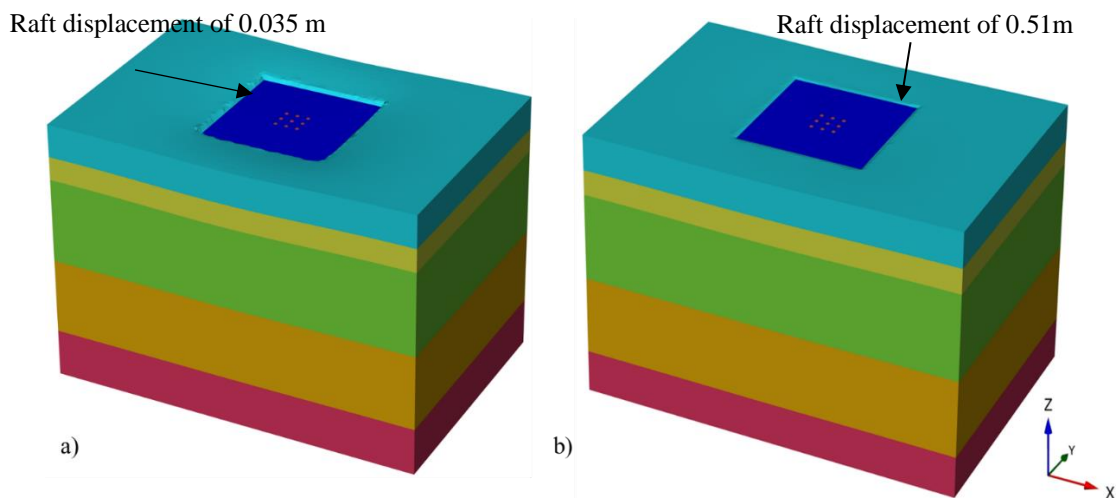
Figure 3.16. FEM model showing the vertical displacements obtained at the end of a) Phase 2 and b) Phase 6

3.1.4.4 Comparison of load distribution

Having the load measured on the top of the piles from the centrifuge, it was considered very important to calibrate the model not only with the displacements but also with the load distribution making the model more accurate. Since the load distribution in the system is one of the main aspects to be assessed, a sensibility analysis of the resistance parameters of the piles was carried out. The values of the shaft and base resistance used to run the FEM model were calculated from the data given by Rodríguez (2016). It should be clarified that the values adopted in the initial numerical model ($FEM_{100\%}$) do not represent the "real" resistance of the piles in the centrifuge model. Nonetheless, it was used as an estimate to perform this analysis. Table 3.10 presents two different simulated cases, the first one ($FEM_{50\%}$) with 50% of the resistance used in the $FEM_{100\%}$ and the second ($FEM_{25\%}$) with just 25 %.

Table 3.10. Shaft and Base pile resistance used in the analysis of sensibility

	Shaft Resistance (kN/m)	Base Resistance (kN)
$FEM_{100\%}$	57	345
$FEM_{50\%}$	28.5	172.5
$FEM_{25\%}$	14.25	86.25

In order to compare and analyze the behavior of the simulations, the Filling Factor (FF) to establish the proportions of load assumed by both piles and the raft was calculated. (Equation 2.1-1). According to the graph presented by Mandolini et al. (2013) (Figure 2.2), for model M3 the percentage of load taken by the raft is 60. This percentage is close to the laboratory results, which gives a good prediction of the behavior of the system.

Table 3.11 presents the variation of the load distribution, comparing the results from the centrifuge with the numerical analysis in both stages. In this case, it is observed how the resistance parameter in the interface is highly sensitive, which directly influences the way load is received by the foundation. When shaft and base resistance is reduced by 25 %, the numerical results match with the centrifuge ones quite well in stage 2. On the contrary, for stage 3, both results are the opposite, and this may be due to problems that present the embedded pile element. The FEM results showed that this element does not take into account the change of

resistance in the soil-pile interface that occurs when the soil passes through a process of consolidation over time. This problem can be mitigated using volume elements. However, it was not an option since, as was explained previously, these elements generate a computational time much higher than the model that is currently used.

Table 3.11. Sensibility analysis of the pile resistance parameters. Comparison between three different cases with FEM and the centrifuge results

Load Distribution	Centrifuge		FEM$_{100\%}$		FEM$_{50\%}$		FEM$_{25\%}$	
	Stage 2	Stage 3	Stage 2	Stage 3	Stage 2	Stage 3	Stage2	Stage 3
Raft (%)	77	54	11	-8	38	37	73	77
Piles (%)	23	46	89	108	62	63	27	23

3.2   Experimental work

Having not enough information to calculate the parameters for the HSM, it was important to conduct laboratory tests that would allow getting the extra data needed. The new tests were carried out using the facility at the University of Los Andes Geotechnical Models Laboratory in Colombia. Two-cylinder containers with soil were prepared. In the first one, three samples of each layer (Figure 2.17) were taken to carry out drained triaxial tests, and consolidation tests were also conducted for each layer. The second container was used to perform a load pile test in the centrifuge with 70g to get the pile resistance parameters.

3.2.1   Soil manufacturing process

Even using a container with different dimensions for practical reasons, the soil manufacturing process was carried out as presented by Rodríguez (2016), since it was tried to reproduce the work in the most precise way. The soil was fabricated in a cylindrical container with an inner diameter of 30 cm and 60 cm in height. As presented in Figure 2.17, the experimental soil represented a clay of variable resistance at depth, from 10 kPa on the surface to 40 kPa at the bottom layer. The soil manufacturing process in the geotechnical centrifuge cast consists of establishing a relation between the vertical stress applied to the soil and the undrained shear strength, evaluated through a mechanical method. Table 3.12 summarizes the soil manufacturing conditions for each layer.

Table 3.12. Quantities and conditions applied in the manufacture of the soil in three layers.

Layer	Theoretical undrained shear strength (kPa)	Average undrained shear strength in layer (kPa)	Vertical stress applied (kPa)	Load applied (kN)	Kaolin dry weight (N)	Weight of water added (N)
1	10 – 20	15	170	12	79.5	103.8
2	20 – 30	27	276	19.5	85.5	111.6
3	30 – 40	38	382	27	90.2	117.8

Next, the steps of this process for the three layers of soil will be briefly presented:

- The kaolin was mixed with an amount of water necessary to obtain 1.5 times its liquid limit using a mechanical mixer for a time average of 30 minutes to ensure mixture uniformity (Figure 3.17);

Figure 3.17. Mixing process of kaolin with water

- At the base of the cylinder cast and on the walls a geotextile was placed. Also, a layer of sand, filter type, was placed on the bottom to ensure drainage (Figure 3.18);

Figure 3.18. Placement of geotextile and the bottom sand layer**.**

- A non-woven geotextile was placed on the sand layer to prevent kaolin from escaping and allowing water to flow. Above the geotextile, the prepared mixture of kaolin and water (slurry) was placed and homogenized. On the homogenized and leveled material, the lateral geotextile was folded encapsulating the mixture (Figure 3.19);

Figure 3.19. Mixture cover with geotextile

- After the mixture was covered with the geotextile, a lid was placed over which the determined load according to the layer level was applied (Figure 3.20);
- The sample was consolidated with different stresses values. The consolidation process was controlled by the Taylor method, aiming to achieve at least 90% of the total consolidation;
- Sand filters were put between layers;

- The steps aforementioned were repeated for the other two layers;

Figure 3.20. Loading with a hydraulic jack.

- During the process of manufacturing the soil, the containers were connected to an external water tank. The function of the tank was to maintain a constant level of external water to ensure pore pressure in the lower sand layer

-

- Also, vane tests were conducted at different depths (Figure 3.21).

Figure 3.21. Vane test

3.2.2   Laboratory tests

Once the soil was fabricated, undisturbed samples were taken at different depths (Figure 2.17) from one of the containers. After extruding, the samples were cut into 100 mm high sections, covered with wax and paraffin, and stored. These were used for the triaxial tests. For the Oedometer tests, the samples were extruded from the tubes and used directly (Figure 3.22 and Figure 3.23).

Figure 3.22. Container and extrusion of samples.

Figure 3.23. Samples from each layer

Figure 3.24 and Figure 3.25 show the development of the oedometer test and the results of the three samples L1, L2, and L3, respectively.
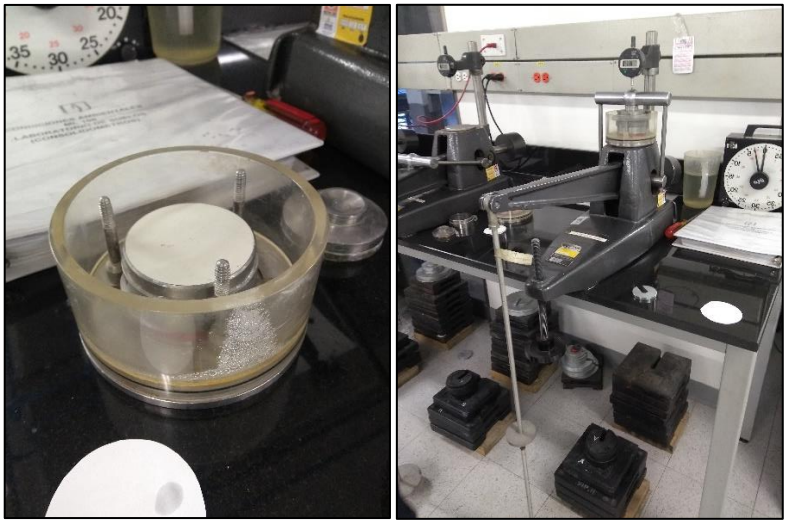
Figure 3.24. Oedometer test
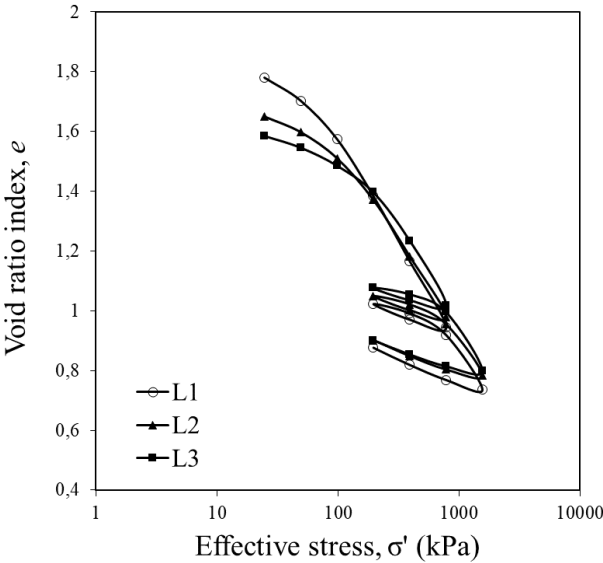
Figure 3.25. Oedometer test results from the layers L1, L2, and L3.

Taking into account that the numerical analysis was done with drained parameters, three isotropically drained consolidated triaxial tests (CID) were conducted at the different layers of the soil profile, L1 to L3. Figure 3.26 and Figure 3.27 show the fabrication of the test samples and the equipment used. Figure 3.40 presents the triaxial test data obtained.
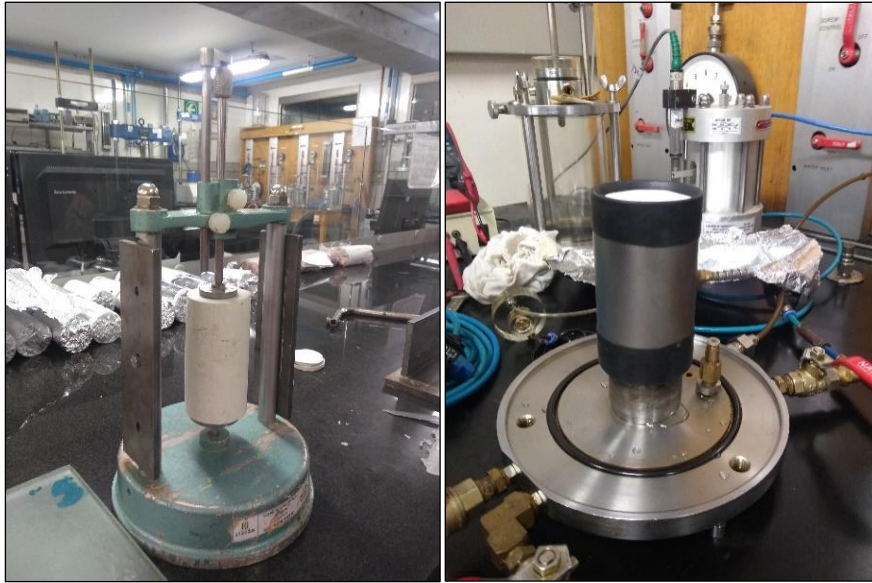
Figure 3.26. Samples fabrication for the triaxial tests

Figure 3.27. The three triaxial equipment
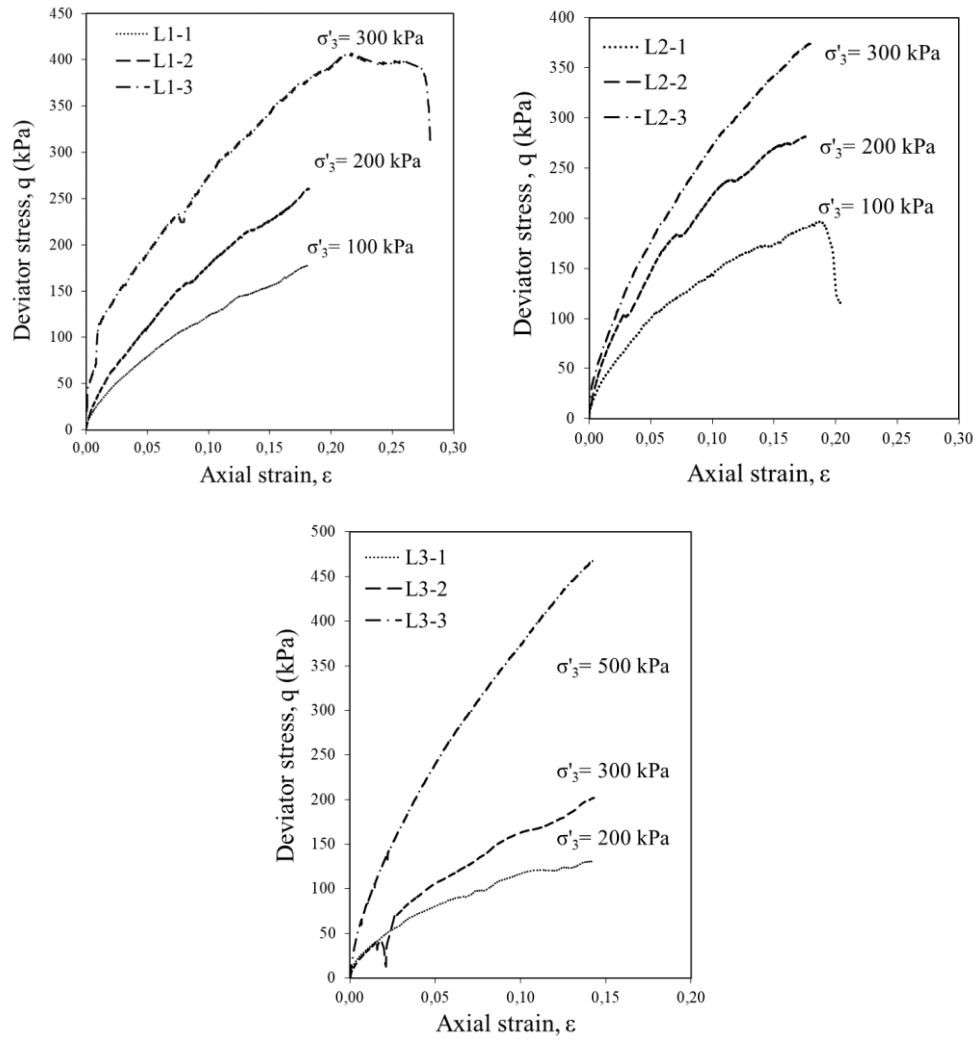
Figure 3.28. CID triaxial test results for layers L1, L2, and L3.

3.2.3 Pile load test in the centrifuge

In order to find the input parameters of the pile needed for the numerical model, it was possible to perform a pile load test on an isolated pile in the centrifuge. The centrifuge used corresponds to a medium scale equipment for the international standards and its characteristics are presented in Table 3.13 and Figure 3.29.
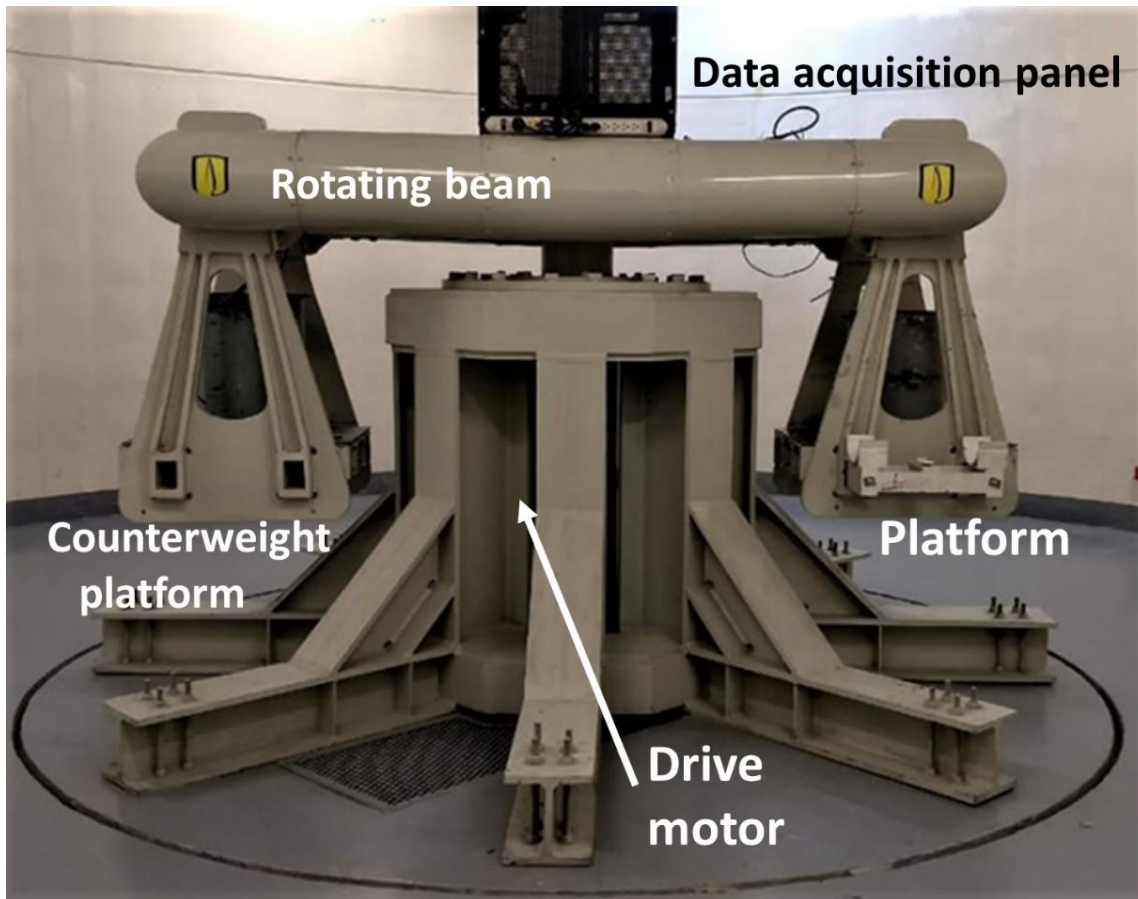
Figure 3.29. Geotechnical centrifuge of The Andes University.

Table 3.13. Geotechnical centrifuge characteristics

Turning radius	1.90 m
Model boxes dimensions	40 cm x 50 cm x 50 cm
Gravitational field maximum	200 g
Maximum model weight	400 kg
Nominal power	400 HP
Channels for data acquisition	50 approx.

3.2.3.1 Instrumentation

The instrumentation of the tests consisted of a pair of miniature rigid load cells, a pair of flexible load cells and an LVDT linear displacement transducer. The instrumentation used is presented below.

- *Linear variable differential transformer (LVDT)*

LVDT is a type of electrical transformer that allows measuring the linear displacement through coils. It was used to measure the pile settlements during the tests with a reading capacity between 1-5cm (Figure 3.30).
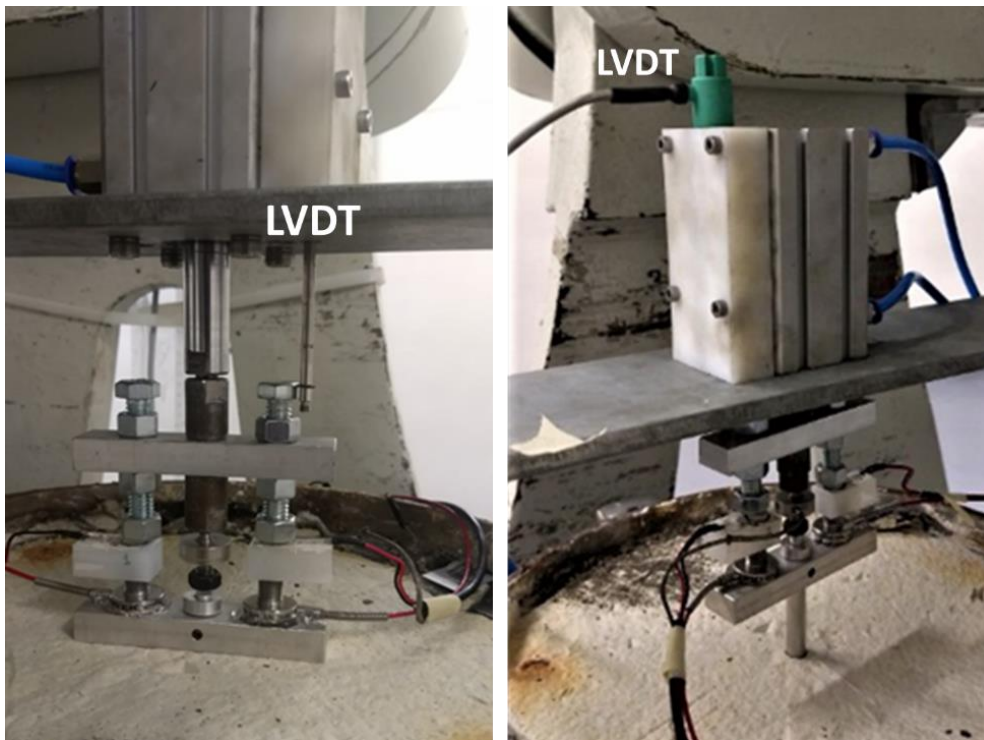
Figure 3.30. LVDT.

The LVDT displacement transducer was installed next to the CP10 pneumatic actuator manufactured by the MICRO company. The instrument calibration was performed in the centrifuge basket, using aluminum plates with known thicknesses that were previously determined using a micrometer. A photo of the calibration process can be seen in Figure 3.31.

Figure 3.31. Calibration setup in the centrifuge.

- *Load cells*

Three types of load cells were used as listed in Table 3.14.

Table 3.14. Load cells. Adapted from Rodríguez (2016)

Type	Details	Use	Main characteristics*
LCM200 FUTEK		To measure the shaft load	Capacity: 113, 225 and 450 kg Diameter: 2.3 cm Error: ± 1%
LCM300 FUTEK		To measure the pile head load	Capacity: 25, 45, 113, 225 and 450 kg Diameter: 3.7 cm Error: ± 3%
A301@25 FLEXIFORCE		To measure the pile shaft load	Capacity: 0.4kN Diameter: 0.9 cm Error: <±3%

* Data obtained from the manufacturer's catalogs.

As shown in Figure 3.32, the Futek LCM 200 and LCM 300 load cells were calibrated in the geotechnical centrifuge basket itself, using metallic disks of known weight. Calibration was performed with maximum loads of approximately 60 N as can be seen in the calibration curves presented in the Appendix B.

Figure 3.32. Assembly for the calibration of Futek load cells.

Figure 3.33 shows the Flexiforce A301 flexible load cells used to determine lateral friction forces in the model. To have a completely horizontal and rigid base for the flexible load cells, rectangular plastic bases were built that also facilitated the calibration process and the test execution process. Calibration was also performed with known masses as shown in Figure 3.34.
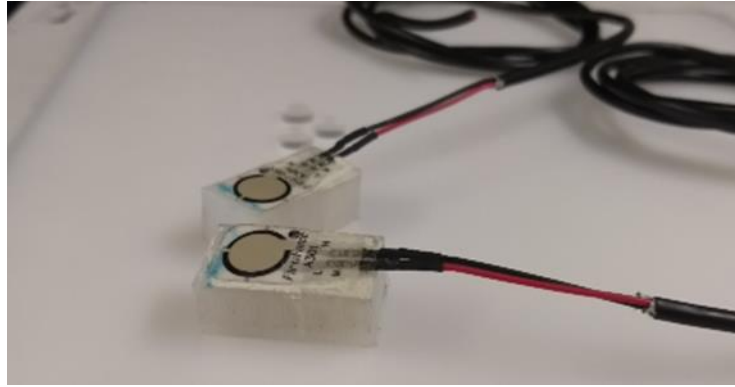
Figure 3.33. Flexiforce load cells.
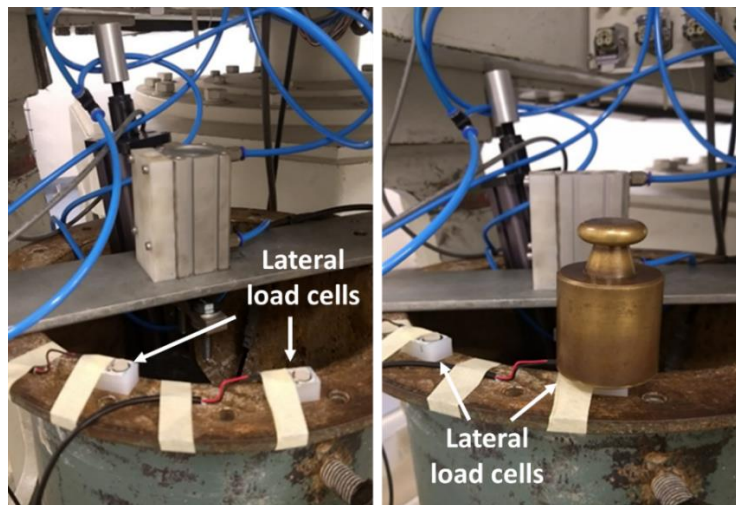
Figure 3.34. Assembly for the calibration of Flexiforce load cells.

3.2.3.2 Pile load test results

The pile shaft and base resistance were needed as input parameters for the element that would numerically simulate the pile. The pile was made of an aluminum bar with a 6 mm diameter and Young's modulus of 70GPa. The outer diameter of the instrumented pile was 10 mm with 400 mm of length. The applied axial load was monitored by a central load cell, and four extra lateral load cells were used to measure the axial load transfer along the pile shaft during the tests. Also, a linear variable differential transformer (LVDT) was used to measure the pile settlements during the test (Figure 3.35).
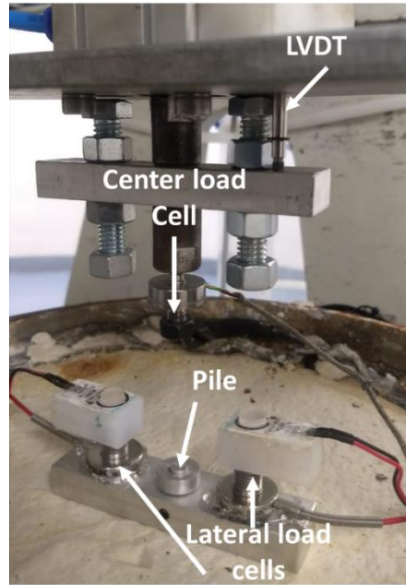
Figure 3.35. Centrifuge model assembly and instrumentation.

The pile installation was carried out at lg at a jacking rate of about 0.5 mm/s (Figure 3.36). After completing model preparation and a final check, the container was transferred to one of the two swinging platforms of the centrifuge (Figure 3.37). The two platforms were then spun up to 70g. This model was tested in two stages: first, without loading the pile till stabilization of the readings so to guarantee the adherence of the pile shaft with the soil; and second, with the subsequent development of the load test. In general, each load increment was held until the cells had reached their steady-state condition before another load increment was further applied. After stopping the centrifuge, vane tests were conducted at different depths to check on the undrained shear strength (Figure 3.38).
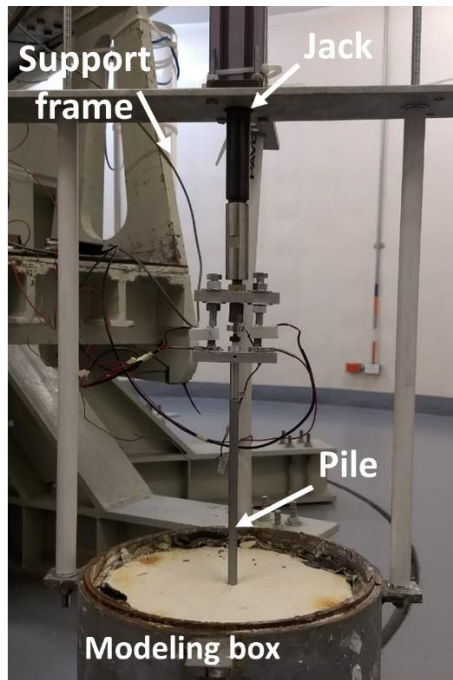
Figure 3.36. Centrifuge model assembly and instrumentation.

Figure 3.37. Container in the centrifuge platform.
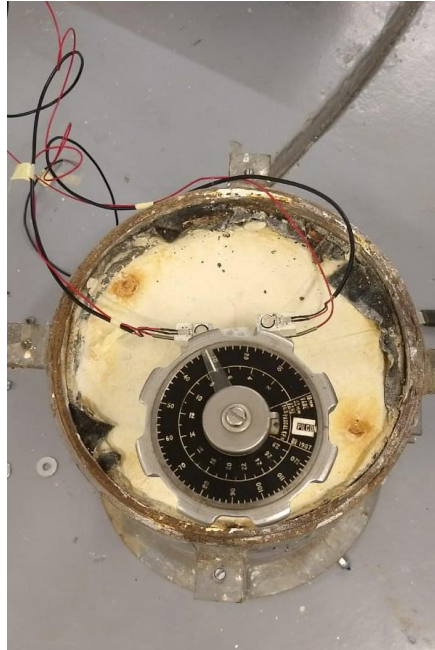
Figure 3.38. Vane tests.

The load and displacement data are shown in Figure 3.39. Test results are expressed in the prototype scale unless stated otherwise. The maximum applied load was 539 kN. Table 3.15 presents the input parameters that were needed for the model, in terms of pile shaft and base resistance for long-term behavior. It was observed that the pile-soil adherence is low, which has consequently generated a significant displacement of the pile.
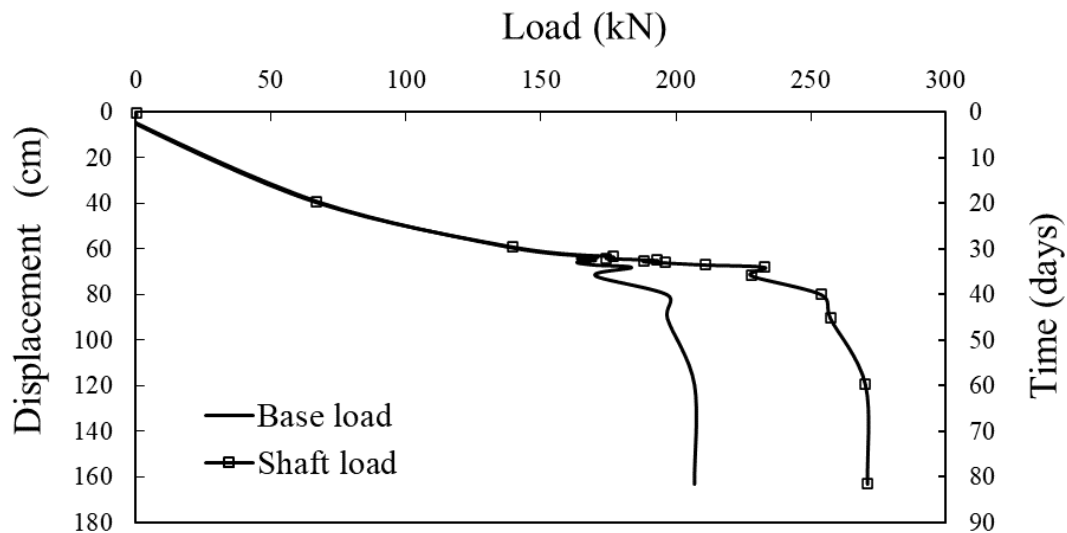
Figure 3.39. Displacement and time *vs* load curves.

Table 3.15. Parameters of the pile

Parameter		
Axial skin Resistance	11.38	kN/m
Base Resistance	205	kN

3.3 Numerical model calibration

To numerically reproduce the behavior of a pile raft foundation system, the mechanical parameters of the HSM were calibrated from the experimental test. In this way, it was possible to experimentally determine the behavior of the soil in a different stress state.

3.3.1 Parameters from laboratory tests

The methodology used to calculate the parameters was the one suggested by Surarak et al. (2012) and Rodríguez-Rebolledo et al. (2019). The results of the oedometer and triaxial tests are presented below.

3.3.1.1 Oedometer tests results

The oedometer tests were conducted on three samples at different layers of the fabricated soil labeled L1, L2, and L3 (Figure 2.17). Table 3.16 shows the values of the reference oedometer modulus (E_{oed}^{ref}, $E_{ur,oed}^{ref}$) and the parameter that defines the dependency level of the strains on the stress state (m), obtained from Figure 3.40.

Table 3.16. Parameters calculated from oedometer tests.

Layer	E_{ur}^{ref} (kPa)	m	E_{oed}^{ref} (kPa)	m
L1	4,976	1.13	830	0.99
L2	6,164	1.08	1,347	0.82
L3	7,707	0.91	2,214	0.5
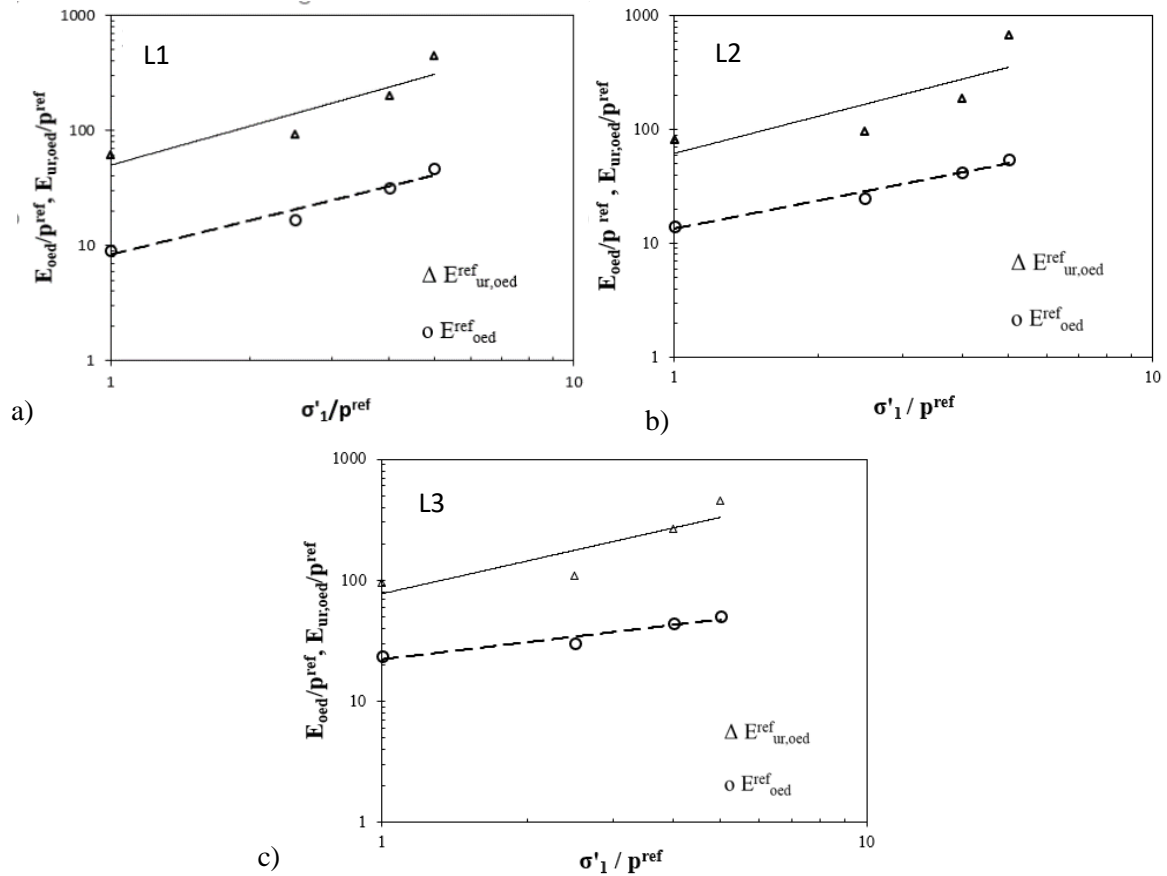
Figure 3.40. Oedometer Modulus vs consolidation pressure calculated from one-dimensional consolidation tests: a) Layer L1, b) Layer L2 and c) Layer L3.

3.3.1.2 Triaxial tests results

Three isotropically drained consolidated triaxial tests (CID) were conducted at the three different layers (Figure 2.17). The confining pressures σ_3 used for the L1 and L2 samples were 100, 200, 300 kPa, and for the L3, σ_3= 200, 300, and 500 kPa. The friction angle (φ') obtained were 25°, 22°, and 18°; whereas, the cohesion (c') was 21, 40,1 kPa, respectively. The reference modulus at 50% of strength (E_{50}^{ref}) and power m determined from the CID tests using double log scale plots are given in Figure 3.41. These values are summarized in Table 3.17.
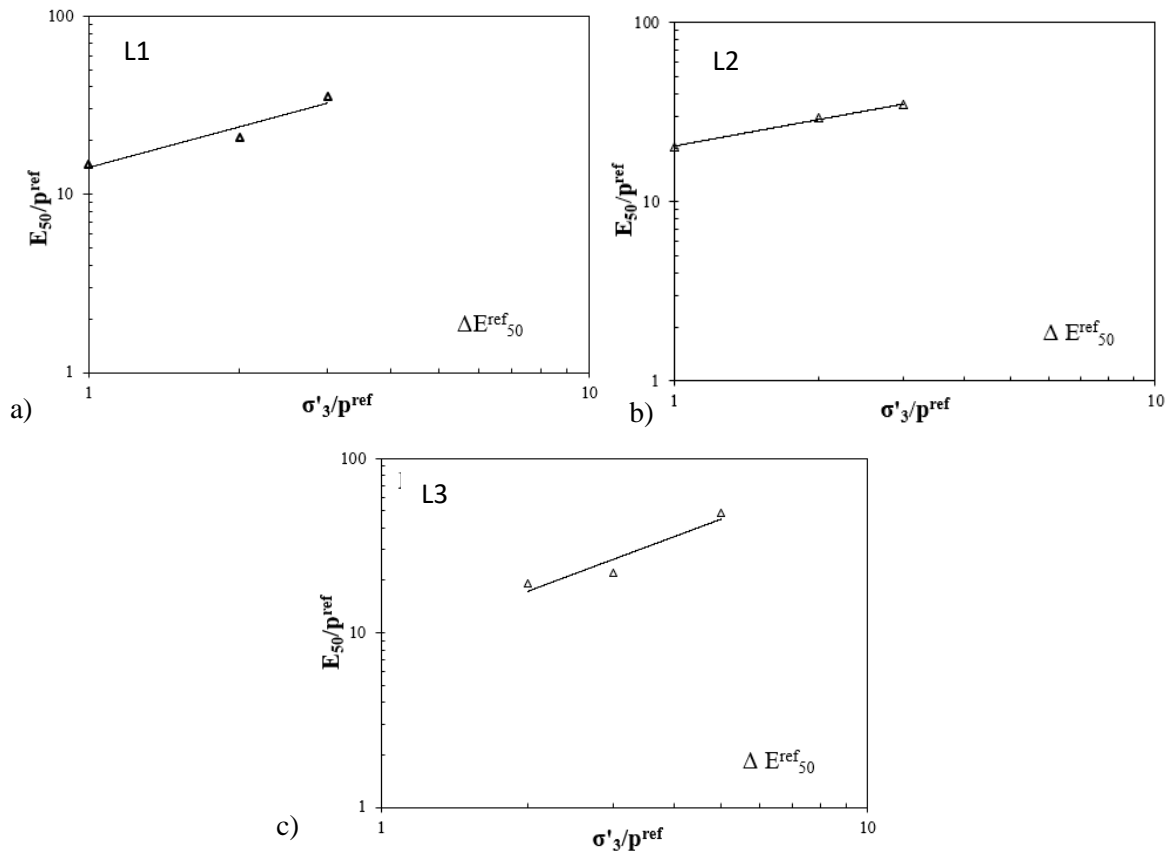
Figure 3.41. Variation in E_{50} with confining pressure: a) Layer L1, b) Layer L2 and c) Layer L3.

Table 3.17. Parameters calculated from triaxial tests.

Layer	E_{50}^{ref} (kPa)	m	ϕ' (°)	c' (kPa)
L1	1,413	0.8	25	21
L2	2,044	0.5	22	40
L3	843	1	18	1

3.3.2 Soil parameters calibration

To calibrate the soil parameters listed in Table 3.16 and Table 3.17, the CID triaxial and oedometer tests were modeled again using the *SoilTest* tool. The results from the three layers reveal good agreements among all the stress-strain and stress path behavior for different confining pressure values ($\sigma3 = 100$, 200, and 300 kPa). Although the L3 layer results calculated

from PLAXIS were not as successful as those of the L1 and L2 layers, since they were underestimated for the confining pressure of 500 kPa, it can be stated that the HSM predictions agree reasonably well with the triaxial test results. To obtain suitable parameters to give the best fit results, the input parameters were adjusted, as is presented in Figure 3.42, Figure 3.43, and Figure 3.44 for layers L1, L2, and L3, respectively. The results from the three layers reveal good agreements among all the stress-strain and stress path behavior for different confining pressure values ($\sigma 3 = 100$, 200, and 300 kPa).

Although the L3 layer results (Figure 3.44) calculated from PLAXIS were not as successful as those of the L1 (Figure 3.42) and L2 (Figure 3.43) layers, since they were underestimated for the confining pressure of 500 kPa, it can be stated that the HSM predictions agree reasonably well with the triaxial test results.

a)

b)

c)

83
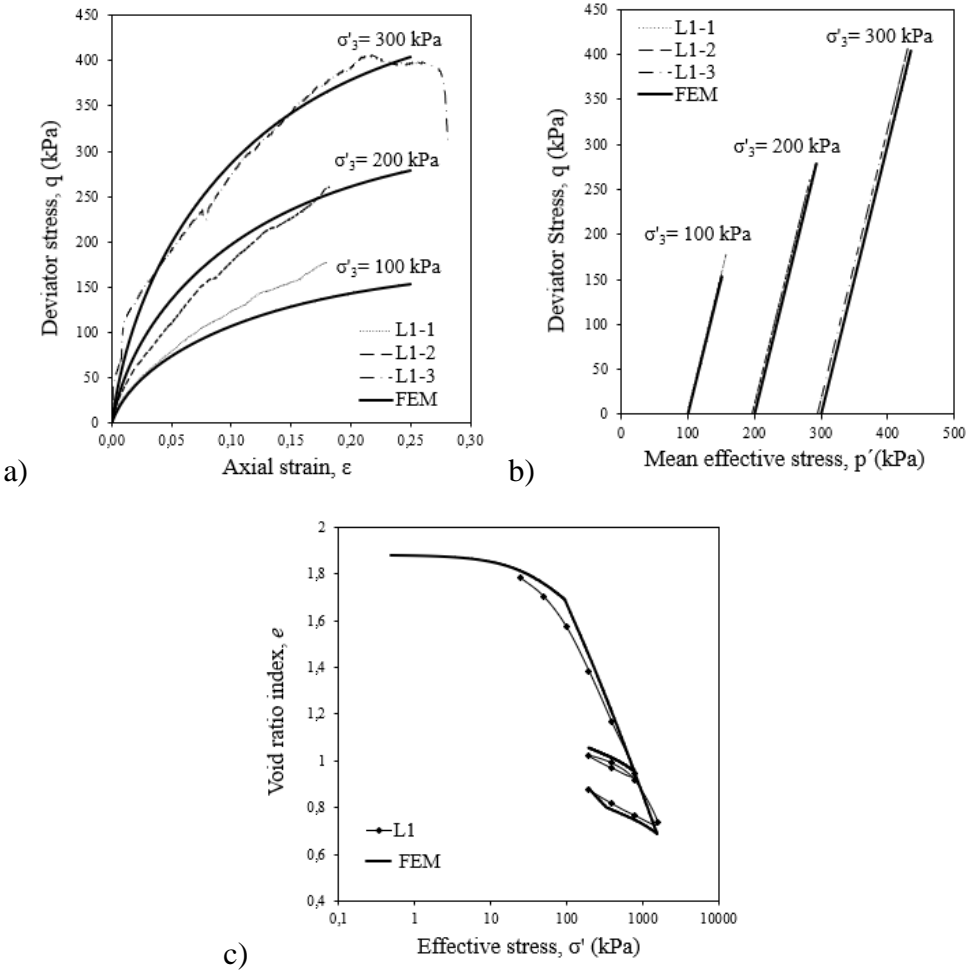
Figure 3.42. CD triaxial and oedometer test results and their FEM simulations with HSM: a) Deviator stress vs axial strain (*q* vs. *ε*), b) Deviator stress vs Mean effective stress (*q* vs. *p′*), c) Void ratio index vs effective stress (*e* vs. *σ′*) of L1 layer.

a)

b)

c)
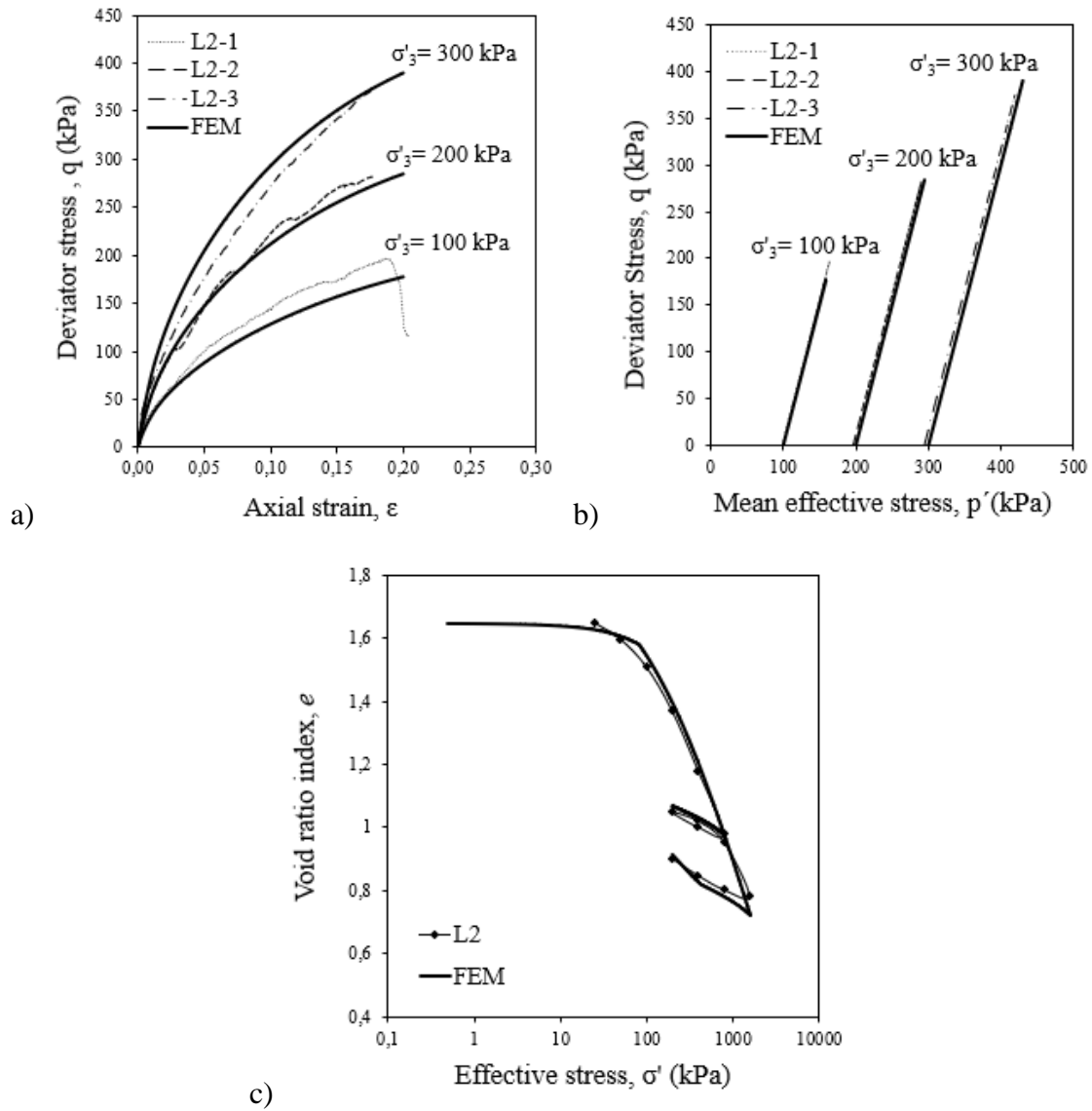
Figure 3.43. CD triaxial and oedometer test results and their FEM simulations with HSM: a) Deviator stress vs axial strain (*q* vs. *ε*), b) Deviator stress vs Mean effective stress (*q* vs. *p′*), c) Void ratio index vs effective stress (*e* vs. *σ′*) of L2 layer.
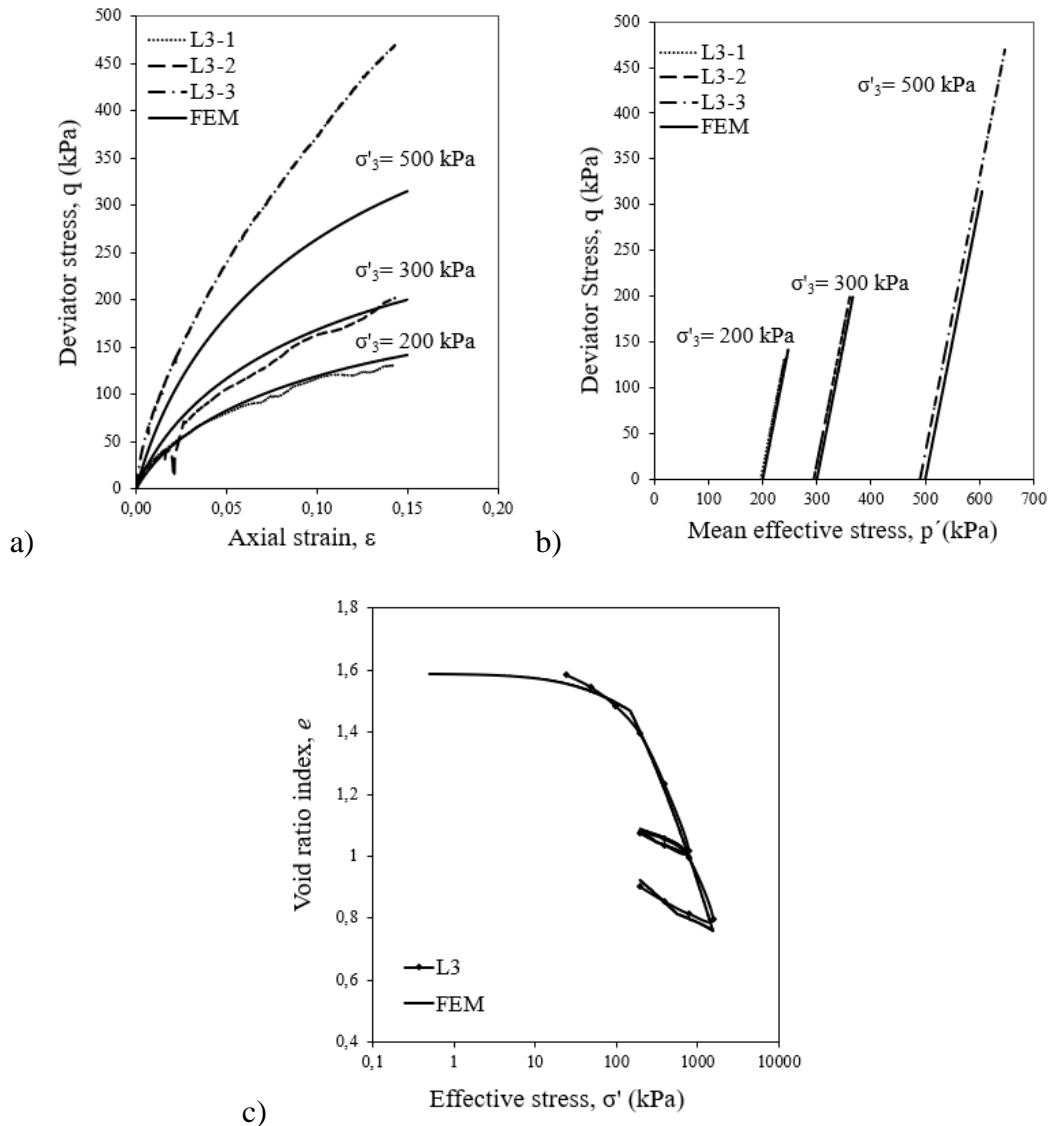
Figure 3.44. CD triaxial and oedometer test results and their FEM simulations with HSM: a) Deviator stress vs axial strain (*q* vs. *ε*), b) Deviator stress vs Mean effective stress (*q* vs. *p'*), c) Void ratio index vs effective stress (*e* vs. *σ'*) of L3 layer.

3.3.3 Validation of the new proposed geotechnical model

The geotechnical parameters calibrated for the different soil layers needed for the new numerical simulations are shown in Table 3.18. The mesh of the new model is presented in Figure 3.45, and the parameters that were obtained from the centrifuge test are summarized in Table 3.19. The equivalent coefficient permeability used for this new model was initially calculated in item 3.1.4.1.

Table 3.18. Geotechnical parameters of the soil profile.

Layer		Z m	γ kN/m³	σ'_0 kPa	σ kPa	σ_P kPa	c' kPa	ϕ °	k_0	k_0^{nc}	E_{50}^{ref} MPa	E_{ur}^{ref} MPa	E_{oed}^{ref} MPa	m	v	OCR
	SL1	0 - 3.5	18.67	10	28	170	11.5	28	1.24	0.53	9.5	30	12	1	0.2	6.07
L1	SL2	3.5 - 6	16.68	30	75	170	21	25	1.2	0.58	1.41	10	1	1	0.2	5.66
	SL3	6 - 9	16.68	50	125	191	21	25	0.97	0.58	1.41	10	1	1	0.2	3.39
L2	SL4	9 - 19	17.03	81	200	223	20	22	0.92	0.62	2.4	15	1.55	1	0.2	2.77
L3	SL5	19-23	17.03	141	342	342	20	17	0.74	0.71	2.5	16	1.58	0.8	0.2	1.27
	SL6	23-28	17.03	176	425	382	20	17	0.69	0.71	2.5	16	1.58	0.8	0.2	1.01
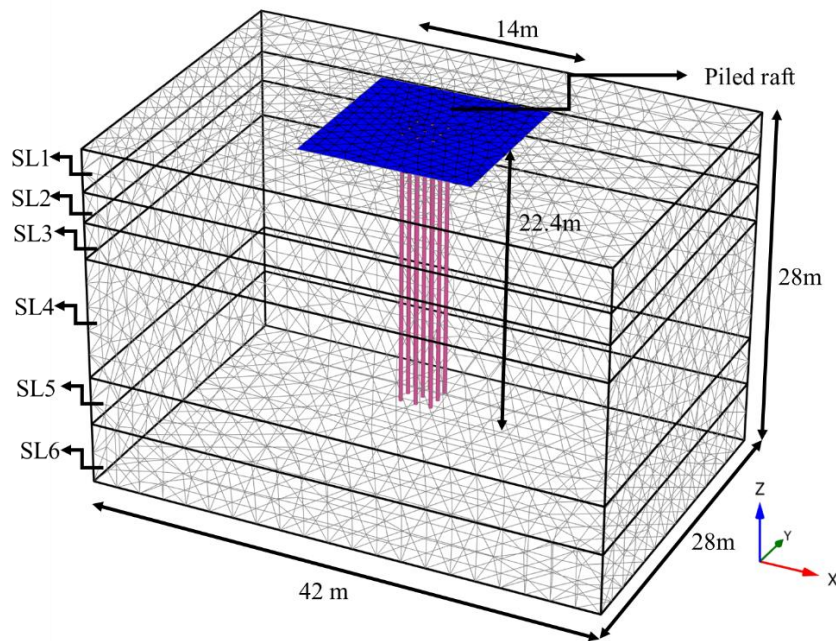
Figure 3.45. Geometry and mesh of the new 3D model developed in PLAXIS.

Table 3.19. Main properties of the embedded beams

Element	Parameter	
	Unit weight	25 kN/m³
	Diameter	0.63 m
Embedded beams (Piles)	Young's modulus	30000 MPa
	Length	22.4 m
	Axial skin Resistance	11.38 kN/m
	Base Resistance	205 kN

3.3.3.1 Comparison of displacements

The displacement-time curve for the piled raft foundation, under vertical loading and pore pressure drawdown, obtained from the centrifuge test are presented along with the results obtained from FEM. Figure 3.46 shows the displacements measured of a point on the soil Es1 with respect to time. In the first stage of the test, the results in the prototype are very close to the one from the laboratory. Regarding the drawdown pore pressure phase, the results move away slightly, although the behavior path is the same.

The displacements on the foundation system in the model were measured in three corners of the raft labeled Er1, Er2 and Er3. The comparison results are plotted in Figure 3.47. The centrifuge model results measured in the three corners of the raft were slightly different; this can be due to a possible uneven load application that shows the not equal distribution of it. When comparing the model and FEM results, it was observed that the two paths are quite close. Already, with the similar results presented of soil and foundation, and the accurate representation of the phenomenon, the numerical model could be considered "calibrated" for the centrifuge tests carried out in the laboratory.
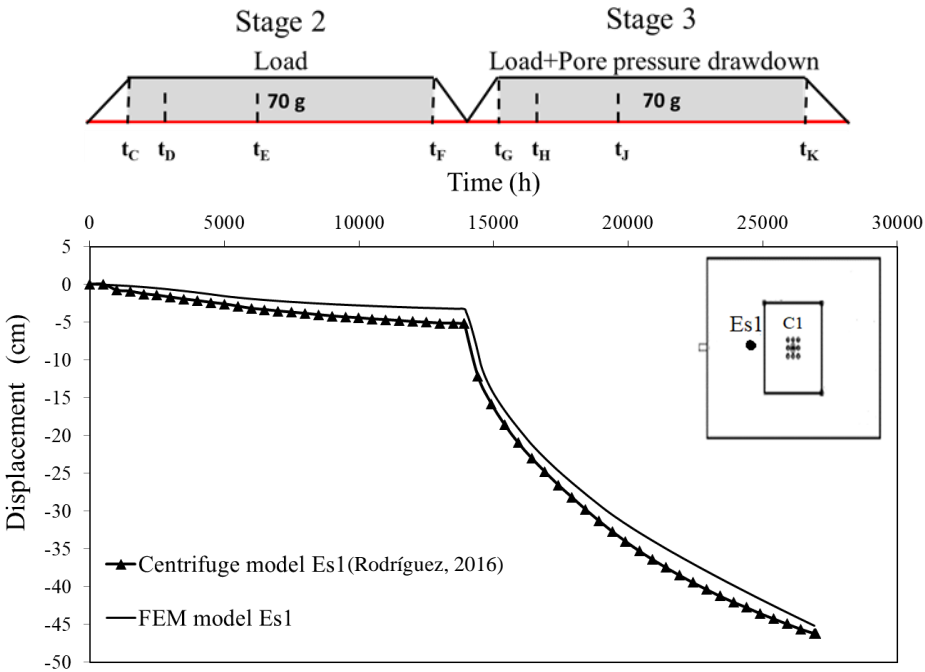
Figure 3.46. Displacements *vs* time curves obtained at point Es1 by centrifuge and FEM models.
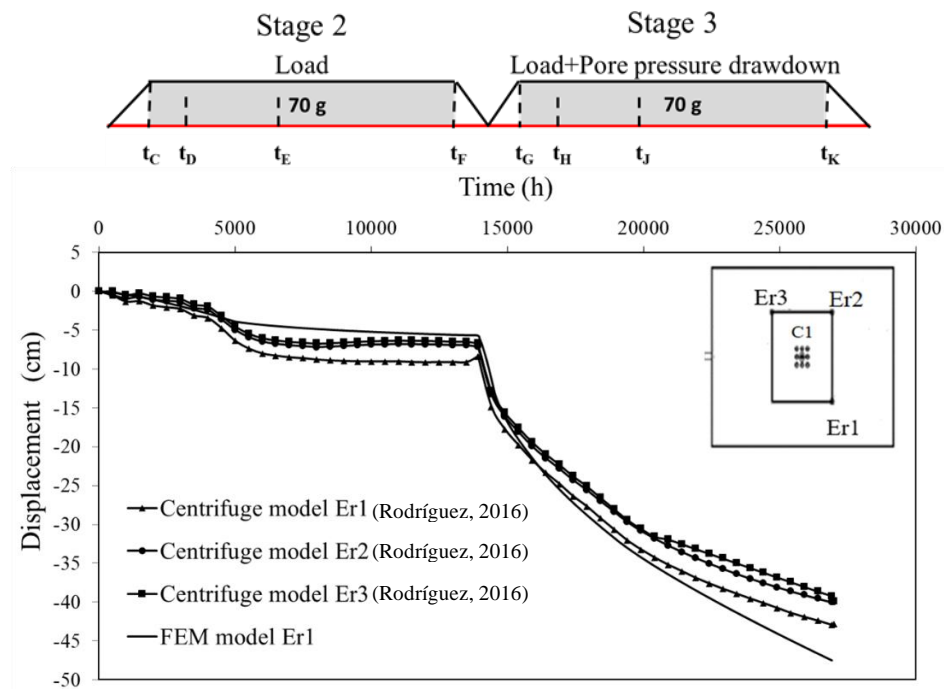
Figure 3.47. Displacements *vs* time curves obtained at raft corner points Er1, Er2 and Er3 by centrifuge and FEM models.

3.3.3.2 Comparison of load distribution

The proposed model showed poor results compared to the laboratory ones when using a calculated theoretical shaft and base pile resistance. In consequence, it was carried out a single pile load test in the centrifuge explained already in detail in item 3.2.3. The new results from the numerical analysis were favorable for stage 2 since they fit with the centrifuge data. Unfortunately, for stage 3 the percentage of load taken by the piles decreased by almost half compared with the stage 2 results. To overcome this problem, the input parameters for this element in stage 3, were adjusted in order to the best fit results when compared with centrifuge data (Table 3.20).

Table 3.21 and Figure 3.48 presents the variation of the load distribution between piles and raft, comparing the centrifuge test results with the numerical analysis (FEM) in both stages. The differences in the load data in the piles, mainly in stage 3, for both models, it is due to the boundary conditions as the model has a rectangular geometry (Figure 3.45). It means that for pile 6 the border condition is much farther than for pile 2, making having a greater mass of soil around it. Consequently, when soil is consolidated by the drawdown pore pressure, it transmits a greater load to the pile 6 than to the 2 that has less amount of soil around it. For stage 2, the

difference between the load measured values and the FEM were 22% and 6% for the piles and raft, respectively. These differences are smaller in stage 3, being 4% for both elements. The FEM results of the present work are in reasonably good agreement with the measured results in the centrifuge test, which means that the numerical model is calibrated.

Table 3.20. Embedded beams modified parameters.

Element	Parameter	Phase 3-6
Embedded beams (Piles)	Axial skin Resistance	40.72 kN/m
	Base Resistance	713 kN

Table 3.21. Comparison between centrifuge and FEM load values measured on the pile head in each of the stages of the test.
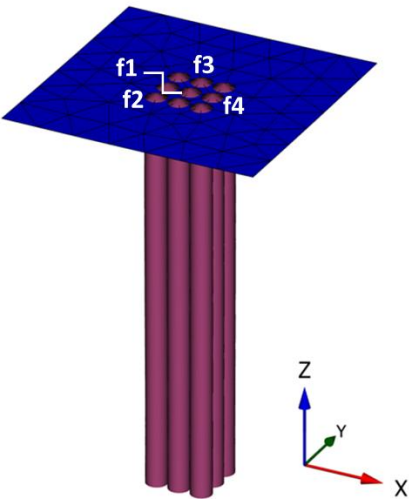
Pile	Stage 2 Centrifuge Load, kN	FEM	Dif. %	Stage 3 Centrifuge Load, kN	FEM	Dif. %
f3	196	226	+15	347	382	+10
f1	173	228	+32	393	477	+21
f4	164	227	+38	463	430	-7
f2	215	241	+12	352	298	-15
	1,753	2,098	+20	3,421	3,293	-4
Pile load %	23	28	+22	46	44	-4
Raft load%	77	72	-6	54	56	+4

	Piles	Raft	Piles	Raft
	Stage 2		Stage 3	
Centrifuge(%)	23	77	46	54
FEM (%)	28	72	44	56
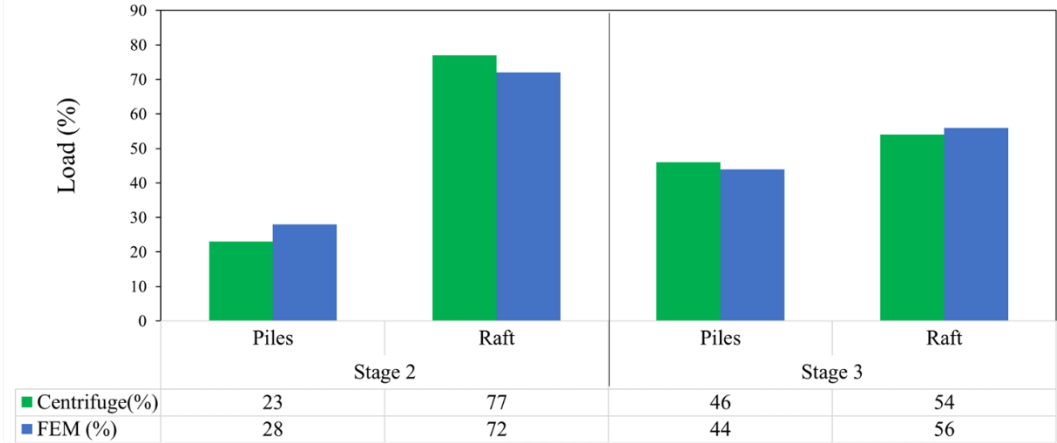
Figure 3.48. Comparison between centrifuge and FEM load values measured on the pile head in each of the stages of the test for model M3.

Having the model calibrated, it was possible to obtain and the variation of the axial forces with depth in piles for three different positions on the raft (Figure 3.49), which allows to properly access the negative skin friction that can be generated. This is an important issue to design piled raft foundations in this type of soft soils since the negative skin friction induces a downdrag force that, depending on each case, should or should not be considered as mentioned by Auvinet and Rodríguez-Rebolledo (2017).

For Phase 2 (Figure 3.49a), the load transmitted by the corner pile is slightly larger (+13 kN) than for the central and border piles. For Phase 6, the settlement developed by pore pressure drawdown has a greater influence on the behavior of the corner piles than on the border and center one, which receive a higher load in the head piles. This can be related to the fact that the influence area of the corner piles is considerably larger than for the others leading to higher values of negative skin friction, which agree with results like those presented by Auvinet and Rodríguez (2017), and Melo (2018). As the pore pressure drawdown developed in Phase 6, the neutral point of the piles stabilized at a depth between 15-16m which is near to 0.75 of the pile length, which is the location suggested for some authors like Prakash and Sharma(1990), and Lam et al. (2009) based on experiments tests.
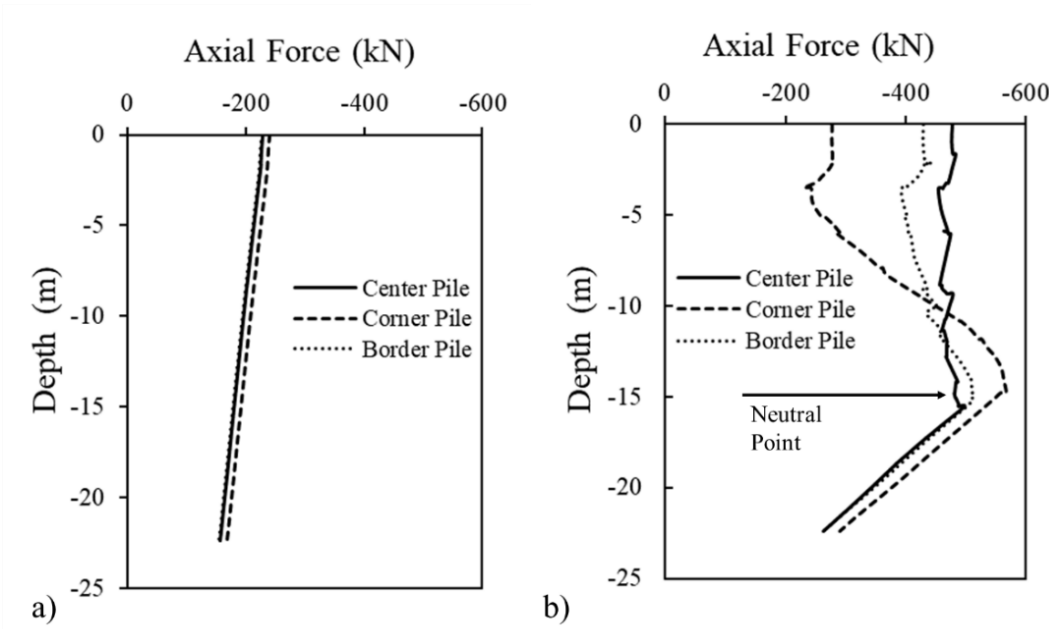
Figure 3.49. Axial forces developed along the piles with different positions in the piled raft (border, corner, and center), for: a) Stage 2 and b) Stage 6.

3.3.4 Different configuration comparison

After calibrating the numerical model, simulations of the other two physical tests that were carried out in the centrifuge (model M4 and M6), were made to compare the results and to understand the behavior of the model.

3.3.4.1 Model M4

M4 model had a piled raft with sixteen piles arranged in the center, with a spacing of two diameters between them. The instrumentation distribution is shown in Figure 3.50 and Figure 3.51. The number of finite elements varied as more piles were included in this analysis. The generated mesh had almost 30,000 elements and was also refined in a volume where the piles were contained.
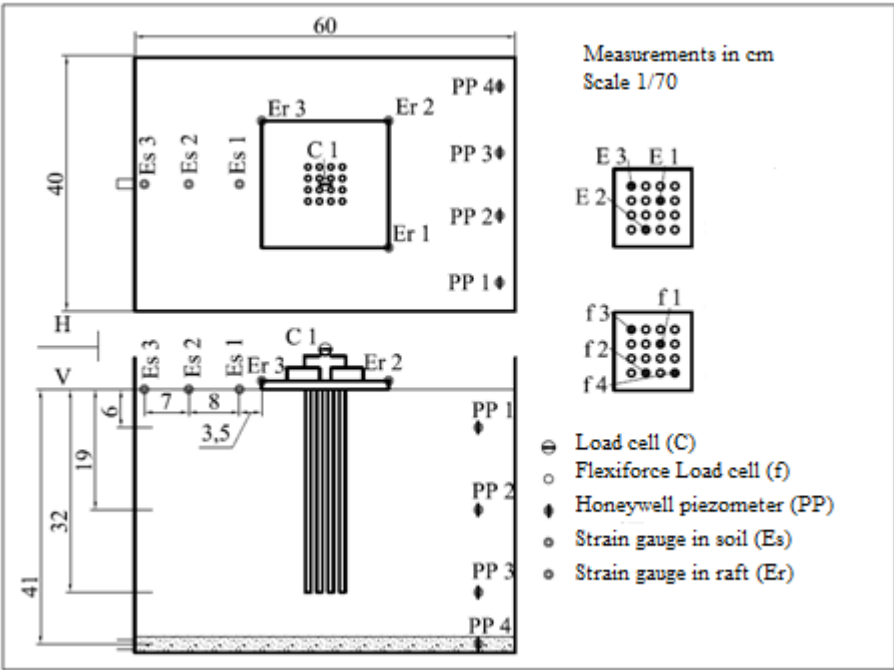
Figure 3.50. Instrumentation distribution of the Reduced scale model M4. Adapted for Rodríguez 2016.

Figure 3.51. Assambly and instrumentation details of M4 model. Rodríguez 2016.

Although some of the centrifuge data were not stable, Figure 3.52 and Figure 3.53 showed the same path behavior for the displacements of both the foundation and the surrounding soil. The centrifuge results for the soil showed higher displacement value, a difference of +81% for stage 2, and +14% for the last stage. As reported by Rodríguez (2016), the centrifuge model seemed to had problems related to the water control equipment, which generated an overload in the model. However, for the piled raft displacement, the FEM values fit between the two measured points on the physical model.
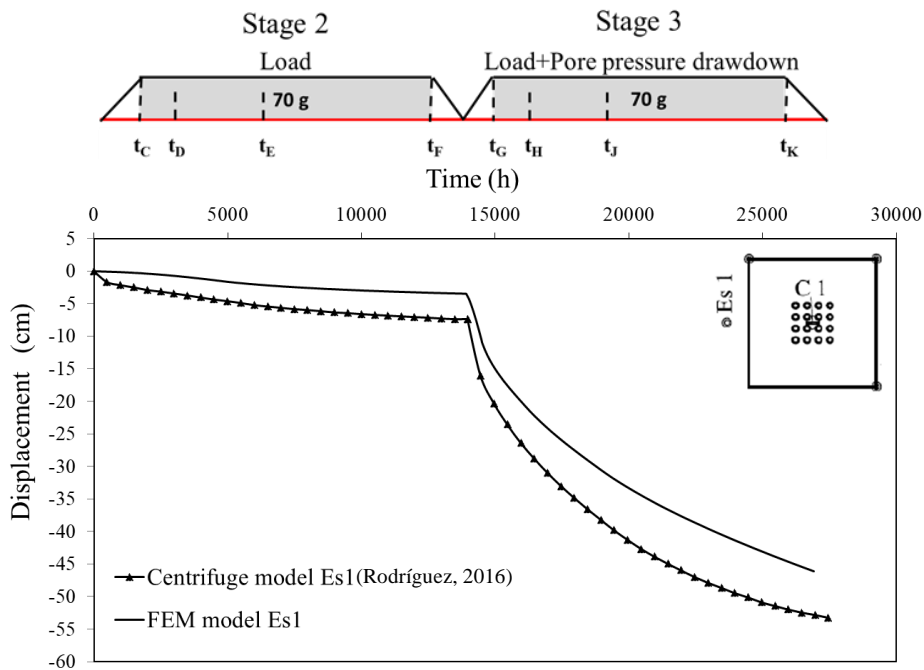
Figure 3.52. Displacements *vs* time curves obtained at point Es1 by centrifuge and FEM models.
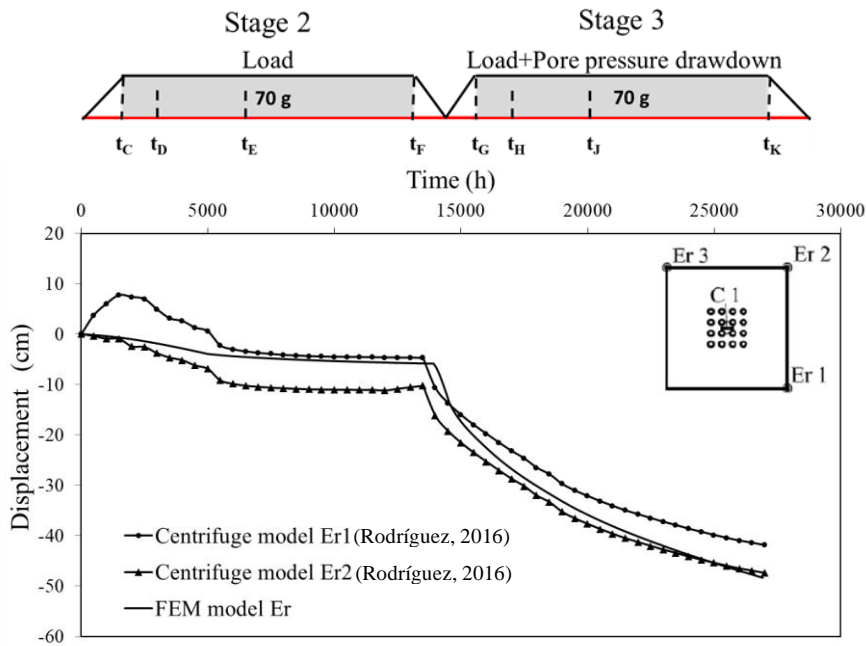
Figure 3.53. Displacements *vs* time curves obtained at raft corner points Er1, Er2 and Er3 by centrifuge and FEM models.

Regarding the percentage of the load supported by the piles, it increased in the last stage, where the pore pressure drawdown was simulated. In general, the difference between the FEM and the centrifuge results is high, as presented in Table 3.22 and Figure 3.54. The centrifuge results showed that the load was not uniformly applied on the raft.

Table 3.22. Comparison of the M4 model between centrifuge and FEM load values measured on the pile top in each of the stages of the test.

| Pile | Stage 2 | | | Stage 3 | | |
| | Centrifuge | FEM | Dif. % | Centrifuge | FEM | Dif. % |
	Load, kN			Load, kN		
f1	114	192	+68	225	375	+66
f2	132	163	+23	222	278	+25
f3	36	153	+325	102	160	+57
f4	142	158	+11	314	157	-100
	1,863	2,644	+42	3,504	4277	+22
Pile load %	26	36	+38	47	58	+23
Raft load%	75	64	-17	53	42	-26

	Stage 2		Stage 3	
	Piles	Raft	Piles	Raft
■ Centrifuge(%)	26	75	47	53
■ FEM (%)	36	64	58	42
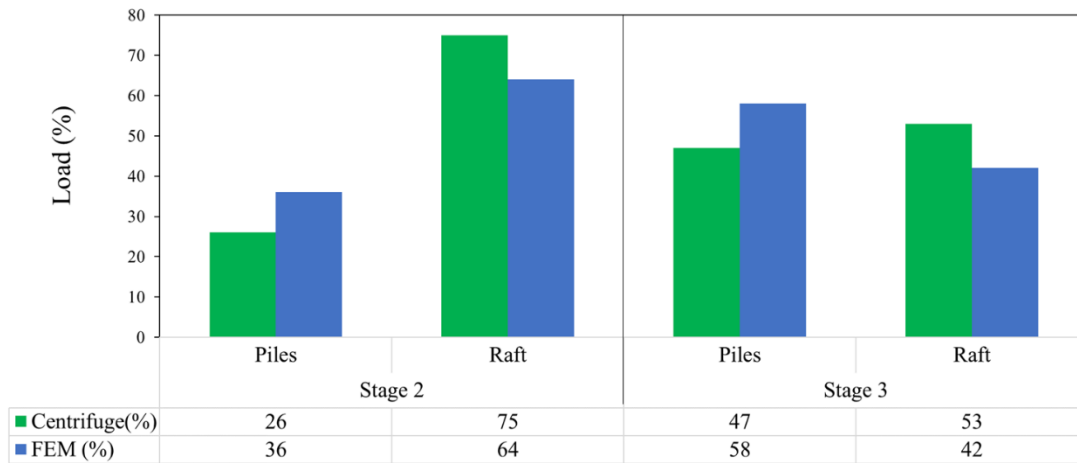
Figure 3.54. Comparison of the M4 model between centrifuge and FEM load values measured on the pile top in each of the stages of the test.

3.3.4.2 Model M6

M6 model had a piled raft with nine piles arranged in the center, with a spacing of nine diameters between them. The instrumentation distribution is shown in Figure 3.55 and Figure 3.56.
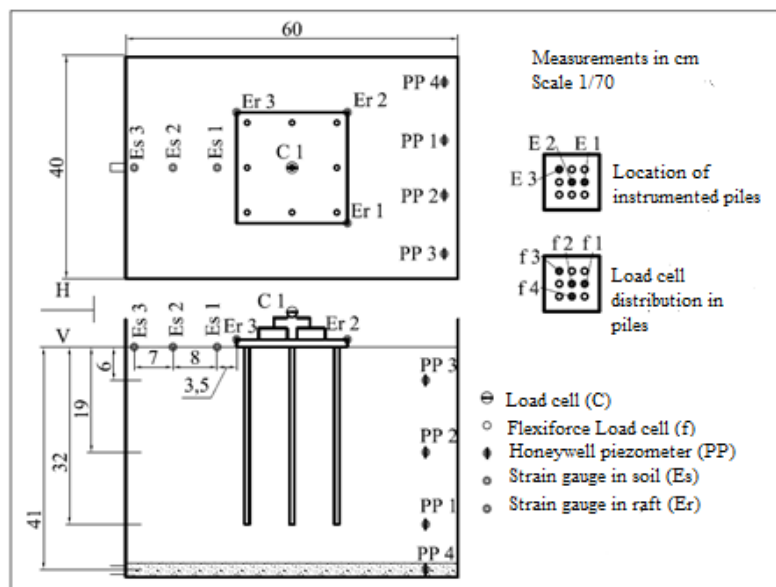
Figure 3.55. Instrumentation distribution of the Reduced scale model M6. Adapted for Rodríguez 2016.
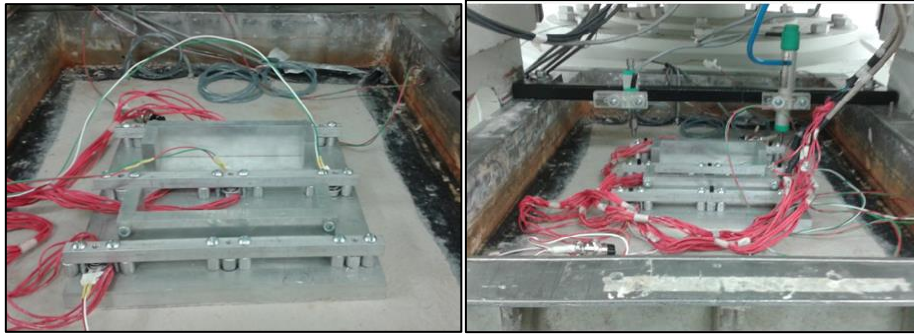
Figure 3.56. Assambly and instrumentation details of M6 model. Rodríguez 2016.

Figure 3.57 shows that FEM displacements results in stage 2 are smaller than the ones from the centrifuge test. As was registered by Rodríguez (2016), the data of the piezometers installed in the model showed a drop in the first two stages, associated with the loss of pressure in the water compensation chamber, installed in the counterweight box; so, the higher displacements can be due to this reason. Figure 3.58 shows that the piled raft settlement difference was just +4% when compared to the soil surrounding it (Figure 3.57) in the FEM analysis, contrary to the behavior shown in the centrifuge results, where the difference is approximately -48%. The variation behavior between the centrifuge model and the numerical model can be presented in a better way in Figure 3.59.
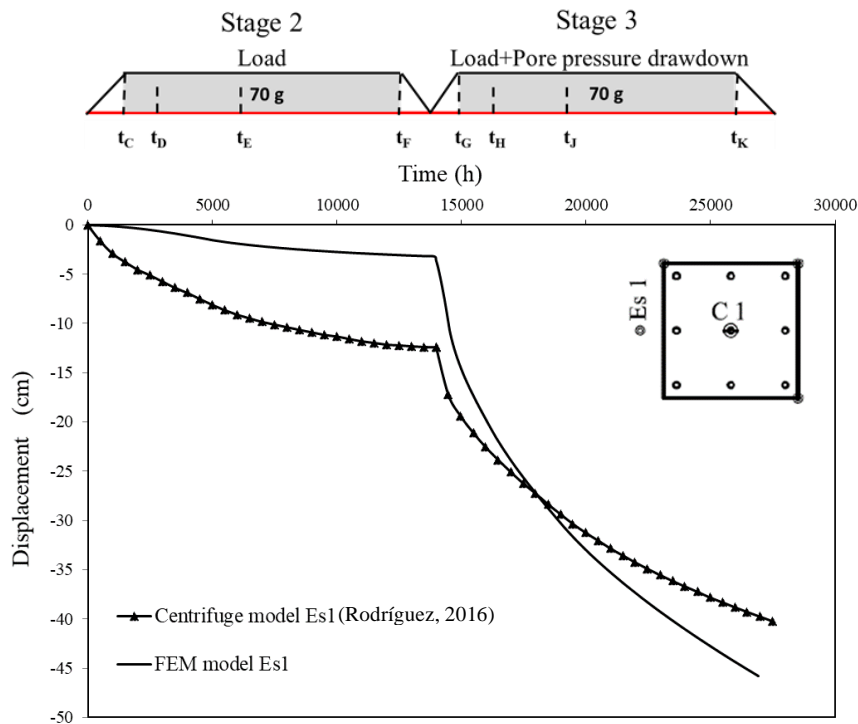
Figure 3.57. Displacements *vs* time curves obtained at point Es1 by centrifuge and FEM models.

95
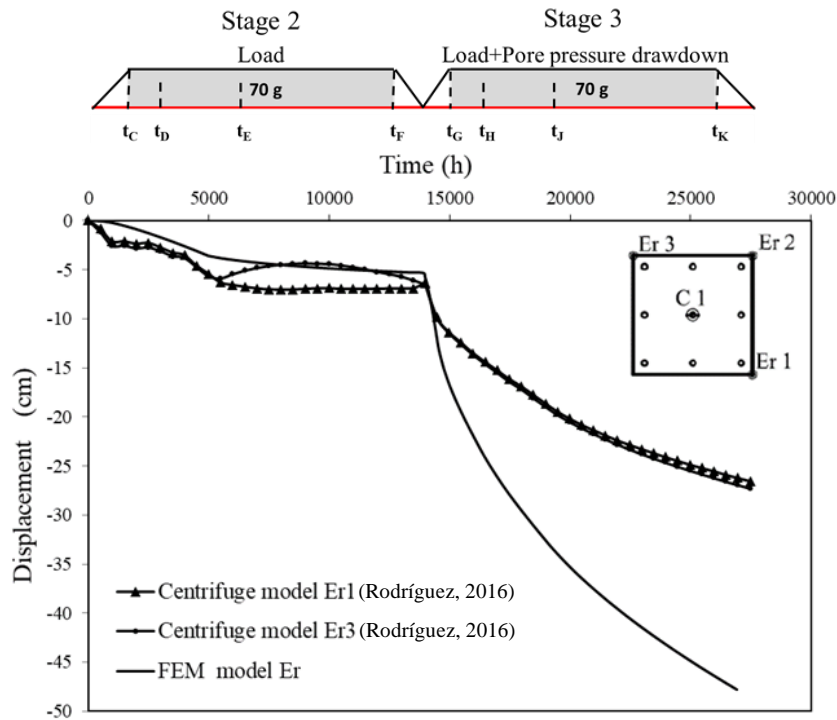
Figure 3.58. Displacements *vs* time curves obtained at raft corner points Er1, Er2 and Er3 by centrifuge and FEM models.
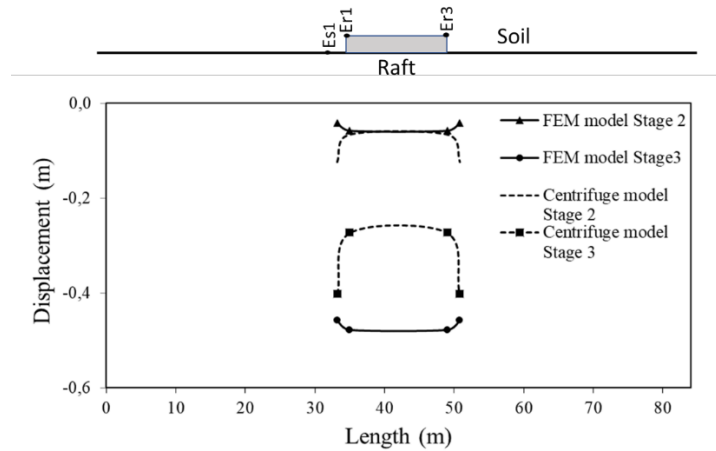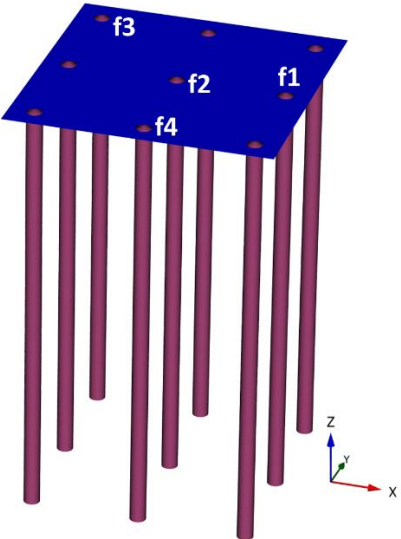
Figure 3.59. Displacement profiles comparison between centrifuge model and FEM model results.

Table 3.23 and Figure 3.60 summarizes the load measured at the pile head and shows significant differences between the centrifuge and FEM results, this can be due to the problems that the model had and the not symmetry application of the load. In general, the piled raft load distribution behaves in the same way in all the three models. The raft supports more than 60%

of the total load applied in stage 2, and this percentage decrease when the pore pressure drawdown occurs in stage 3.

Table 3.23. Comparison of the M6 model between centrifuge and FEM load values measured on the pile top in each of the stages of the test.

Pile	Stage 2			Stage 3		
	Centrifuge	FEM	Dif. %	Centrifuge	FEM	Dif. %
	Load, kN			Load, kN		
f3	155	278	+79	434	367	-18
f2	307	269	-14	429	315	-36
f1	107	274	+156	268	351	+31
f4	387	278	-39	612	361	-69
	1,915	2,485	+29	3,925	3,207	-22
Pile load %	26	34	+30	53	44	-20
Raft load%	74	66	-12	47	56	+19
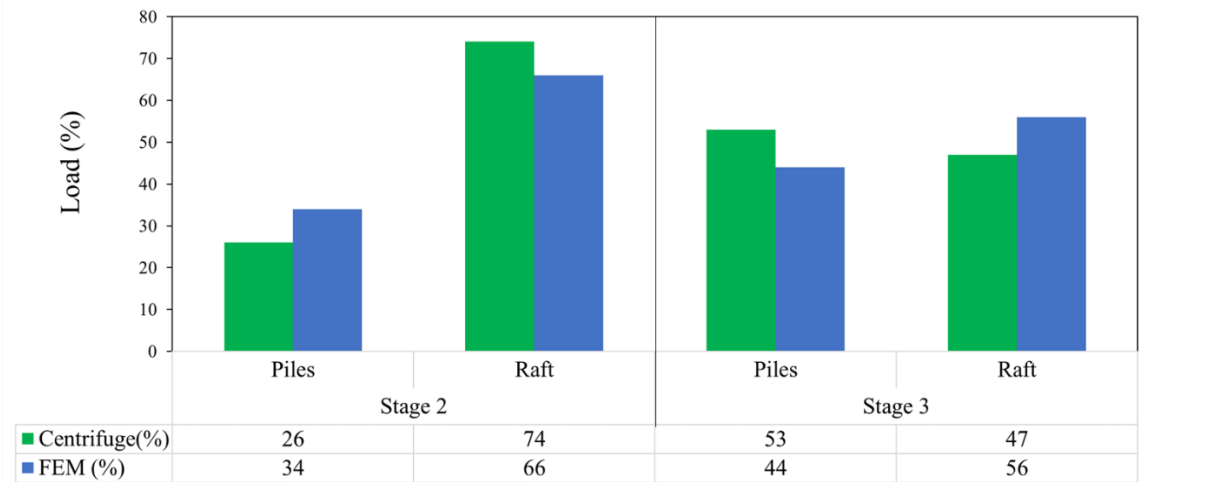
Figure 3.60. Comparison of the M6 model between centrifuge and FEM load values measured on the pile top in each of the stages of the test.

3.3.5 Analysis of the influence of boundary conditions on the model's response

To analyze the boundary effect on the results, the calibrated model (Model 1 with 42x28 m) was extended in both horizontal directions. The boundaries for Model 2 (with 84x84 m) were located at 2,5B (B= raft width) from the raft, as shown in Figure 3.61.
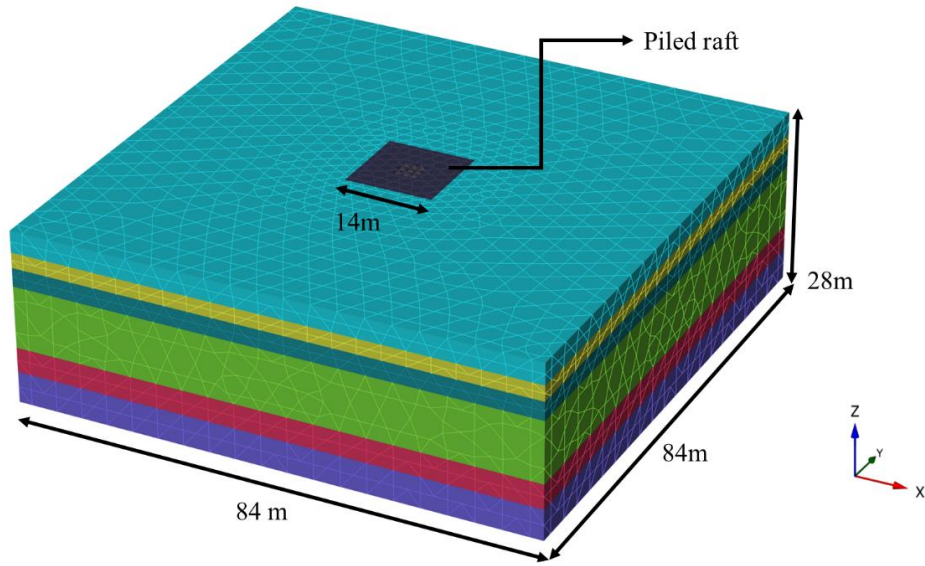
Figure 3.61. Geometry and mesh of Model 2 developed in PLAXIS.

Figure 3.62 shows the displacements generated in stage 2 (load-consolidation) for both of the models. It can be observed that the boundaries had an important influence on the results, showing that Model 1 presents more significant displacements than Model 2. That difference is summarized in Table 3.24, being greater the ones referring to the points more influenced by the load, Es1, and Er3 with -69% and -75%, respectively.
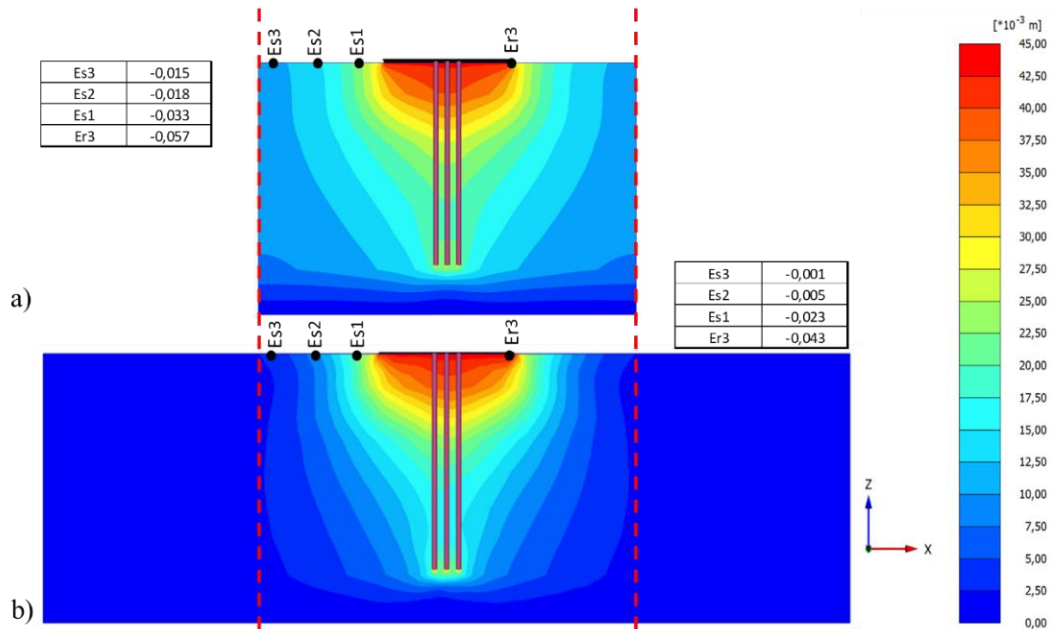
Figure 3.62. Displacements of Stage 2.a) Model 1. b) Model 2 (All values in meters).

Table 3.24. Comparison of displacements between Model 1 and Model 2 in Stage 2.

Point	Model 1 Displacements (m)	Model 2 Displacements (m)	Difference (%)
Es3	-0.015	-0.001	-6
Es2	-0.018	-0.005	-30
Es1	-0.033	-0.023	-69
Er3	-0.057	-0.043	-75

In Figure 3.63 are comparing the displacements in stage3 that involves regional subsidence, and it confirms the same behavior of the previous stage. Figure 3.63b shows that not only the area under the foundation is the one that presents the most significant displacements, but also the areas near the boundaries behave in similar way. The differences are around -70% between the models, being the biggest (-79%) for the point located on the piled raft (Er3) (
Table **3.25**).

Table 3.25. Comparison of displacements between Model 1 and Model 2 in Stage 3.

Point	Model 1 Displacements (m)	Model 2 Displacements (m)	Difference (%)
Es3	-0.44	-0.328	-75
Es2	-0.441	-0.328	-74
Es1	-0.452	-0.346	-77
Er3	-0.475	-0.374	-79
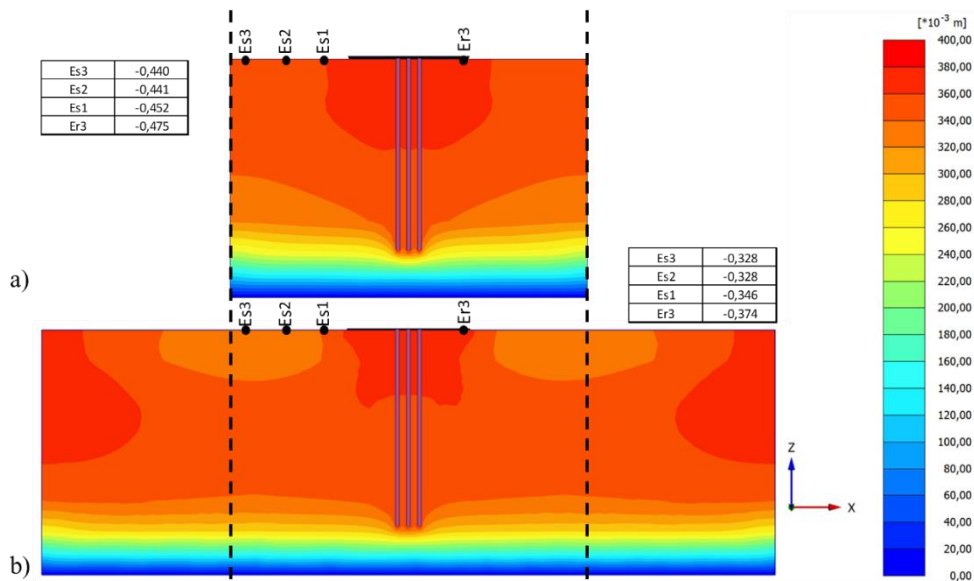
Figure 3.63. Displacements of Stage 3.a) Model 1. b) Model 2 (All values in meters).

This difference between the settlements also influences the load distribution in the foundation elements. As mentioned in item 3.3.3.2, no symmetry was observed in the load distribution in the piles in Model 1; this can be due to its rectangular geometry, making the boundaries on the axis-x have a more considerable influence on the piled raft as they are closer than the ones on axis-y

3.4   Chapter summary

In this chapter, a numerical model using FEM was proposed to identify the most sensitive parameters for this type of simulation, also to define the types and stages of analyses that had the best fit to the physical model, and to obtain additional (Chapter 4) results to those measured in it. In Figure 3.64 presents the summary of the chapter.
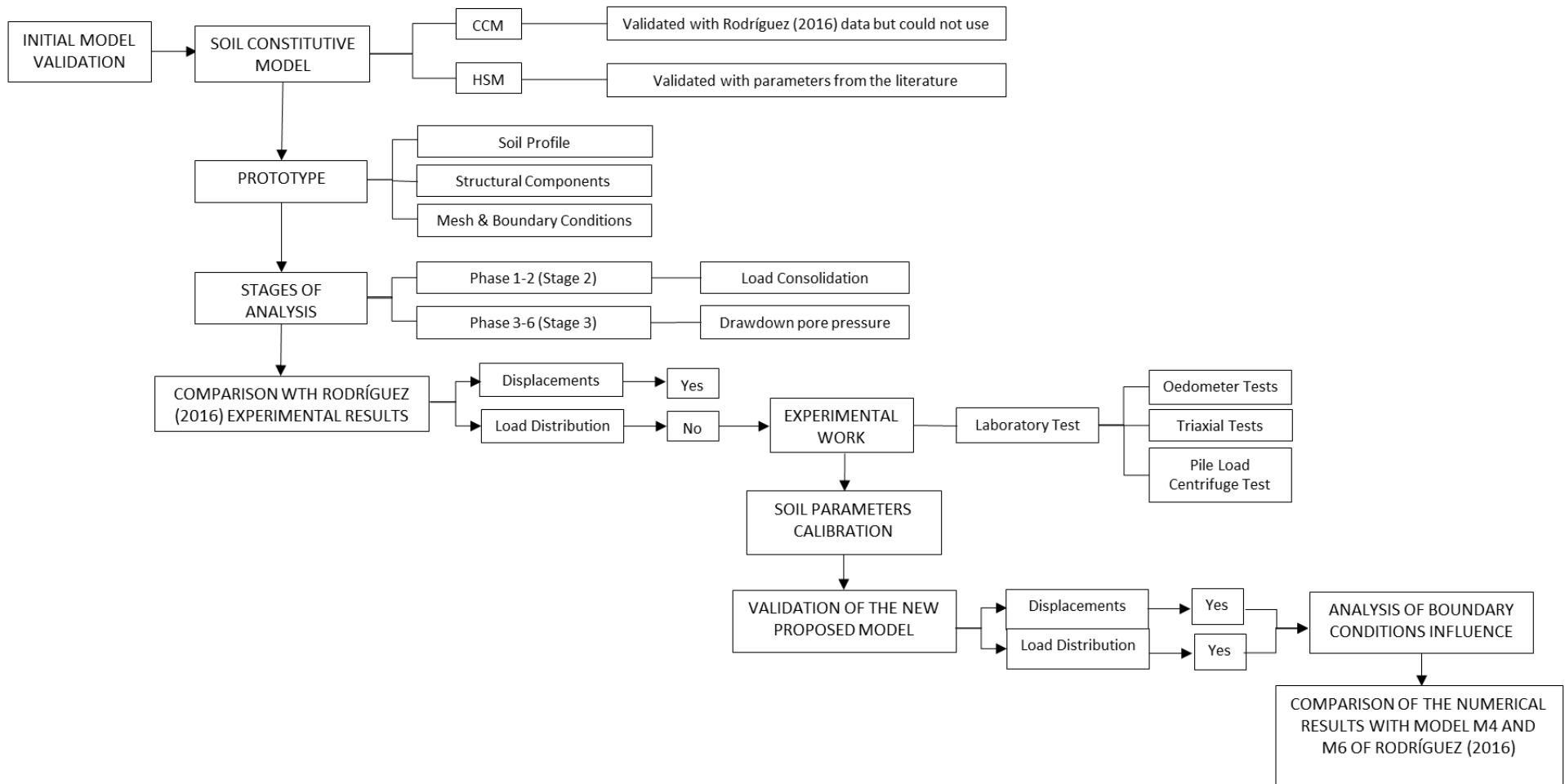
Figure 3.64. Chapter Summary.

CHAPTER 4

In this chapter are presented and discussed the results of the parametric analyses varying geometric parameters on the 3D model that was calibrated in the previous chapter.

Specifically, this part of the work presents a comparative analysis of the results obtained, establishing the influence of loading and drawdown water pore pressure on the responses of the models M3 to M8.

4. RESULTS: PARAMETRIC ANALYSES AND CONTRIBUTIONS FOR PILED RAFT FOUNDATION DESIGN

The results of the parametric analysis will be divided and presented into four main parts as shown in Figure 4.1.
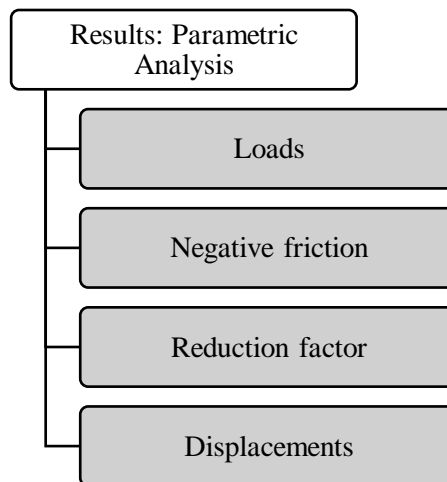
Figure 4.1. Results-Parametric analysis outline.

The results focus on assess the pile's load distribution, vertical displacements, neutral point, and negative friction along pile in the center, border, and corner positions.

Each configuration was modeled with four different conditions (C1, C2, C3, and C4), varying geometric parameters that are described in Table 4.1. As the number of results is extensive,

some graphs will be presented and analyzed in this chapter, and the others will be presented in Appendix I.

Table 4.1. Parametrical variables for all models (M3-M8).

Condition	L/D	H/L	L (m)	H (m)	D (m)
C1	35.5	1.25	22.4	28	0.63
C2	35.5	3	22.4	67.2	0.63
C3	50	1.25	31.5	39.7	0.63
C4	50	3	31.5	94.5	0.63

Load-settlement curves (Figure 4.2) to determine the foundation system's workable load capacity (Q_w) were obtained from numerical simulations. The criteria used in this research was related to foundation displacement, it means that Q_w is the load obtained when the piled raft displacement reached is equal to 10% of the pile diameter. The load to be applied (Q_{adm}) on the piled raft is equal to Q_w divided by a safety factor of three. This process was performed for each configuration with four different conditions. Table 4.2 listed the configurations of models with the load that was applied for condition C1.
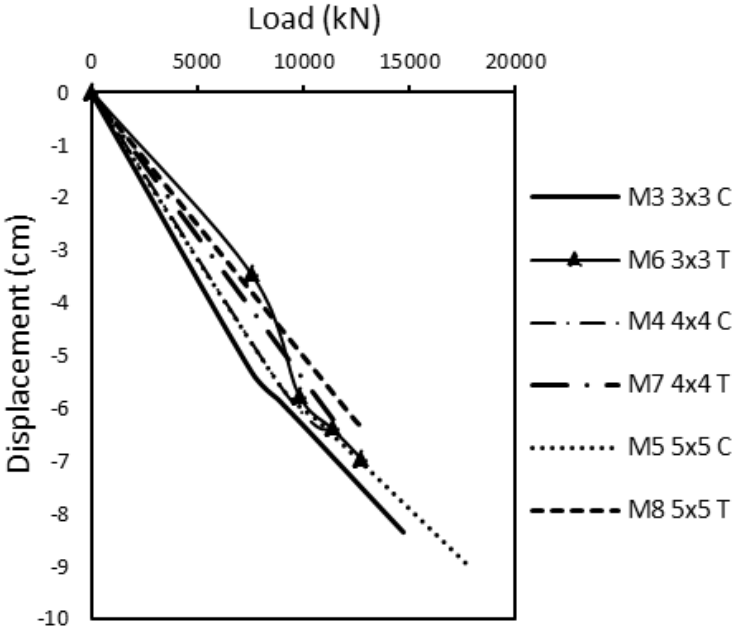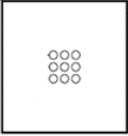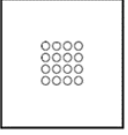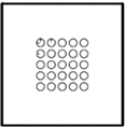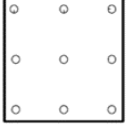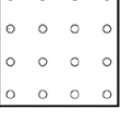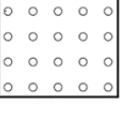
Figure 4.2. Load-settlement curves for configurations models M3 to M8 simulated with condition C1.

Table 4.2. Variation of ultimate bearing capacity of models M3 to M8 simulated with condition C1.

Configuration models	Q_w (kN)	Q_{adm} (kN)
M3 3x3C	9898	3299
M4 4x4C	10584	3528
M5 5x5C	10878	3626
M6 3x3T	11368	3789
M7 4x4T	11662	3887
M8 5x5T	12642	4214

From the beginning part, some insights can already be pointed out about the foundation behavior. As was expected, the load capacity increases with the increasing number of piles. This load capacity increase is also observed when the piles' distribution in the raft changes, an aspect that will be analyzed more deeply in the comparisons that will be presented later.

As previously mentioned, to understand the piled raft behavior including settlements, moments and load percentage that each element supports, piles displacements, and load distribution along them, it is important to understand the load transfer mechanism from the raft to the piles and soil (Chow, 2007) The results obtained considering these aspects will be presented and discussed next.
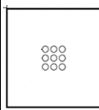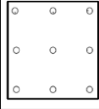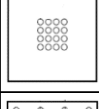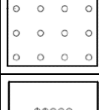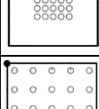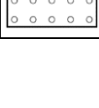
4.1 Analysis of loads and proposed graphs

An analysis of the load displacement curves results aims to establish a change that can be presented in the load supported by the piles when the pore pressure abatement process takes place in the soil. With the results of the load distribution, it was possible to establish a proportion of the total load that is assumed by the piles. Table 4.3 and Figure 4.3 summarizes the load percentage taken by each of the elements of the foundation and their variation in the 1/70 scale models for conditions C1, C2, C3, and C4.

In general, it is observed that systems with the piles distributed in the whole area of the raft (T) are more efficient since they receive higher loads with similar settlements. In these cases, the load percentage assumed by the raft is less than the percentage assumed by the piles, this being an advantage in cases where a separation between the soil surface and the raft may occur as happened in conditions C3 and C4. This separation can be identified due to the small percentage of load that the raft receives and can be numerically modeled in PLAXIS using interface elements that allow simulating this problem by admitting discontinuities between the finite elements.

It is also possible to perceive that in the configurations with distributed piles (T) the load that reaches the head of the piles is much higher when compared to the load received by the piles located in the center of the foundation (C) (Figure 4.4 and Appendix D).

Table 4.3. Load distribution.

Configuration		Condition C1							Condition C2							Condition C3							Condition C4						
		Load (kN)	Stage 2			Stage 3			Load (kN)	Stage 2			Stage 3			Load (kN)	Stage 2			Stage 3			Load (kN)	Stage 2			Stage 3		
			Head Load (kN)	Piles %	Raft %	Head Load (kN)	Piles %	Raft %		Head Load (kN)	Piles %	Raft %	Head Load (kN)	Piles %	Raft %		Head Load (kN)	Piles %	Raft %	Head Load (kN)	Piles %	Raft %		Head Load (kN)	Piles %	Raft %	Head Load (kN)	Piles %	Raft %
M3 3x3C		8919	1454	16	84	4113	46	54	8201	1358	17	83	3897	48	52	8756	2382	27	73	6267	72	28	8300	1803	22	78	4512	54	46
M6 3x3T		9409	2567	27	73	5375	57	43	8430	2554	30	70	5120	61	39	8952	2847	32	68	7970	89	11	8527	2845	33	67	7479	88	12
M4 4x4C		9148	3011	33	67	6638	73	27	8397	2648	32	68	6039	72	28	9214	3704	40	60	9193	100	0	8691	3566	41	59	8703	100	0
M7 4x4T		9507	3430	36	64	6776	71	29	8430	4184	50	50	6499	77	23	9278	5134	55	45	9172	99	1	8723	5086	58	42	8716	100	0
M5 5x5C		9246	3368	36	64	7033	76	24	8888	3613	41	59	7560	85	15	9409	5010	53	47	8840	94	6	8625	4580	53	47	8961	100	0
M8 5x5T		9834	6200	63	37	7979	81	19	8756	5712	65	35	7333	84	16	9638	6998	73	27	9661	100	0	8952	7047	79	21	8964	100	0
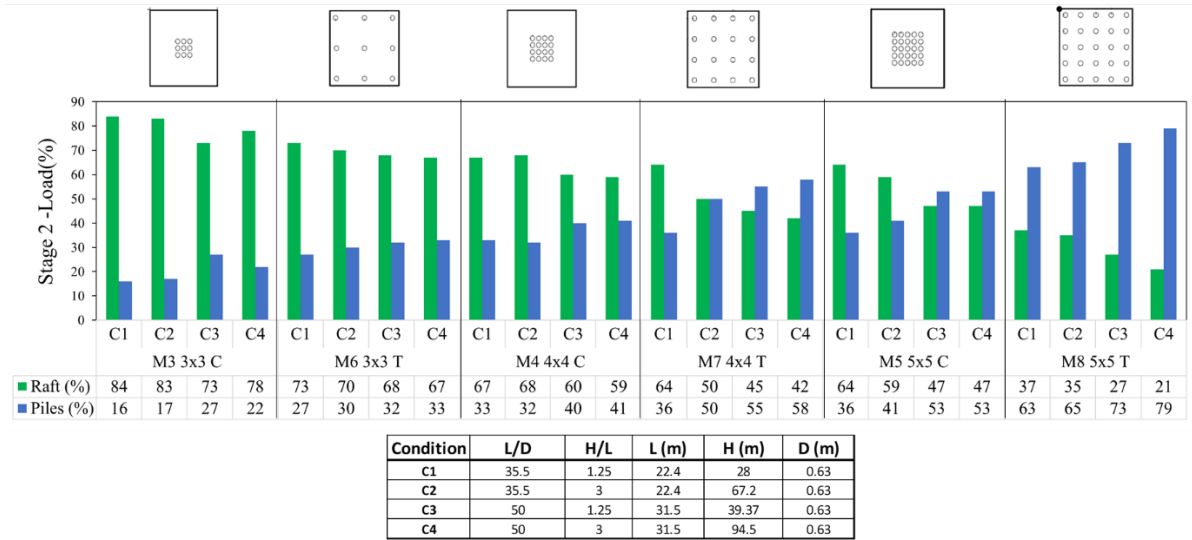
a)
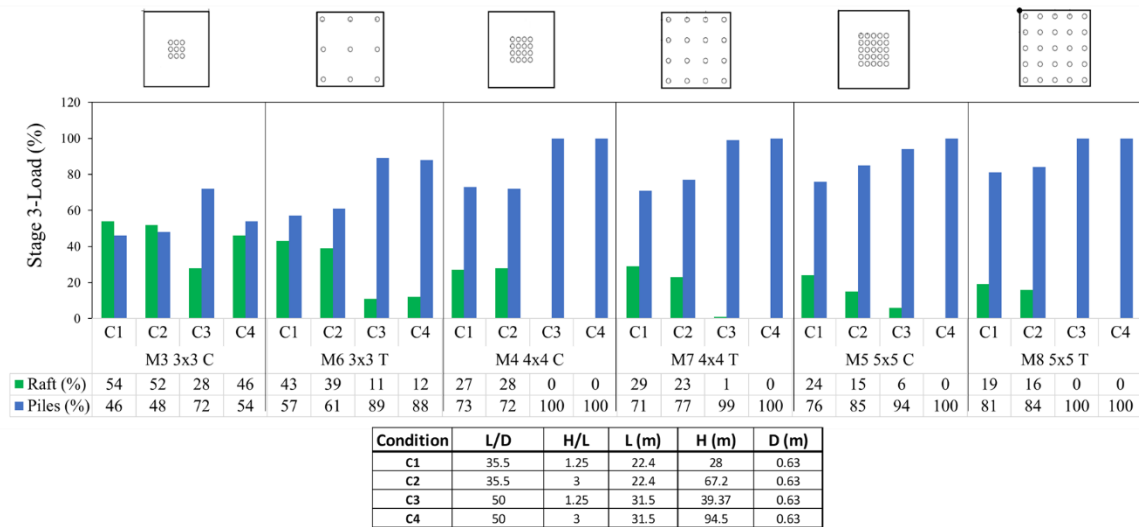
b)

Figure 4.3. Load Distribution for configurations M3 to M8 a) Stage 2 and b) Stage 3.
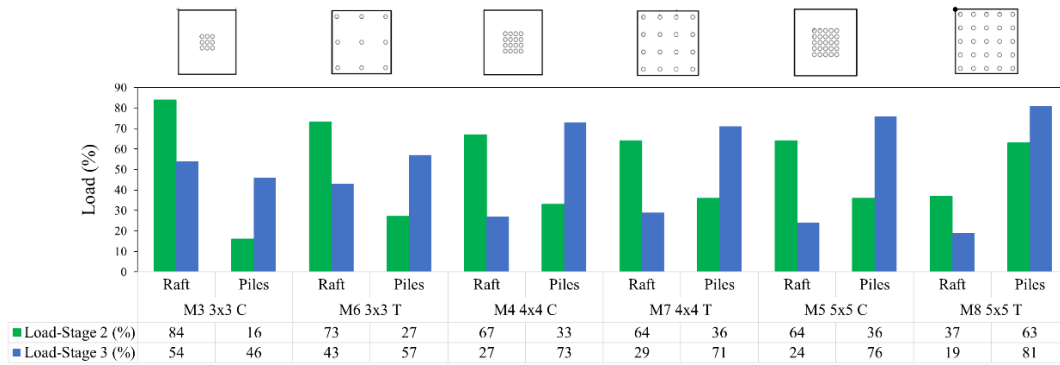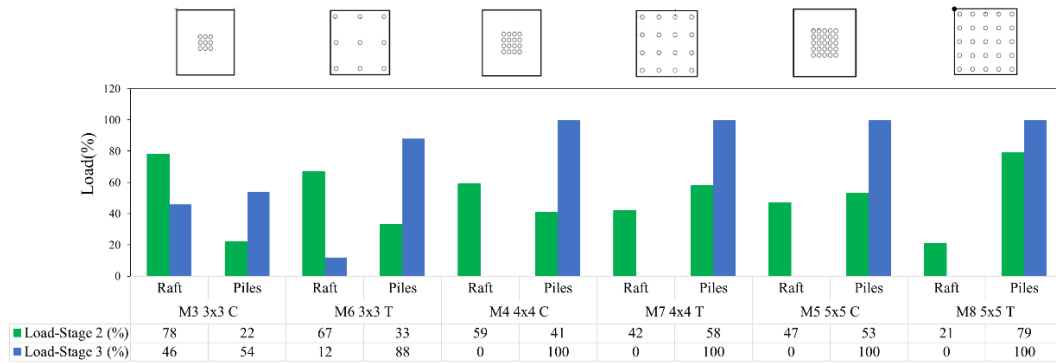
Figure 4.4. Load distribution comparing both stages for all configurations M3 to M8. a) Condition C1 and b) Condition C4.

When the piled spacing increased (Figure 8), the load shared by the piles also increased. This phenomenon occurred because the soil around the piles was mobilized to resist the applied load. When piled spacing was increased, the stress in the mobilized zone was not overlapped resulting larger capacity carried by the piled (Tran et al., 2012a).

For centered piles configurations (C), mainly M3 where the separation is very small (s=2D) the set of piles works as a single block. For small spacings the piles have their transfer mode affected and the peripheral piles absorb more loads than the internal piles (Velloso & Lopes, 2012). The central piles behave like a block in conjunction with the soil trapped between them, this behavior is not wanted, and a minimum spacing must be established so that this condition does not occur. Withaker (1957) and Sowers et al. (1961) indicate that for a small spacing, less than close to 2D, the block behavior characterized by lost of efficiency. When the separation increases the efficiency of the system increases as well and the influence of the group effect decreases, and each pile can be analyzed separately.

4.1.1 Proposed graphs of ALM vs Head pile load percentage

In piled raft systems, it is important to define the load percentages that will be supported by the raft and piles and, in specific cases where the regional subsidence phenomenon occurs, to evaluate the variation of that proportion. Some authors have proposed correlations that allow these percentages to be estimated. Next, the criteria of Mandolini et al., (2013) and lateral area will be explained. Then, the proposed graphs with the results obtained in this work will be presented.

4.1.1.1 Mandolini et al., (2013) criterion

As explained in Chapter 2 (item 2.1), Mandolini et al. (2013) criterion allow estimating the percentage of load that will be supported by the raft. Consequently, knowing this value, the load percentage received in by the piles can also be defined.

On the graph proposed by Mandolini et al. (2013), the results obtained in the numerical models for each of the conditions in Table 4.3 and the results obtained by Rodríguez (2016) are presented in Figure 4.5. According to this author, this criterion was used to make a comparison of the model's responses tested in the centrifuge, since the Filling Factor (FF) presented by Mandolini et al. (2013), allows including the variables that influence the response of the piled raft systems.

In Figure 4.5a it can be seen that the percentage of the load supported by the raft in all models is located within the interval proposed by Mandolini et al. (2013) as expected. Initially, the loads are transmitted to the system in a proportion >70% for the raft and <30% for the piles, as explained by Rodríguez (2016). However, in Stage 3, the Mandolini et al. (2013) criterion cannot be considered since when the drawdown pore pressure occurs in the soft soils studied, a regional subsidence phenomenon appears. This can generate an increase in the resistance at the pile-soil interface that favors a load transfer from the raft to the piles, or a separation of the raft and the supporting soil since the settlement suffered by the soil can be greater than the one from the whole system. This causes the component to completely lose its load capacity. This is observed in the models evaluated with conditions C3 and C4 that were presented in Table 4.1.
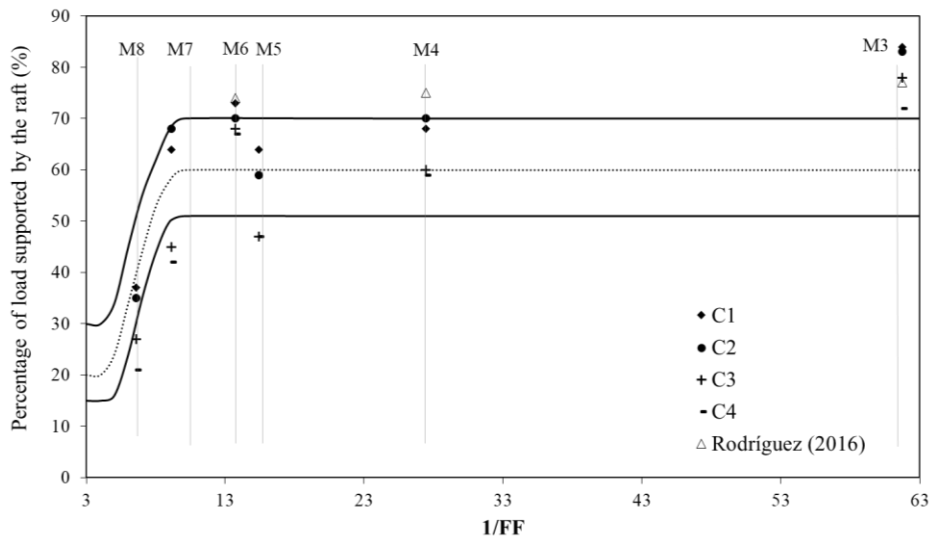
a)
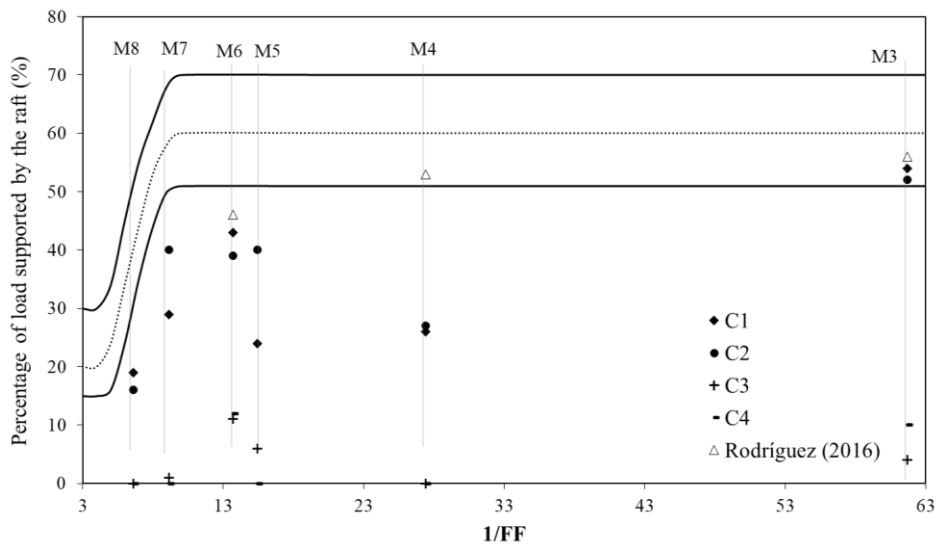
b)

Figure 4.5. Mandolini et al. (2013) Criteria: a. Stage 2, b. Stage 3.

4.1.1.2 Lateral area criterion

As it was observed, with the regional subsidence phenomenon, the piled raft must be analyzed with different criteria than those usually considered. Although the FF factor proposed by Mandolini et al. (2013) includes different variables that influence the system response, it does not contemplate the lateral area of the piles, a characteristic that defines the shaft resistance of this component and variable necessary to understand the behavior of piled raft in soft soils.

According to the Mexican standard norm "*Normas Técnicas Complementarias Para Diseño Y Construcción De Cimentaciones*" (NTCDC C, 2004) of Mexico City, a place affected by the problems generated by regional subsidence, in soft soils the piles of a piled raft must be calculated (design) to support the total weight of the structure and thus ensure its stability. When the material is in the consolidation process, the raft can lose support from the soil and, as already mentioned, also lose its load-bearing capacity. In these cases, the load capacity of the system must be calculated only with the piles and considering:

- Individual piles: sum of the tip load capacity plus the shaft load capacity of each pile;

- Foundation as a whole: sum of the individual tip load capacities plus the shaft load capacity of a pile with a geometry equal to the envelope of the group of piles.

That is,

$$Q_t = C_P + C_F \tag{4.1}$$

Where

$$C_p = (c_u N_c * F_R + p_v)A_p \tag{4.2}$$

$$C_F = A_L f F_R \tag{4.3}$$

where

Q_t= Total load capacity

C_p= Tip load capacity

C_f= Shaft load capacity

c_u = Cohesion of soil

N_c= Bearing capacity factors

p_v= Effective vertical stress

A_p= Area of the pile base

A_L= Pile lateral area

f= Average pile-soil lateral adherence

F_R = Resistance factor

To evaluate Q_t considering the sum of the individual capacities of the piles, A_L will be calculated using the expression:
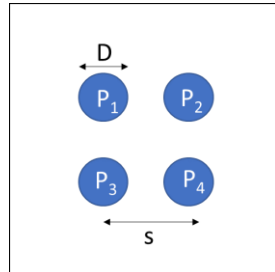
Figure 4.6. A_{L1}

$$A_{L1} = N_P \pi D L \tag{4.4}$$

And to evaluate Q_t as a whole foundation, A_L will be calculated as:
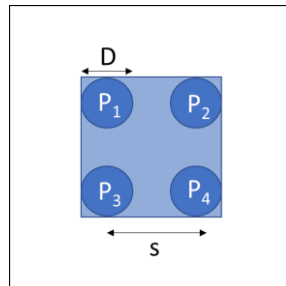
Figure 4.7. A_{L2}

$$A_{L2} = (s * (N_P - 1) + D)4L \tag{4.5}$$

Where

N_P = Number of piles

4.1.1.3 Proposed graphs based on lateral area criterion

It can be seen that A_{L1} and A_{L2} consider all the geometric variables that influence the response of the piled raft systems built-in cohesive soils, that are, number, diameter, spacing, and length

of the piles, characteristics evaluated in this parametric analysis. For this reason, these areas were used to assess the results obtained in all the models.

Figure 4.8 shows the percentage of load that reaches the head of the piles vs the lateral area A_{L1}. This area neglects the spacing between the piles, that is, disregards the configurations that work as a group of piles (M3, M4, M5).

a)

b)
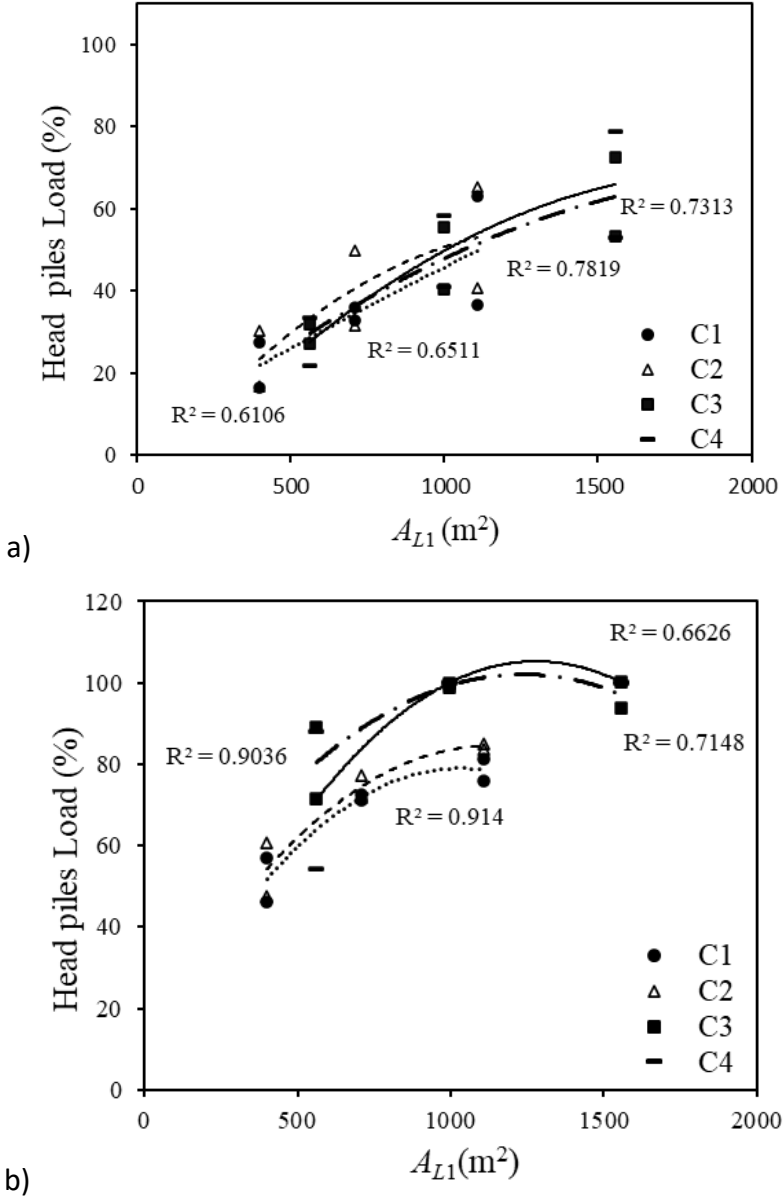
Figure 4.8. % Head piles load vs A_{L1}: a) Stage 2, b) Stage 3.

On the other hand, the lateral area A_{L2} is calculated considering this spacing, that is, it would not be the most adequate to evaluate the configurations where the piles of the system work as

113

individuals (Figure 4.9). Consequently, each configuration should be evaluated with a different A_L that corresponds to the smallest area calculated for each model (A_{LM}).

$$A_{LM} = \text{Smallest area between } (A_{L1} \text{ and } A_{L2}) \tag{4.6}$$
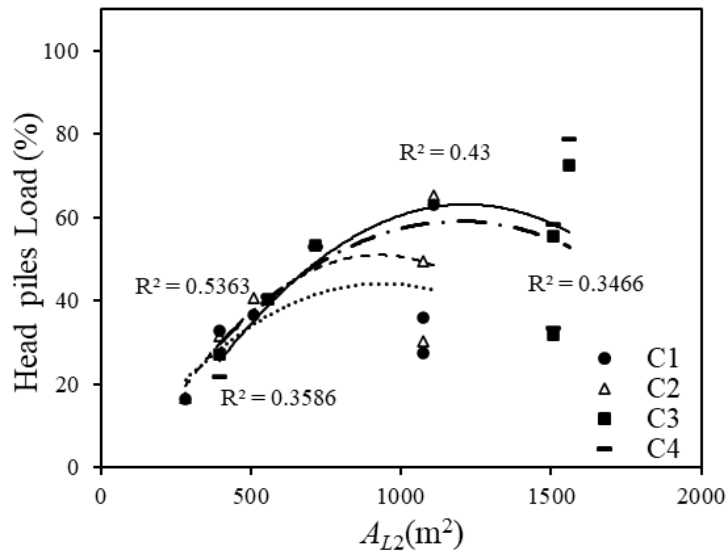
a)
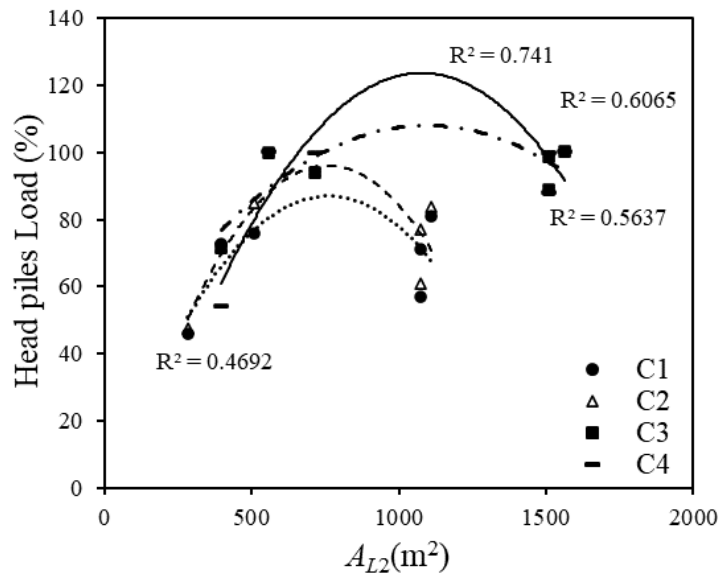
b)

Figure 4.9. % Head piles load vs A_{L2}: a) Stage 2, b) Stage 3

The This criterion is illustrated in Figure 4.10. Once the A_{LM} value is defined, the percentage of load that will be supported by the piles can be estimated, which can vary between the upper

114

and lower limits of the gray band (Figure 4.11). Knowing this percentage, it will also be possible to calculate the load supported by the raft in both stages.
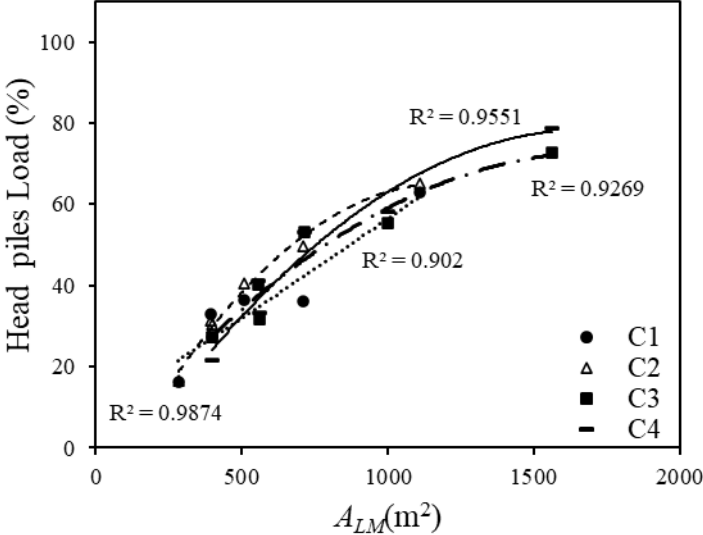
a)
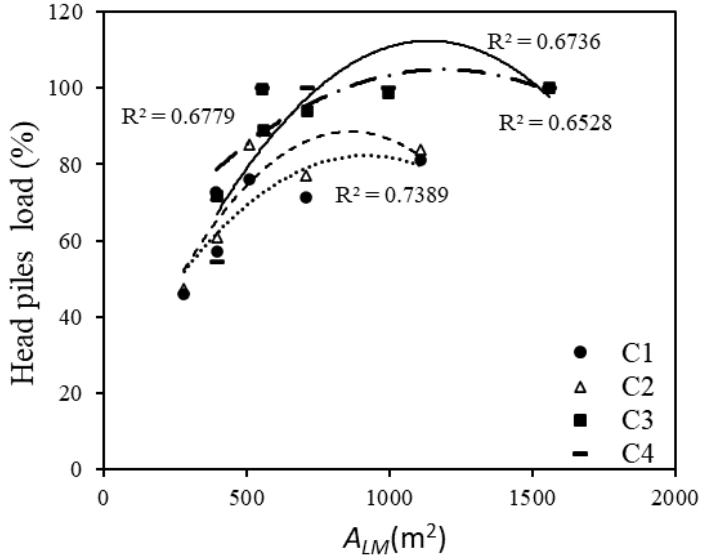
b)

Figure 4.10. % Head piles load vs Minor lateral area A_{LM}: a) Stage 2, b) Stage 3.
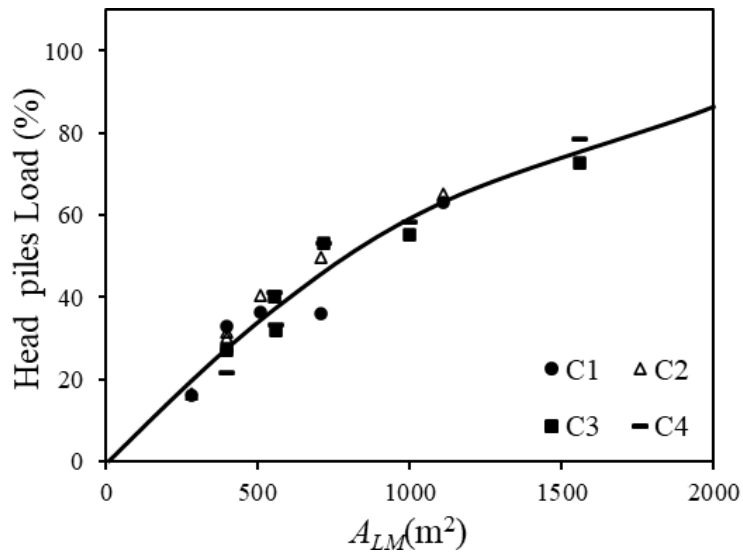
a)
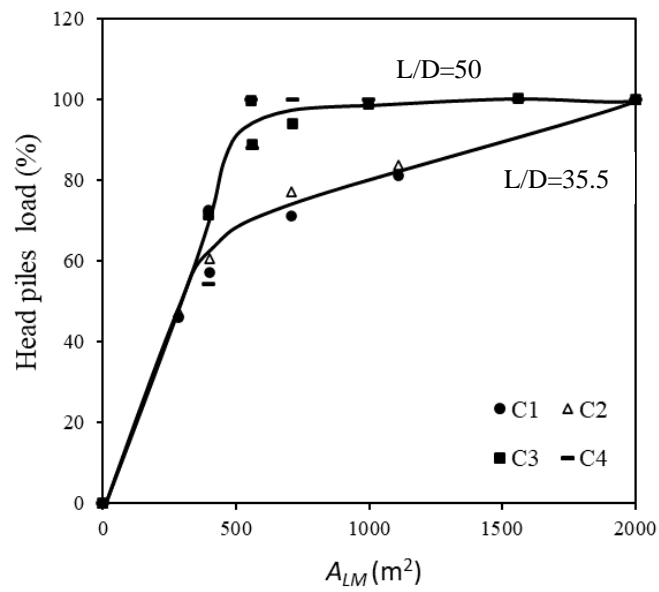
b)

Figure 4.11. Proposed graphs for % Head piles load vs Minor lateral area A_{LM}: a) Stage 2, b) Stage 3.

4.2   Negative friction analyses

From the graphs and results found in the numerical modeling of this research the magnitude of negative friction was obtained by subtracting the load value at the head of the pile from the load at the neutral level NP (neutral point), as illustrated in Figure 4.12.
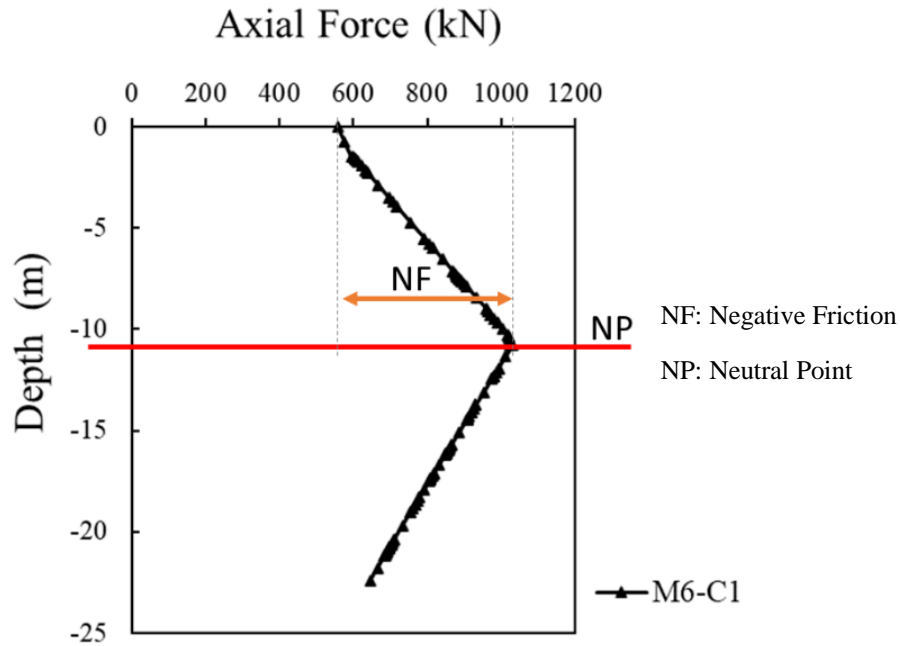
Figure 4.12. Negative friction in a corner pile of the model M6 with the C1 condition.

In order to compare all the configuration models in the four conditions, the negative friction is presented in Figure 4.13 as a percentage equivalent to the increase in the load measured at the pile head in stage 3. It is observed that the slenderest piles located at the border and corner of the raft are the ones that developed most of the friction load as expected since the center piles receive mainly the head load or at the tip. When the models with the same number of piles are compared, it can be observed that when $s > 2D$ a higher percentage of negative friction is generated, mainly for conditions C1 and C2. For all models in conditions C3 and C4, the negative friction value increases more than double in the center pile, which does not happen with the border and corner piles. As stated by Lee 1993, this is due to the influence area (greater volume of soil to be displaced) and the interaction effect between the piles.

When the results C1 and C2 or C3 and C4 are compared, no marked differences are observed, which shows that the thickness H of the profile does not have a significant influence on the behavior of the problem analyzed as verified with the distribution of the loads on the head of the piles.
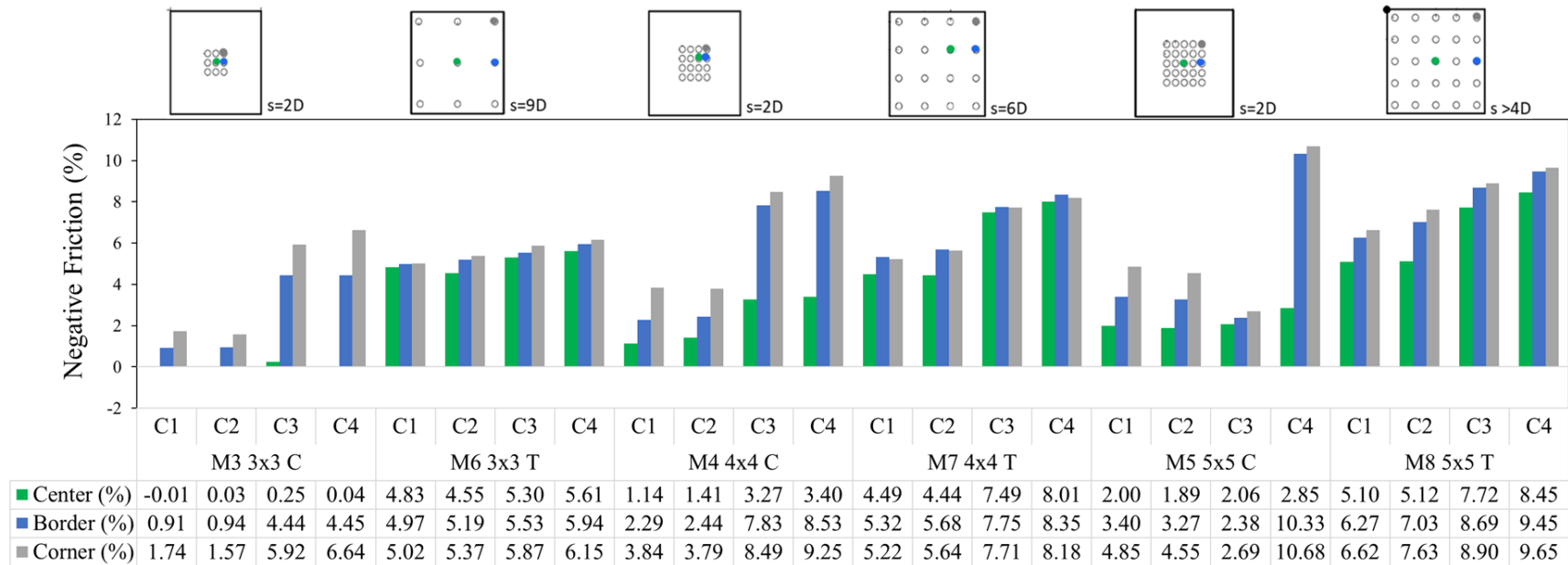
	C1	C2	C3	C4	C1	C2	C3	C4	C1	C2	C3	C4	C1	C2	C3	C4	C1	C2	C3	C4	C1	C2	C3	C4
		M3 3x3 C				M6 3x3 T				M4 4x4 C				M7 4x4 T				M5 5x5 C				M8 5x5 T		
■ Center (%)	-0.01	0.03	0.25	0.04	4.83	4.55	5.30	5.61	1.14	1.41	3.27	3.40	4.49	4.44	7.49	8.01	2.00	1.89	2.06	2.85	5.10	5.12	7.72	8.45
■ Border (%)	0.91	0.94	4.44	4.45	4.97	5.19	5.53	5.94	2.29	2.44	7.83	8.53	5.32	5.68	7.75	8.35	3.40	3.27	2.38	10.33	6.27	7.03	8.69	9.45
■ Corner (%)	1.74	1.57	5.92	6.64	5.02	5.37	5.87	6.15	3.84	3.79	8.49	9.25	5.22	5.64	7.71	8.18	4.85	4.55	2.69	10.68	6.62	7.63	8.90	9.65

Condition	L/D	H/L	L (m)	H (m)	D (m)
C1	35.5	1.25	22.4	28	0.63
C2	35.5	3	22.4	67.2	0.63
C3	50	1.25	31.5	39.37	0.63
C4	50	3	31.5	94.5	0.63

Figure 4.13. Percentage of Load increase by negative friction (%).

	M3 3x3 C				M6 3x3 T				M4 4x4 C				M7 4x4 T				M5 5x5 C				M8 5x5 T			
	C1	C2	C3	C4	C1	C2	C3	C4	C1	C2	C3	C4	C1	C2	C3	C4	C1	C2	C3	C4	C1	C2	C3	C4
Center (m)	14.20	0.54	1.86	0.73	11.27	15.21	9.99	10.26	15.52	15.21	16.19	17.03	12.16	11.24	14.24	14.79	16.54	14.41	14.86	16.77	14.69	13.94	14.74	15.35
Border (m)	12.11	11.69	14.61	13.70	10.76	13.41	10.78	10.69	14.54	13.41	16.52	17.04	11.81	10.91	14.24	14.93	13.86	15.43	19	19	13.39	12.94	17.04	17.44
Corner (m)	11.20	10.61	13.52	13.56	10.78	12.69	10.98	11.21	13.66	12.69	17.09	17.38	11.75	10.56	14.9	14.76	13.81	14.69	19	19	13.44	13.61	17.82	17.53

Condition	L/D	H/L	L (m)	H (m)	D (m)
C1	35.5	1.25	22.4	28	0.63
C2	35.5	3	22.4	67.2	0.63
C3	50	1.25	31.5	39.37	0.63
C4	50	3	31.5	94.5	0.63

Figure 4.14. Neutral Point Location.

As observed in Figure 4.13 and Figure 4.14, the corner pile developed greater negative friction since it is given by the weight of the soil volume that is transferred to the pile which is greater in that position. The corner piles were chosen to present the comparison between all the models in the different conditions.

As mentioned by Leung 2004, the shifting on the neutral point plane reflects the relative movement between the pile and the surrounding soil. Thus, in piles from configurations that developed higher negative friction (M5 and M8), the neutral point is located higher when compared between all (Figure 4.14 and Figure 4.16). On the contrary, M3 and M6 with less negative friction have the neutral point located lower than the midpoint of the piles around 0.6L.
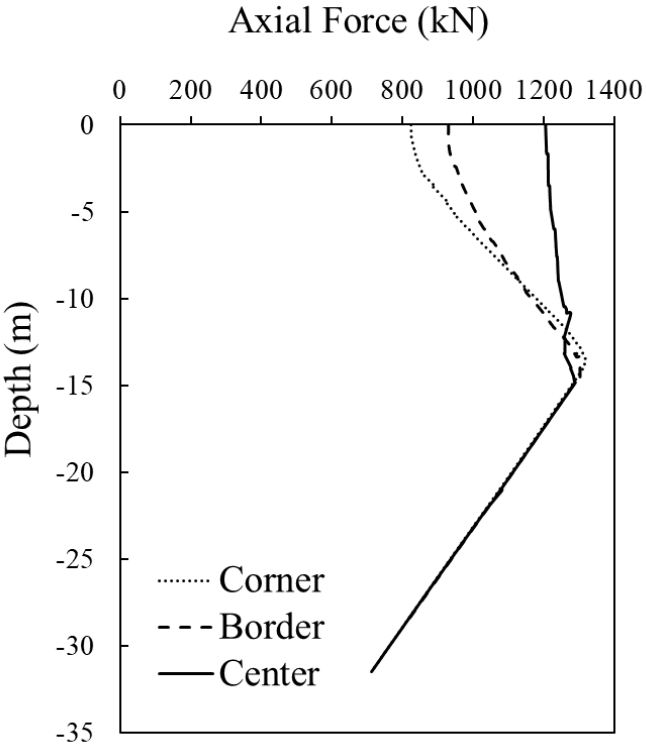
Figure 4.15. Axial force for model M3 with the condition C4.
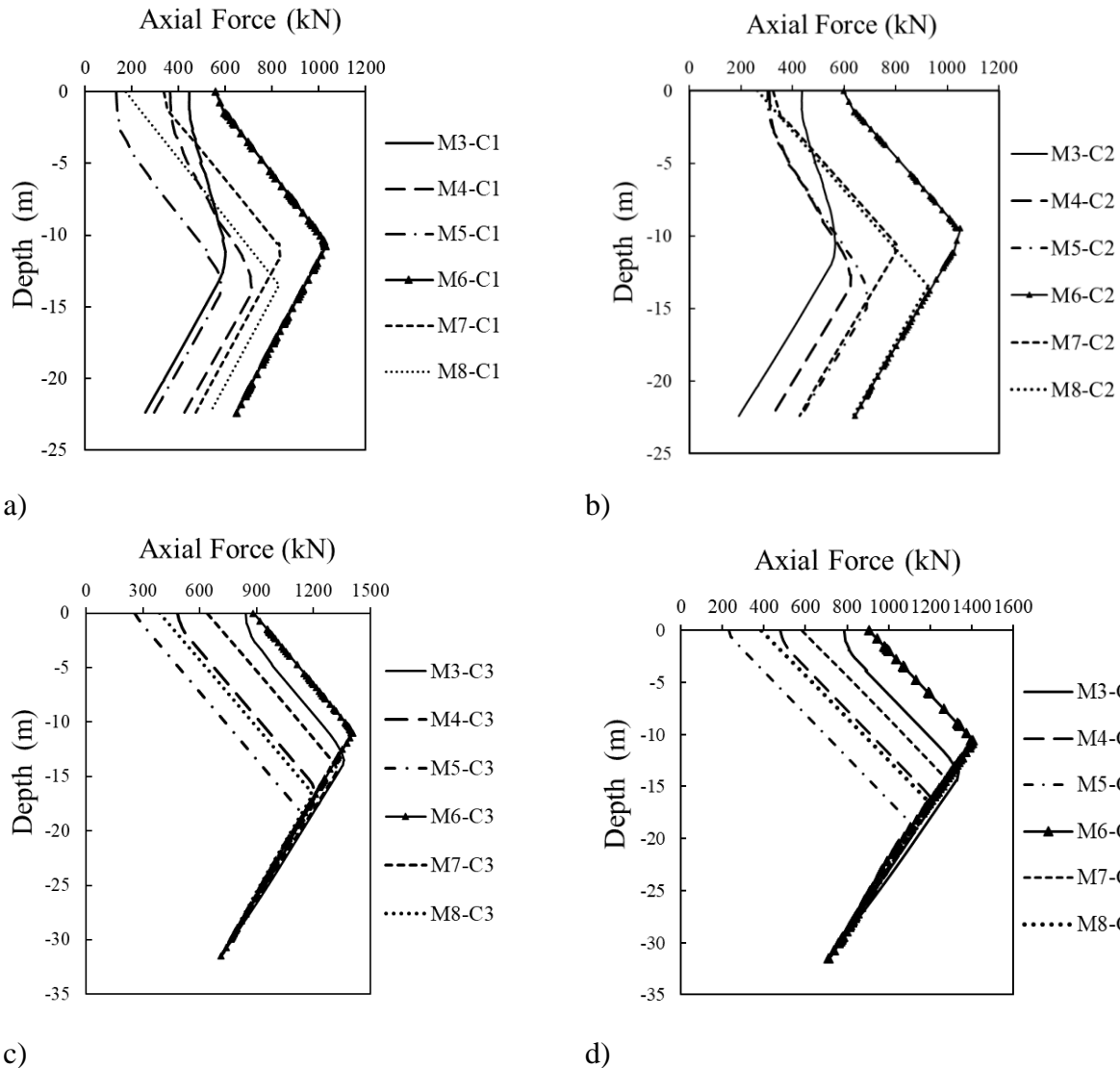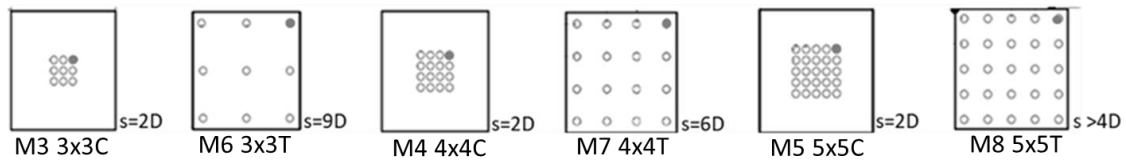
Figure 4.16. Negative friction developed along the corner piles: a) C1, b) C2 c) C3 and d) C4.

4.3 Proposed Reduction factors (*CR*) and graphs of ALM Vs CR

As mentioned by Melo (2018), quantifying negative friction depends on numerous variables and a faster and more simplified way of considering this axial load in design is through reduction factors, as proposed by Jeong et al. (1997). The factors proposed by the authors apply to the magnitude of negative friction estimated for an individual pile. The methodology

proposed recommended reduction factors for square groups of 9 to 25 piles with s= 2.5D and 5D (Table 4.4).

When comparing the methodology proposed by them and this research, it is noted that authors analyzed the negative friction developed in the piles of a group caused by overload, unlike this work, in which it was analyzed the negative friction due to water pore pressure drawdown. Furthermore, they didn't consider the raft stiffness and the geotechnical model used by them is not representative of the conditions presented in the soil that was used in this work.

Having similar soil conditions and purpose of study (negative friction-regional subsidence), were compared (to expand and propose) the reduction factors used in the simplified methodology proposed by Melo (2018) (Table 4.5) as follows:

$$NF = C_R \, C_F \qquad\qquad \textbf{(4.7)}$$

Where C_F is the pile shaft limit lateral load capacity in undrained conditions and C_R is the proposed reduction factors given by Equation (4.8):

$$C_R \; = \frac{NF}{C_F} \qquad\qquad \textbf{(4.8)}$$

Table 4.4. Negative friction reduction factors (modified - Jeong et al., 1997).

	s=2.5D			s=5D		
Groups	**Corner pile**	**Perimeter pile**	**Interior pile**	**Corner pile**	**Perimeter pile**	**Interior pile**
3x3	0.58	0.4	0.22	0.93	0.88	0.72
5x5	0.5	0.38	0.19	0.9	0.84	0.65
6x6	0.5	0.38	0.18	0.89	0.82	0.63

Table 4.5. Reduction factors proposed as a simplified methodology for evaluating the negative friction in pile groups (modified – Melo, 2018).

Analysis Type	Raft rigidity	Pile Position	Moderate Water pore pressure drawdown	Extreme Water pore pressure drawdown
Serviceability limit state (SLS)	Flexible	Center	0.15	0.80
		Border	0.20	0.80
		Corner	0.30	0.90
s=7.5D to 10D	Rigid	Center	0.20	0.50
		Border	0.10	0.50
		Corner	0.08	0.60
Ultimate limit state (ULS)	Flexible	Center	0.10	0.40
		Border	0.15	0.50
		Corner	0.15	0.60
s=4D to 6D	Rigid	Center	0.15	0.30
		Border	0.20	0.50
		Corner	0.35	0.80

4.3.1 Graphs proposed

The reduction factors were calculated for each of the configuration's models in the 4 different conditions as presented in Figure 4.17. The results for M3 show that the C_R are very low and, in some cases, equal to zero mainly in the piles center. This can be due to the small spacing (s=2D) that makes the piles behave like one large pile, which does not allow the center pile to perform and develop negative friction.

Also, it can be seen that the C_R increase as the profile presents a greater pore pressure drawdown and greater negative friction is developed on the piles.
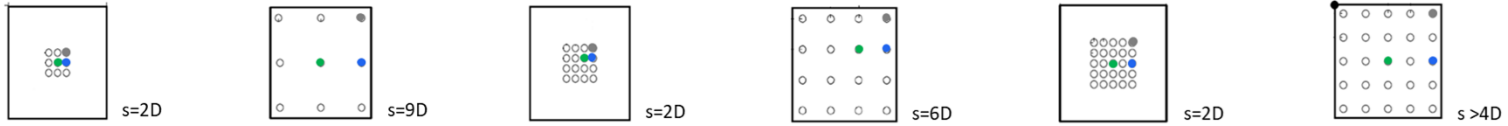
		M3				M4				M5				M6				M7				M8			
		C1	C2	C3	C4	C1	C2	C3	C4	C1	C2	C3	C4	C1	C2	C3	C4	C1	C2	C3	C4	C1	C2	C3	C4
C_R	Center	0.00	0.00	0.01	0.00	0.08	0.09	0.16	0.15	0.14	0.12	0.10	0.13	0.34	0.29	0.26	0.24	0.32	0.28	0.38	0.38	0.38	0.34	0.40	0.41
	Border	0.06	0.07	0.21	0.20	0.16	0.16	0.39	0.40	0.24	0.21	0.48	0.48	0.36	0.33	0.27	0.25	0.38	0.36	0.39	0.39	0.47	0.47	0.45	0.46
	Corner	0.12	0.11	0.28	0.30	0.27	0.24	0.42	0.43	0.34	0.29	0.50	0.50	0.36	0.34	0.28	0.27	0.38	0.36	0.39	0.38	0.49	0.51	0.46	0.47

Condition	L/D	H/L	L (m)	H (m)	D (m)
C1	35.5	1.25	22.4	28	0.63
C2	35.5	3	22.4	67.2	0.63
C3	50	1.25	31.5	39.37	0.63
C4	50	3	31.5	94.5	0.63

Figure 4.17. Reduction factors, C_R.

Although the two research cannot be compared directly due to the different parameters used, Table 4.6 shows the comparison between the parameters and results obtained by Melo (2018) and the ones for M6 model.

Table 4.6. Comparison.

	Analysis type	B=L (m)	Np	D (m)	s (m)	A_L (m^2)	Piles L (m)	Raft	Water pore pressure drawdown	Pile Position	C_R
Melo (2018)	Serviceability limit state (SLS)	15x15	16	0.5	7.5 D	628	25	Rigid	Extreme	Center	0.3
										Border	0.45
										Corner	0.6
M6 (C3-C4)	SLS	14x14	16	0.63	6D	561	31.5	Rigid	Extreme	Center	0.38
										Border	0.39
										Corner	0.42

As the reduction factors obtained in the M6 configuration are consistent, a third proposed graph was analyzed (Figure 4.18) that estimates the value of C_R for piles located in the center, border, and corner of the system, using the area A_{LM} previously defined. The results of the criterion proposed is presented in Figure 4.19.

The reduction factors proposed in this research aim to facilitate the estimation of negative friction in the center, border, and corner piles since this axial load on the foundation with pile groups will be known more quickly. Furthermore, they are representative of typical cases of serviceability and breakdown limit states for drawdown conditions with moderate and extreme pore pressure.
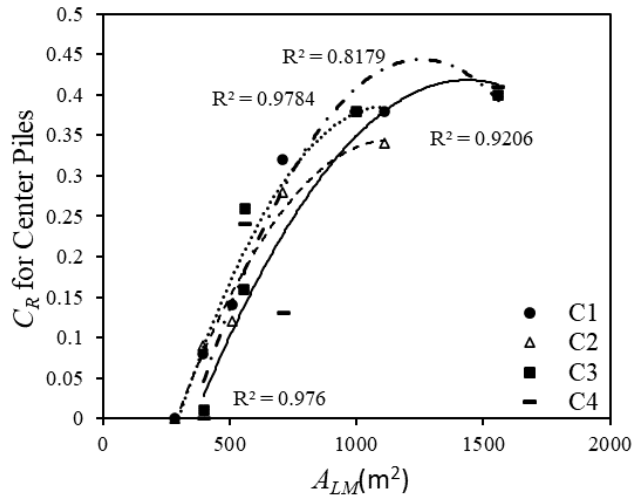
a)
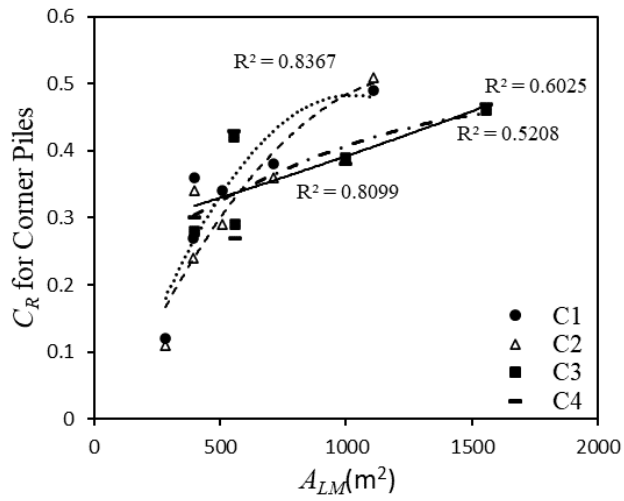
b)
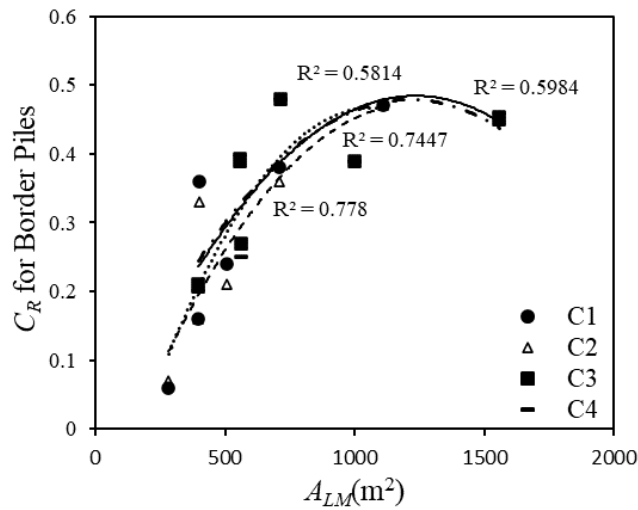
c)

Figure 4.18. C_R : a. C_R for center piles, b. C_R for corner piles, c. C_R for border piles.
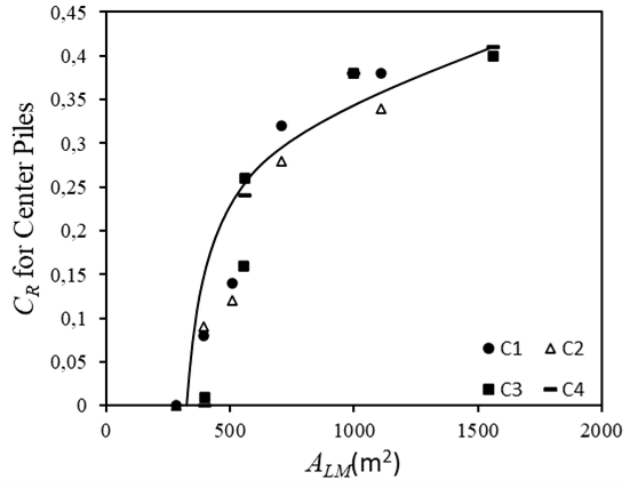
a)
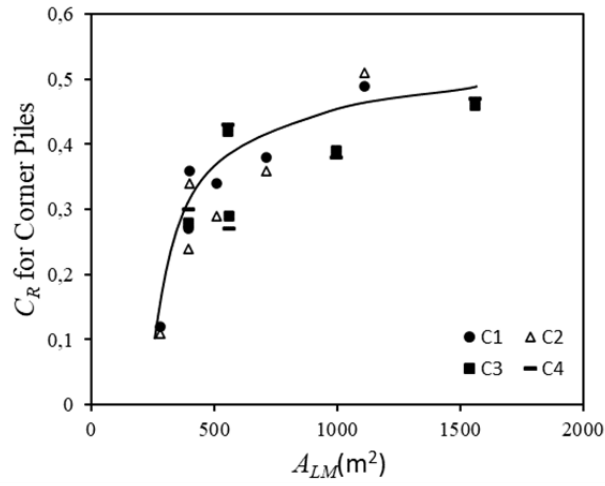
b)
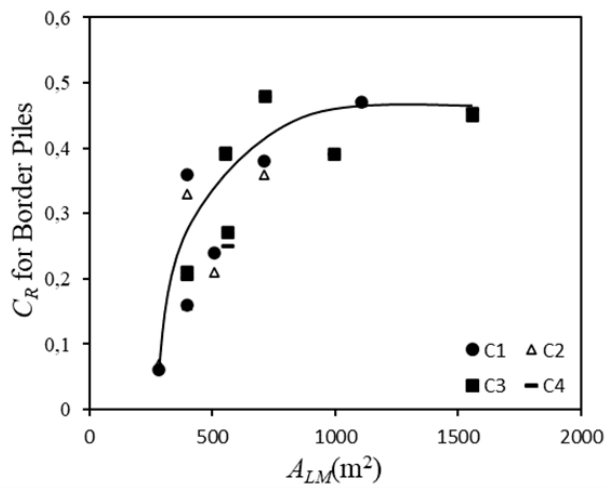
c)

Figure 4.19. C_R graphs proposed: a) C_R for center piles, b) C_R for corner piles, c) C_R for border piles.

4.4 Analyses of displacements and proposed graphs of A_{LM} vs vertical effective displacements

As piled raft systems are used to reduce total and/or differential settlements in soft soils affected by regional subsidence (which causes excessive settlements and therefore possible failures in structures), it was important to assess the vertical effective displacements (δ_{Yeff}) suffered by the models. For each of the models (M3 to M8) simulated with the four conditions (C1 to C4) were established the δ_{Yeff} (normalized in the graph with the pile diameter) profiles along the central axis. The variable δ_{Yeff} predicted for the piled raft is defined as:

$$\delta_{Yeff} = \delta_{Ytotal} - \delta_{Ysub} \tag{4.9}$$

where δ_{Ysub} is the superficial subsidence induced by drawdown pore pressure and δ_{Ytotal} is the total vertical displacement predicted for the piled raft.

Since the C1 and C4 presented the biggest differences between each other, only the vertical displacements reached in each of the stages are discussed next, and the results from the other two conditions (C2 and C3) are in Appendix E.

When load consolidation occurs (Stage 2), the vertical displacements in the configurations with more piles and distributed in the whole raft (T) are smaller compared to the displacements achieved by the other configurations, as expected (Figure 4.20 and Figure 4.21).
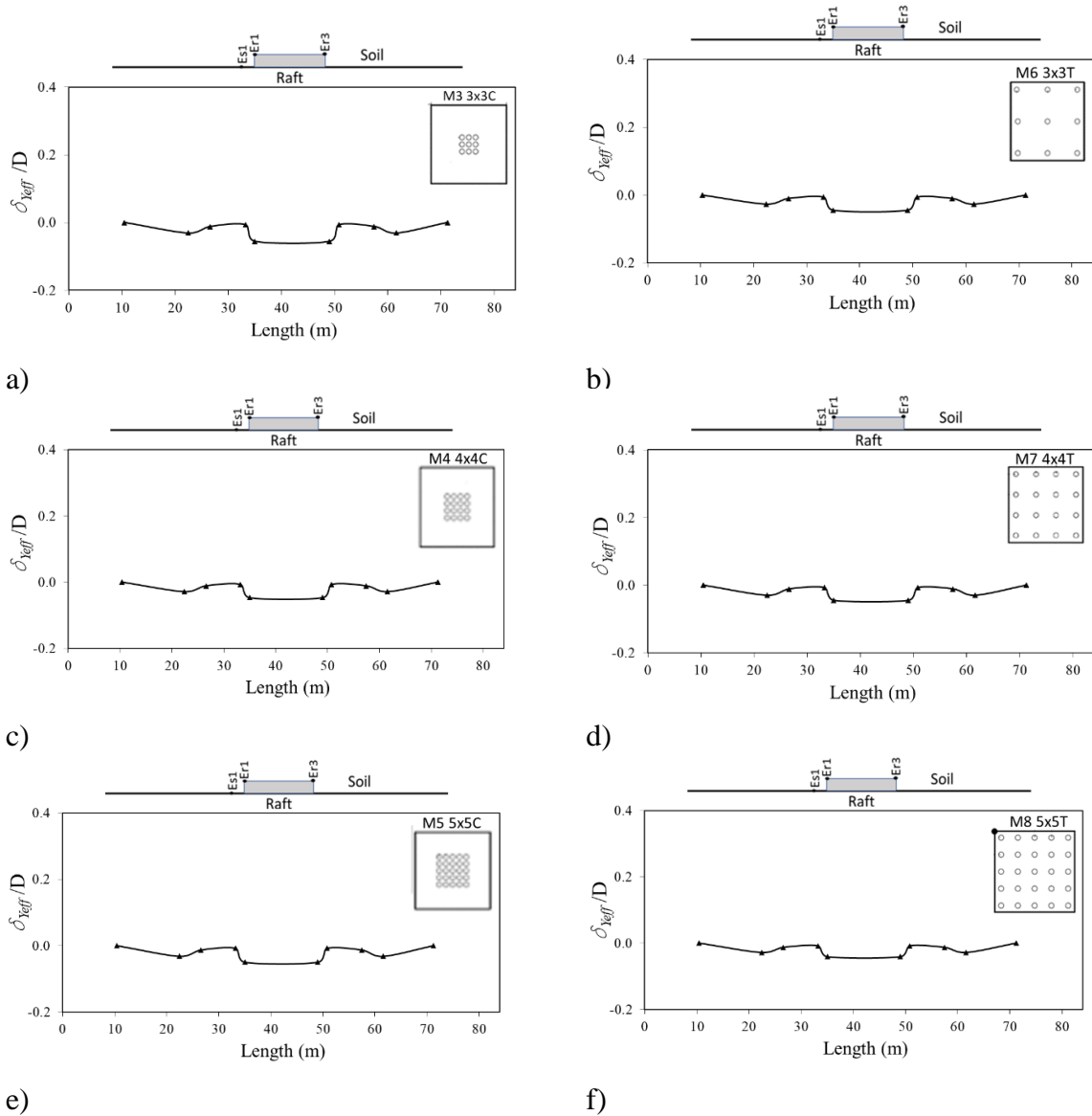
Figure 4.20. Normalized vertical effective displacements (δ_{Yeff}/D) vs length profile for Condition 1 (C1) in Stage 2: a) M3, b) M6, c) M4, d) M7, e) M5 and f) M8.
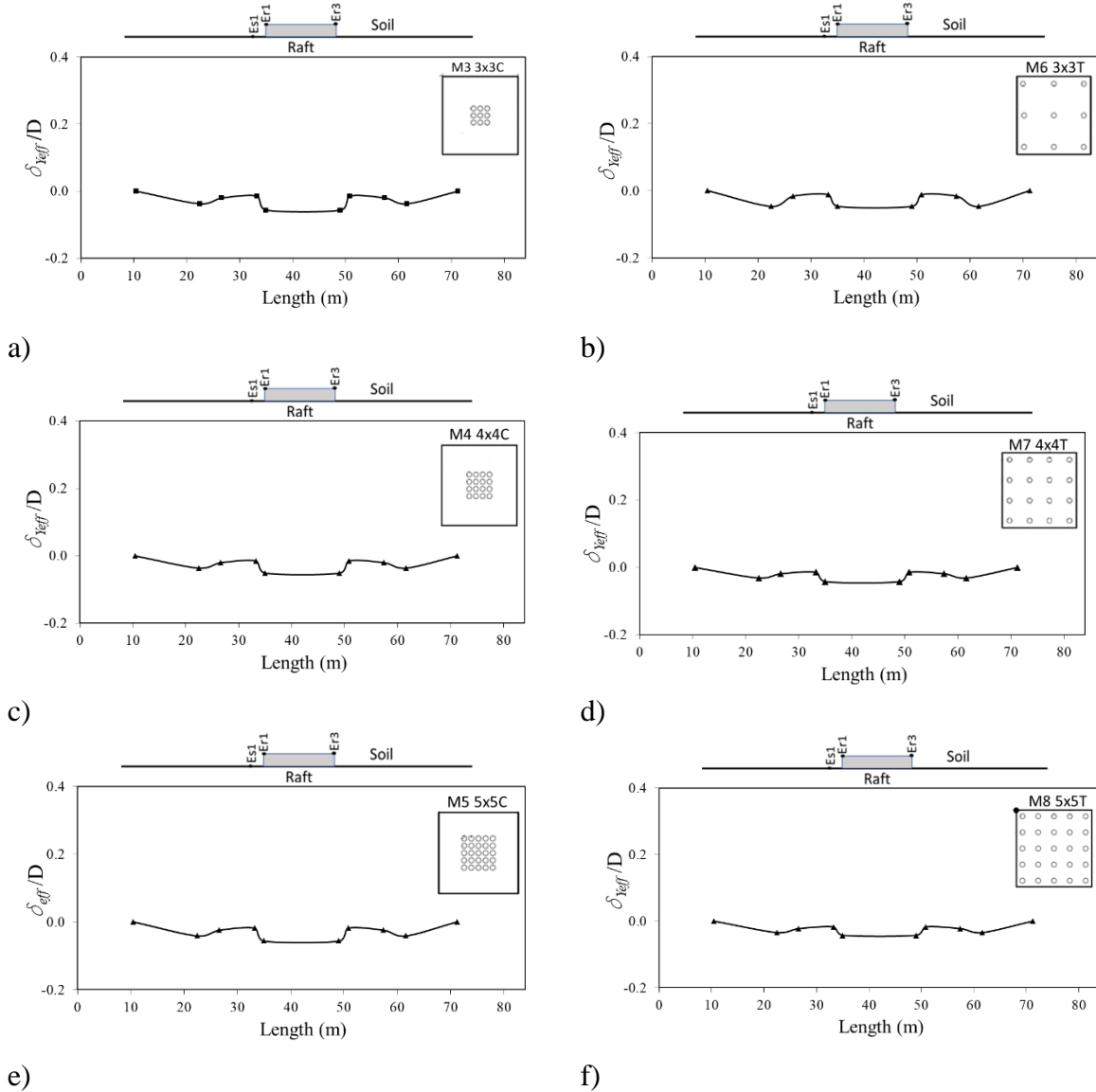
Figure 4.21. Normalized vertical effective displacements (δ_{Yeff}/D) vs length profile for Condition 4 (C4) in Stage 2: a) M3, b) M6, c) M4, d) M7, e) M5 and f) M8.

When the drawdown pore pressure occurred (Stage 3), greater vertical displacements were generated in the configurations with piles in the center (M3, M4, and M5) compared to lower values obtained with the piles distributed throughout the raft (M6, M7, and M8) (Figure 4.22 and Figure 4.23). At this stage, under conditions C1 and C2, the piled raft accompanies the displacements generated by regional subsidence. On the other hand, in conditions C3 and C4 there is an apparent protrusion that occurs when the system is not capable of accompanying the settlement of the soil layer (Figure 4.23c to Figure 4.23f). This is due to an extreme effect generated by regional subsidence and over-reinforcement of the system, that is, the number of piles is greater than what would be necessary. The apparent protrusion can cause the separation

130

of the raft (item 4.1 and 4.1.1) and the rupture of the supporting structure. It is necessary to clarify that this does not occur in the M3 and M6 models, precisely because of the lower number of piles in the system. It is necessary to clarify that this does not occur in M3 and M6 models, because of the lower number of piles in the system.

It is evident that a system with more piles is not necessarily more efficient. As already mentioned, the objective of piled raft type foundations is to be able to reduce total and differential settlements, either directly or by accompanying the vertical displacements produced in soils susceptible to regional subsidence problems.
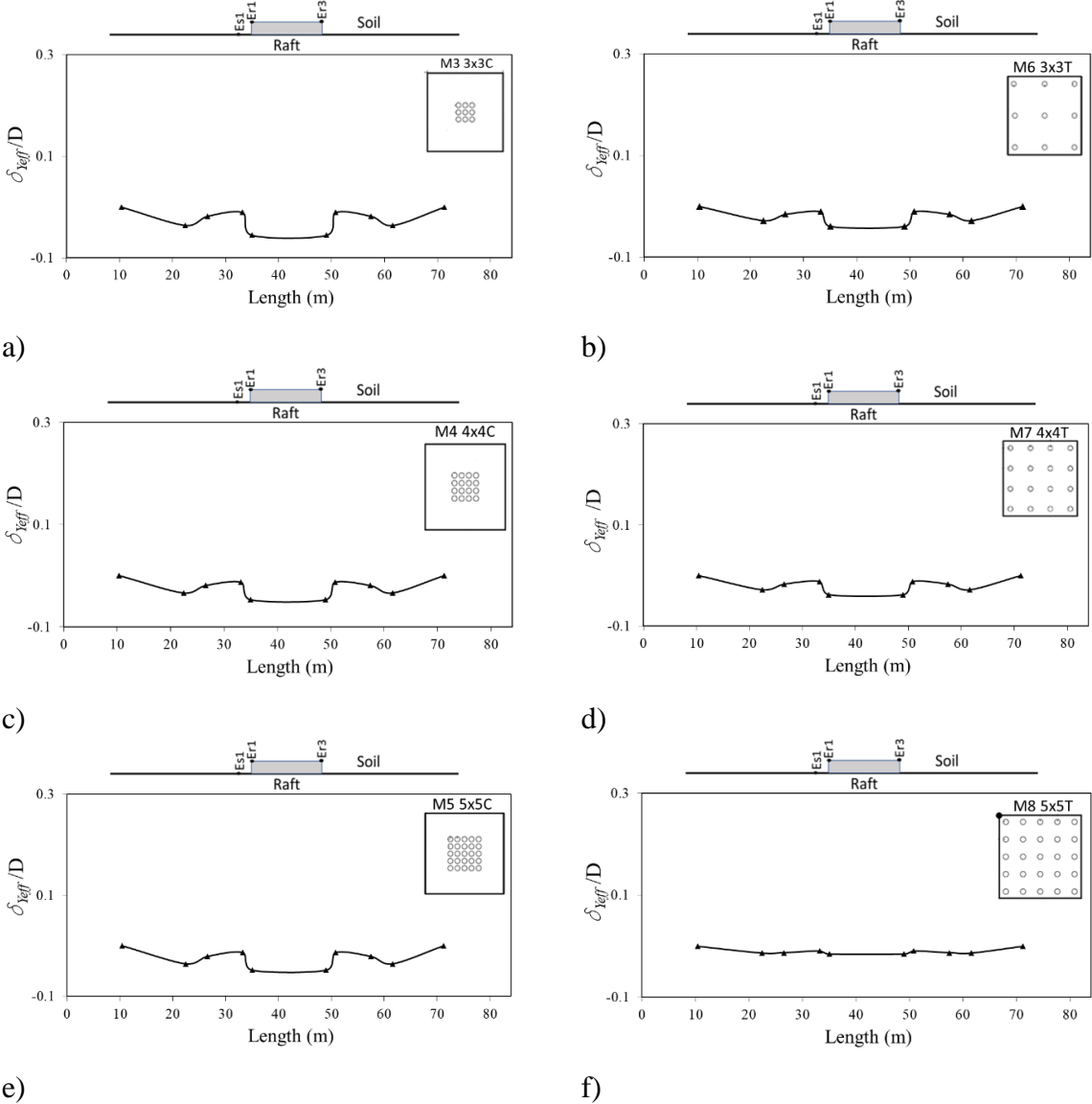
Figure 4.22. Normalized vertical effective displacements ($\delta_{Yeff}/$D) vs length profile for Condition 1 (C1) in Stage 3: a) M3, b) M6, c) M4, d) M7, e) M5 and f) M8.
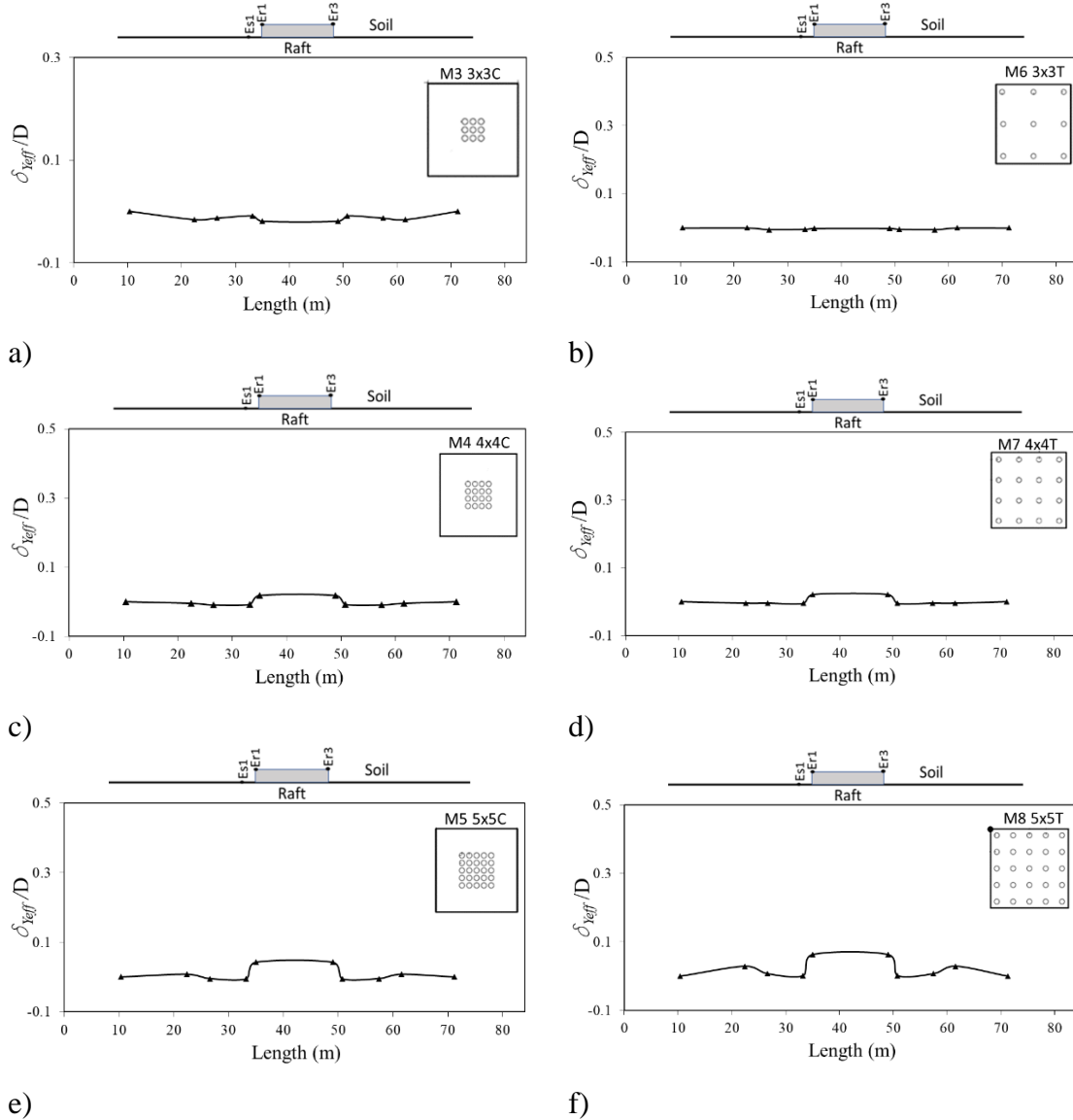
Figure 4.23. Normalized vertical effective displacements (δ_{Yeff}/D) vs length profile for Condition 4 (C4) in Stage 3: a) M3, b) M6, c) M4, d) M7, e) M5 and f) M8.

4.4.1 Graphs proposed

As in the previous items, the A_{LM} area is related to the δ_{Yeff} to propose graphs that allows estimating the settlement value when piled raft systems are used in soft soils prone to regional subsidence. As shown in Figure 4.24a, it is possible to estimate the δ_{Yeff} when load consolidation occurs (Stage 2).

When the water drawdown pore pressure occurs (Stage 3), vertical displacements equivalent to the system settlement or an apparent protrusion can be estimated as previously mentioned (Figure 4.24b).
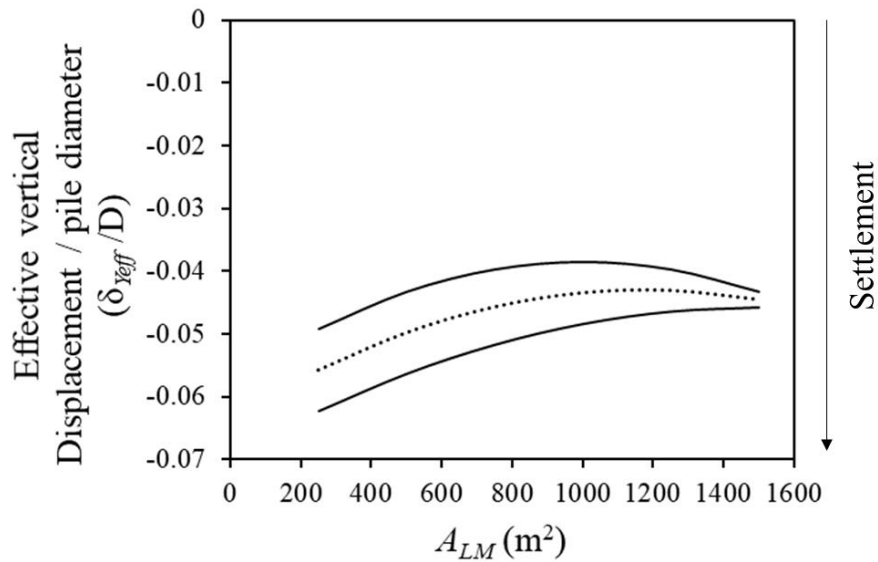
a)
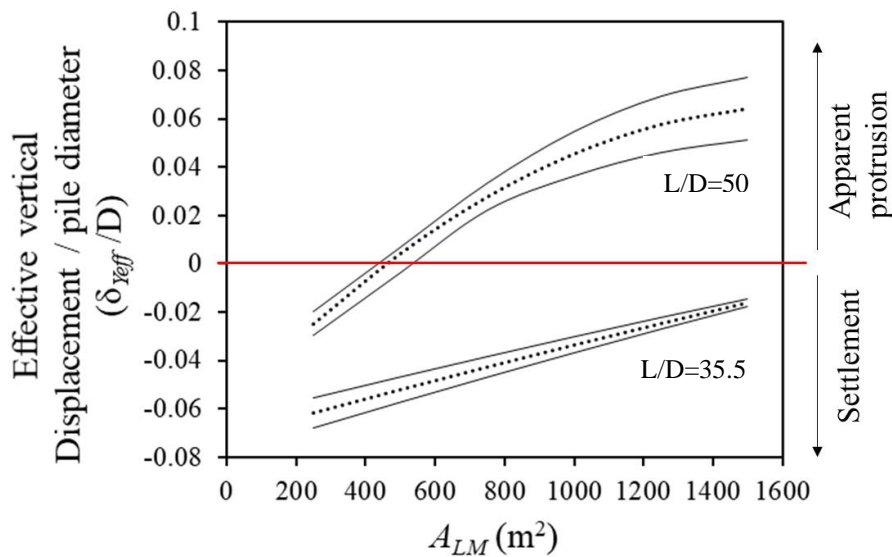
b)

Figure 4.24. Graphs proposed for predicted Effective vertical displacement/ pile diameter (δ_{Yeff}/D) *vs* Minor Lateral Area (A_{LM}): a) Stage 2 b) Stage 3.

4.5   Chapter summary

This chapter has presented the results of a parametric analysis carried on for the models M3 to M8 with four different conditions (C1, C2, C3, and C4), varying geometric parameters that are described in Table 4.1. Three main aspects were assessed with the results obtained from the models: loads. Negative friction and displacements.

It was assessed the load transfer mechanism in the system in both stages (load and drawdown water pore pressure) for each of the elements of the piled raft as presented in Table 4.3. The Filling Factor (FF) was used as one of the criteria to analyze the load in the system (Figure 4.5). It was observed that for all models in the four conditions, the raft assumes the highest percentage of the total load in stage 2 (initial loading stage). This load percentage decreases in stage 3 (drawdown water pore pressure) and can be due to an increase in the resistance at the pile-soil interface that favors a load transfer from the raft to the piles.

The results obtained showed that adherence is an important factor regarding the load capacity and response in general of this type of system. Consequently, a lateral area criterion was described and used to also assess the transfer load between the system elements. From the results obtained a graph was proposed between the minor lateral area (A_{LM}), among the sum of the pile's lateral areas (A_{L1}) and the lateral area assuming a big pile that wraps around the pile group (A_{L2}), and the percentage of load reaching the piles in both stages. The graph was presented in Figure 4.11.

It was presented the results of the negative friction developed in three piles located in different positions in the raft (Figure 4.13) for all the configurations in the four proposed conditions. Results showed that the slenderest piles located at the border and corner of the raft are the ones that developed most of the negative friction load, as expected, since the center piles receive mainly the head load or at the tip. When the models with the same number of piles are compared, it can be observed that when s> 2D a higher percentage of negative friction is generated, mainly for conditions C1 and C2. For all models in conditions C3 and C4, the negative friction value increases more than double in the center pile, which does not happen with the border and corner piles.

In Figure 4.14 and Figure 4.16 the results obtained for the neutral point were presented. Thus, in piles from configurations that developed higher negative friction (M5 and M8), the neutral point is located higher when compared between all. On the contrary, M3 and M6 with less negative friction have the neutral point located lower than the midpoint of the piles around 0.6L.

Quantifying negative friction depends on numerous variables and a faster and more simplified way of considering this axial load in design is through reduction factors, as proposed by Jeong

et al. (1997). The factors proposed by the authors apply to the magnitude of negative friction estimated for an individual pile.

With the aim of finding a simpler and faster way to analyze, evaluate or/and quantify the negative friction, the methodologies proposed by Jeong et al. (1997) and Melo (2018) were introduced. These methodologies propose reduction factors for specific conditions presented in Table 4.4 and Table 4.5. Using the methodologies and the results obtained in this research, new reduction factors were proposed (Figure 4.16). It was also proposed a graph in Figure 4.19, that estimates the value of C_R or piles located in the center, border, and corner of the system, using the area A_{LM} previously defined.

It was assessed the displacements generated by the load consolidation but also the ones due to the regional subsidence. From the results, it was observed that piled raft systems that have piles grouped in the center of the raft have a higher settlement compared to those that have piles distributed throughout the raft area.

In Figure 4.23 it was observed that an apparent protrusion in the models with more piles occurs when the system is not capable of accompanying the excessive settlement of the soil layer. This is due to an extreme effect generated by regional subsidence and over-reinforcement of the system.

At last, it was also suggested to relate the area A_{LM} with the maximum vertical displacements to propose a criterion that allows estimating the settlement value when piled raft systems are used in soft soils (Figure 4.24).

CHAPTER 5

5. CONCLUSIONS AND RECOMMENDATIONS

In this research, a numerical model using the finite element method, that represents the behavior of a piled raft system founded on a soft consolidating soil, was developed based on physical models tested in a centrifuge by Rodríguez (2016). This soil profile was composed by three layers of soft soil (kaolin) divided into two layers that work as a filter and a bottom layer as drainage, and was modeled using The Hardening Soil constitutive model. The configuration of the piled raft that is being used for the calibration is a model with nine piles distributed in the raft center. Also, a parametric analysis was carried out with varying geometric parameters and conditions of different configuration models, a total of 50 numerical analyses.

The conclusions obtained through the calibration and the parametric analysis carried out with the three-dimensional numerical modeling in this present research are:

5.1   Conclusions

- It was possible to develop a three-dimensional numerical model of finite elements that reproduces soil and foundation structure displacements due to not only to consolidation caused by load, but also to drawdown of the water pore pressure (regional subsidence).

- The model is very sensitive to the resistance of the interface generated between soil-pile, which makes the calculation of this parameter very important. It can be observed that when both shaft and base pile resistance is reduced 25% of its initial value, the load taken by the raft increases in a 60% in the load-consolidation stage.

- The resistance that the embedded pile element used does not consider the change of the resistance when the soil is modified by the process that had suffered (drawdown pore pressure stage). Regarding displacement values, it can be concluded that they do not change in a large magnitude when this parameter is modified.

136

- It was possible to assess the load transfer mechanism that occurs in the system when the drawdown water pore pressure occurs and to establish a proportion of the load that was assumed by each of the elements in both stages.

- When the results were analyzed with the Filling Factor (FF), including all models in the four conditions, it can be noticed that the raft assumes the highest percentage of the total load in stage 2 (initial loading stage). This load percentage decreases in stage 3 (regional subsidence) and can be due to an increase in the resistance at the pile-soil interface that favors a load transfer from the raft to the piles, or a separation of the raft and the supporting soil. This is so, since the settlement suffered by the soil can be greater than the one from the whole system, causing the component to completely lose its load capacity. Moreover, it can result in their rupture if the project was carried out with operating loads very close to the maximum theoretical load conditions.

- Based on the results, it was established that in extreme cases of regional subsidence, the loss of contact between the raft-soil could occur, since it was observed was that in some models the piles assume 100% of the total load when the drawdown pore pressure happens.

- Piled Raft systems with the piles distributed in the whole area of the raft(T) are more efficient since they receive higher loads with similar settlements. In these cases, the load percentage assumed by the raft is less than the percentage assumed by the piles, which is an advantage in cases where a separation between the soil surface and the raft eventually occurs.

- It was observed, that with the regional subsidence phenomenon, the piled raft must be analyzed with different criteria than those usually considered. The results obtained showed that adherence is an important factor when regarding the load capacity, and the response in general of this type of system. Consequently, a graph was proposed between the minor lateral area (A_{LM}), between the sum of the pile's lateral areas (A_{L1}) and the lateral area assuming a big pile that wraps around the pile group (A_{L2}), with the percentage of load reaching the piles in both stages.

- The axial load on the pile induced by negative friction depends on the position of the pile within the group and the spacing between the piles. When the models with the same

number of piles are compared, it can be observed that when s> 2D a higher percentage of negative friction is generated.

- When the configuration has s≤2D the piles are working as a group and the center pile developed almost no negative friction. The slenderest piles located at the border and corner of the raft are the ones that developed most of the friction load as expected since the center piles receive mainly the head load or at the tip.

- The corner pile developed greater negative friction since it is given by the weight of the soil volume that is transferred to the pile which is greater in that position.

- The neutral point (NP) of a pile depends on a balance of acting and resisting forces that develop along it. When there is an increase in negative friction due to pore pressure drawdown (stage 3), a greater depth location of the NP in the pile is observed, varying slightly from the previous level (in stage 2).

- There is a range of neutral level depth for the center, border, and corner piles within a group. This depth is generally less for corner and border piles than for piles in the center.

- Thus, in piles from configurations that develop higher negative friction (s> 2D), the neutral point is located higher when compared between all. On the contrary, models with less negative friction (s≤2D) have the neutral point located lower (near the pile tip) than the midpoint of the piles around 0.6L.

- Reduction factors (C_R) were determined for the shaft resistance as a design tool to obtain the negative friction magnitude of piles located in the center, border, and corner of the raft. A graph between the C_R and the A_{LM} was proposed for each of the piles in three different locations (center, border, and corner).

- The reduction factors and the graphs proposed in this research will facilitate the estimation of the negative friction, once the axial load on the foundation with groups of piles will be quickly known to be considered in a design.

- Regarding foundation settlements, it was observed that there is an indirect way of analyzing the development of negative friction in piles, as this load has a direct effect on the magnitude of vertical displacements of the foundation.

- It was shown that piled raft systems that have piles grouped in the center of the raft have a higher settlement compared to those that have piles distributed throughout the raft area since settlements are influenced by the spacing and the number of piles.

- It was observed that an apparent protrusion in the models with more piles that occurs when the system is not capable of accompanying the excessive settlement of the soil layer. This is due to an extreme effect generated by regional subsidence and over-reinforcement of the system, that is, the number of piles is greater than what would be necessary. This apparent protrusion can cause the separation of the raft and the rupture of the supporting structure.

- It is also evident that a system with more piles is not necessarily more efficient, and an exercise of optimization needs to be carried out to have a good cost-efficiency foundation design.

- A graph was proposed for predicted Effective vertical displacement/ pile diameter (δ_{Yeff}/D) vs Minor Lateral Area (A_{LM}) for piled raft systems founded in soft soils that suffer regional subsidence. This graph is of extreme practical importance but must be tested and validated in field situations

5.2   Recommendations

This research studied the behavior of piled raft systems founded in soft soils suffering regional subsidence, trying to cover a reasonable number of parameters. However, having already a calibrated model and knowing that the problem studied is a complex one in which many variables are involved, future research and parametric analysis can be concentrated on the following aspects:

- Variation not only of the pile's diameter but also of relation s/D to expand the knowledge and look for the possibility of new graphs that help in the design of the system.

- Analysis of the relative rigidity of the raft and piles, controlling the ratio between the raft thickness and the pile diameter. This relationship influences the conditions for distributing the load in the head of the piles and the proportion that is assumed by these.

- Analysis of the piled raft behavior when subjected to a different percentage of drawdown pore pressure.

REFERENCES

ALBERRO, J. & HERNÁNDEZ, R. (2000). Proceso de consolidación y fricción negativa inducida, en pilas, pilotes y muros. Series del Instituto de Ingeniería, UNAM, 619: 61.

ALNUAIM, A.M., EL NAGGAR, M.H. & EL NAGGAR, H. (2018). Performance of micropiled rafts in clay: Numerical investigation. Computers and Geotechnics, 99: 42–54.

ALNUIAM, A.; EL NAGGAR, H. & EL NAGGAR, M. H. (2013). Performance of piled-raft system under axial load. 18th International Conference on Soil Mechanics and Geotechnical Engineering, Paris, France, 2417: 2663-2666.

AUVINET-GUICHARD, G. & RODRÍGUEZ-REBOLLEDO, J.F. (2017). Criteria for the design of friction piles subjected to negative skin friction and transient loads. Ingeniería, investigación y tecnología. 18: 279-292

AUVINET, G. & HANELL, J.J. (1981). Negative skin friction on piles in Mexico city clay. 10th International Conference on Soil Mechanics and Foundation Engineering, ICSMFE, Stockholm, Sweden, 4:7.

AUVINET, G. & DÍAZ-MORA, C. (1981). Programa de computadora para predecir movimientos verticales de cimentaciones. Instituto de Ingeniería Series, UNAM, 438.

AUVINET, G. & RODRÍGUEZ-REBOLLEDO, J.F. (2001). Friction piles in consolidating soils. 15th International Conference on Soil Mechanics and Foundation Engineering, ICSMFE, Istanbul, Turkey, 843–846.

AUVINET, G., & RODRÍGUEZ, J.F. (2002). Modelling of friction piles in consolidating soils. International Deep Foundations Congress, IDFC, Orlando, Florida, 224-235.

BAJAD, S.P. & SAHU, R.B. (2008). An experimental study on the behaviour of vertically loaded piled raft on soft clay. 12th International Association for Computer Methods and Advances in Geomechanics, IACMAG, Goa, India, 84-91.

BALAKUMAR, V. (2008). Experimental Studies of Model Piled Raft on Sand and Field Study of Prototype Behavior. PhD Thesis, Anna University, Chennai India, 358.

BANERJEE, S., JOY, M. & SARKAR. (2016). Parametric Study and Centrifuge-Test Verification for Amplification and Bending Moment of Clay–Pile System Subject to Earthquakes. Geotechnical and Geological Engineering 34:10.

BAREÑO, E & RODRÍGUEZ, E. (1999). Clays Shrinkage (in Spanish). Undergraduate Thesis, Universidad Nacional de Colombia, Bogotá, Colombia. 155.

BJERRUM, L., JOHANNESSEN, I.J., & EIDE, O. (1969). Reduction of negative skin friction on steel piles to rock. 7th International Conference on Soil Mechanics and Foundation Engineering, ICSMFE, México DF, México, 2:27-34.

BOWLES, J.E. (1997). Foundation analysis and design. McGraw-Hill, New York, EEUU, 5th ed. 1024.

BOZOZUK, M. (1972). Downdrag Measurements on a 160-Ft Floating Pipe Test Pile in Marine Clay. Canadian Geotechnical Journal, 9:127-136.

BRIANÇON, L., HAZA-ROSIER, E., THOREL, L., DAMIEL, D. & COMBARIEU, O. (2011). Recommendations for design, construction and control of rigid inclusion ground improvements. IREX's Soil Specialist Cluster, 317.

BRIAUD, J. L., JEONG, S., Y BUSH, R. (1991). Group effect in the case of downdra, Geotechnical Engineering Congress, GEC, Colorado, EEUU, 1:505-518.

BRINKGREVE, R.B.J., KUMARSWAMY, S., & SWOLFS, W. M. (2018). Reference Manual PLAXIS 3D, 470.

BRINKGREVE, R.B.J., KUMARSWAMY, S., & SWOLFS, W. M. (2018). Material Models Manual PLAXIS, 240.

BROWN, P.T. (1969a). Numerical analyses of uniformly loaded circular rafts on deep elastic foundations. Geotechnique, 19:399-404.

BROWN, P.T. (1969b). Numerical analyses of uniformly loaded circular rafts on elastic layers of finite depth. Geotechnique, 19:301-306.

BROWN, P T; WIESNER, T.J. (1975). The behaviour of uniformly loaded piled strip footings. Soils and foundations, 15:13–21, 1975.

BURLAND, J.B. (1967). Deformation of soft clay. University of Cambridge, Cmbridge, England.

BURLAND, J.B, KALRA, J.C. (1986). Queen Elizabeth II Conference Centre: Geotechnical aspects. Proceedings of the Institution of Civil Engineers, 80:1479–1503.

CANADIAN GEOTECHNICAL SOCIETY (1978). Canadian Foundation Engineering Manual. Canadian Geotechnical Society. Foundations Committee. 399.

CHAN. R.K.S. (2006). Negative Skin Friction on Piles in Consolidating Ground. Master Thesis. Hong Kong University of Science and Technology, Hong Kong, China, 319.

CHENG, Song e colab. Centrifuge modeling of response of bridge due to exploiting groundwater. Yantu Lixue/Rock and Soil Mechanics, 2011.

CHO, J., LEE, J. H., JEONG, S., & LEE, J. (2012). The settlement behavior of piled raft in clay soils. Ocean Engineering, 53:153-163.

CHOW, Y.K., YONG, K.Y., & SHEN, W.Y. (2001). Analysis of piled raft foundations using a variational approach. International Journal of Geomechanics, 1:129-147.

CHOW, H.S.W. (2007). Analysis of Piled Raft Foundations with Piles of Different Lengths and Diameters. PhD Thesis, University of Sidney, Sidney, Australia, 358.

CHOW, Y.K. (1986). Analysis of vertically loaded pile groups. International journal for numerical and analytical methods in geomechanics, 10:59–72.

CHOW, Y.K. (1987). Iterative analysis of pile-soil-pile interaction. Geotechnique, 37:321–333.

CLANCY, P. & RANDOLPH, M.F. (1993). An approximate analysis procedure for piled raft foundations. International Journal for Numerical and Analytical Methods in Geomechanics. 17:849–869.

COMODROMOS, E.M. & BAREKA, S.V. (2005). Evaluation of negative skin friction effects in pile foundations using 3D nonlinear analysis. Computers and Geotechnics, 32:210-221.

CUI, ZD., TANG, YQ. & YAN, XX. (2010). Centrifuge modeling of land subsidence caused by the high-rise building group in the soft soil area. Environmental Earth Sciences, 59:1819–1826.

CUNHA, R.P., BEZERRA, J.E., ZHANG, H.H. & SMALL J.C. (2004). Back analyzed parameters from piled foundations founded on tropical porous clay. GeoSupport: Innovation and Cooperation in the Geo-Industry, 1-12.

CUNHA, R.P., POULOS, H.G. & SMALL, J.C. (2001). Investigation of design alternatives for a piled raft case history. Journal of Geotechnical and Geoenvironmental Engineering ASCE, 127:635-641.

DAI, G., SALGADO, R., GONG, W. & ZHANG, Y. (2012). Load test on full-scale bored pile groups. Canadian Geotechnical Journal, 49:1293-1308.

DAO, T.P.T. (2011). Validation of PLAXIS embedded piles for lateral loading. Magister's dissertation, Delft University of Technology, Delft, Holland, 113.

DAVIS, E.H. & POULOS, H.G. (1972). Rate of settlement under two-and three dimensional conditions. Geotechnique, 22:95–114.

DUNCAN, J.M. & CHANG, CY. (1970). Nonlinear analysis of stress and strain in soils. Journal of Soil Mechanics & Foundations Division, ASCE, 96:1629–1653.

DURÁN, J.E. (2003). Optimizing a piled raft foundation system in the lake Bogotá deposit. (In Spanish). III Encuentro Nacional de Ingenieros de Suelos y Estructuras, Escuela Colombiana de Ingeniería "Julio Garavito", Bogotá, Colombia, 2-65.

EL-MOSSALLAMY. Y. (2011). Modelling the behaviour of piled raft applying PLAXIS 3D Foundation Version 2. PLAXIS Practice: 10-13.

EL-MOSSALLAMY, Y., LUTZ, B. & RICHTER, T. (2006). Innovative application of piled raft foundation to optimize the design of high-rise buildings and bridge foundations. 10th Arab Structural Engineering Conference, Kuwait city, Kuwait, 347-358.

EL-MOSSALLAMY, Y. & FRANKE, E. (1997). Piled rafts: numerical modelling to simulate the behaviour of piled raft foundations. ARCADIS, Trischler & Partner, 4.

ELWAKIL, A.Z. & AZZAM, W.R. (2015). Experimental and numerical study of piled raft system. Alexandria Engineering Journal, 55:547-560p.

ENDO, M., KAWASAKI, T. & SHIBATA, T. (1969). Negative skin friction acting on steel pipe pile in clay. 7th International Conference on Soil Mechanics and Foundation Engineering, ICSMFE, México DF, México, 2:86-92.

ERGUN, M.U., & SÖNMEZ, D. (1995). Negative skin friction from surface settlement measurements in model group tests. Canadian Geotechnical Journal, 32: 1075-1079.

FELLENIUS, B. H. (1984). Negative skin friction and settlement of piles. 2nd International Seminar Pile Foundations, Nanyang Technological Institute, Singapore, 18.

FRANKE, E., LUTZ, B. & EL-MOSSALLAMY, Y. (1994). Measurements and numerical modelling of high rise building foundations on Frankfurt clay. American society of civil engineers, ASCE, 1325–1336.

FULLER, M.L. (1908). Summary of the controlling factors of artesian flows. US Government Printing Office, 319:51.

GARZÓN, J.C. (2011). Evaluation of settlements for consolidation generated by lowering water table (In Spanish). Magister's dissertation. Universidad Nacional de Colombia. Bogotá, Colombia, 120.

GOH, S.H. & ZHANG, L. (2017). Estimation of peak acceleration and bending moment for pile-raft systems embedded in soft clay subjected to far-field seismic excitation. Journal of Geotechnical and Geoenvironmental Engineering, 143.

GU, L., WANG, Z., HUANG, Q., YE, G., & ZHANG, F. (2020). Numerical investigation into ground treatment to mitigate the permanent train-induced deformation of pile-raft-soft soil system. *Transportation geotechnics*, *24*, 100368.

HAIN, S.J. & LEE, I.K. (1978). The Analysis of Flexible Pile Raft System. Geotechnique, 28:65–83.

HEWITT, V.M. (2011). Possible Effects of the Negative Friction over Piles Induced by the Bogota Soils Subsidence Phenome. (In Spanish). Magister's dissertation, Universidad Nacional de Colombia, Bogotá, Colombia, 159.

HOOPER, J.A. (1973). Observations on the behaviour of a piled-raft foundation on london clay. Proceedings of the institution of Civil Engineers. 55:855-877.

HORIKOSHI, K. & RANDOLPH, M.F. (1996). Centrifuge modelling of piled raft foundations on clay. Geotechnique, 46:741-752.

HORIKOSHI, K.; RANDOLPH, M.F. A (1998). Contribution to optimum design of piled rafts. Geotechnique, 48:301-317.

HUANG, T., ZHENG, J.H., GONG, W. (2014). Research on negative skin friction on pile by a simple model experiment. Applied mechanics and materials, 693-696.

INOUE, Y. (1979). Behaviour of negative skin friction on steel pipe pile driven in alluvial deposits. Recent developments in the design and construction of piles, ICE, London, UK, 237-224.

JANBU, N. (1963). Soil compressibility as determined by odometer and triaxial tests. European Conference on Soil Mechanics and Foundation Engineering (ECSMFE), Wiesbaden, Germany, 1:19-25.

JANDA, T., CUNHA, R.P., KUKLÍK, P. & ANJOS, G.M. (2009) Three dimensional finite element analysis and back analysis of CFA standard pile groups and piled rafts founded on tropical soil. Soil and Rocks, v. 32:1, p. 3- 18.

JEONG, S., KIM, S. & BRIAUD, J.L. (1997). Analysis of Downdrag on Pile Groups by the Finite Element Method. Computers and Geotechnics, 21:143-161.

JEONG, S., LEE, J. & LEE, C.J. (2004). Slip effect at the pile-soil interface on dragload.

Computers and Geotechnics, 31:115-126.

KATZENBACH, R e colab. Piled raft foundation: interaction between piles and raft. *Darmstadt Geotechnics*, v. 4, n. 2, p. 279–296, 1998.

KEENAN, G H; BOZOZUK, Michael. Downdrag on a three-pile group of pipe piles. 1985, [S.l: s.n.], 1985. p. 1407–1412.

KEMPFERT, H.G., and GEBRESELASSIE, B. 2006. Excavations and Foundations in Soft Soils. In Excavations and 617 Foundations in Soft Soils. Springer-Verlag, Berlin/Heidelberg.

KHANMOHAMMADI, Mohammadreza; FAKHARIAN, Kazem. Evaluation of performance of piled-raft foundations on soft clay: A case study. *Geomechanics and Engineering*, 2018.

KONDNER, R.L. (1963). Hyperbolic stress-strain response: cohesive soils. Journal of the Soil Mechanics and Foundations Division, 89:115–144.

KUWABARA, F. & POULOS, H.G. (1989). Downdrag forces in group of piles. Journal of Geotechnical Engineering, 115:806-818.

LADE, P.V. (2005). Overview of constitutive models for soils. ASCE Geotechnical Special publication, 184: 1-34.

LAM, S.S.Y, C.W.W., Leung, C. & Chan, S. (2009). Centrifuge and numerical modeling of axial load effects on piles in consolidating ground. Canadian Geotechnical Journal. 46:10-24.

LEE, C.Y. (1993). Pile groups under negative skin friction. Journal of geotechnical engineering, 119:1587–1600.

LEE, C. J., BOLTON, M. D., & AL-TABBAA, A. (2002). Numerical modelling of group effects on the distribution of dragloads in pile foundations. Geotechnique, 52:325-335.

LEE, C.J., & N.G., Charles W.W. (2004). Development of Downdrag on Piles and Pile Groups in Consolidating Soil. Journal of Geotechnical and Geoenvironmental Engineering, 130:905–914.

LEE, J., Kim, Y., & Jeong, S. (2010). Three-dimensional analysis of bearing behavior of piled raft on soft clay. Computers and Geotechnics, 37:103-114.

LEUNG, C.F., LIAO, B., CHOW, Y., SHEN, R. & KOG, Y. (2004). Behavior of Pile Subject to Negative Skin Friction and Axial Load. Soils and Foundations, 44:17–26.

LEUNG, C.F. (2009). Negative skin friction on piles. India Geotechnical Society, 827-836.

LITTLE, J.A. (1994). Downdrag on piles: Review and recent experimentation. 1994, Geotechnical Special Publication, ASCE, p. 1805-1826.

LOBO-GUERRERO, A. (1992). Geology and Hidrogeology of the Bogotá City (In Spanish), VII Jornada Geotécnicas de la Ingeniería de Colombia, 20.

LUO, R., YANG, M. & Li, W. (2018) Normalized settlement of piled raft in homogeneous clay. Computers and Geotechnics, 103:165–178.

MALI, S. & SINGH, B. (2017). Behavior of large piled-raft foundation on clay soil. Ocean

Engineering, 149:205–216.

MANDOLINI, A., DI LAORA, R., & MASCARUCCI, Y. (2013). Rational Design of Piled Raft. Procedia Engineering, 57:45–52.

MELO, B. (2018). Evaluation of negative friction in piles groups founded on soft soils (In Portuguese), Magister's dissertation, Universidade de Brasília, Brasília, DF, Brasil, 143.

NETO, P.M.S. (1981). Methods for calculating negative friction in piles: study and discussion (In Portugues). Magister´s dissertation . Universidade Federal do Rio de Janeiro, Rio de Janeiro, Brasil, 251.

NG, C.W.W. (2014). The state of the art centrifuge modelling of geotechnical problems at HKUST. Journal of Zhejiang University SCIENCE A, 15:1–21.

NG, H.K., KARASUDHI, P., & LEE, S.L. (1976). Prediction of negative skin friction and settlement in piles due to fill surcharge. Geotechnical Engineering,7:25-45.

NORDAL, S. (1999) Present of PLAXIS. Beyond 2000 in Computational Geotechnics-10 Years of PLAXIS International, Balkema, Rotterdam, 45–54.

O'NEIL, M W. (1996). Case histories of pile-supported rafts. Report for ISSMFE, Technical Committee TCl8, University of Houston.

O'NEILL, M.W., GHAZZALY, O.I. & HA, H.B. (1977). Analysis of three-dimensional pile groups with nonlinear soil response and pile-soil-pile interaction. Offshore Technology Conference, Houston, Texas, EEUU.

OKABE, T. (1977). Large negative friction and friction-free pile methods. 679–682.

PATIL, J.D., VASANVALA, S.A. & SOLANKI, C.H. (2013). A study on piled raft foundation: state of art. International Journal of Engineering Research and Technology, 2:1464–1470.

PLOMP, A; MIERLO, W.C. (1948). Special problems, effects of drainage by well points on pile foundations. 2nd ICSMFE, Rotterdam, 4:141–148.

POOROOSHASB, H. B.; ALAMGIR, M.& MIURA, N. Negative Skin Friction on Rigid and Deformable Piles. Computers and Geotechnics, v. 18, 2: 109 -126.

POULOS, H.G. (2001). Piled raft foundations: design and applications. Geotechnique, 51(2): 95-113.

POULOS, H. G.; SMALL, J. C.; CHOW, H. (2011). Piled raft foundations for tall buildings. Geotechnical Engineering Journal of the SEAGS& AGSSEA, v.42, n 2:78-84.

POULOS, H.G. (1994). An approximate numerical analysis of pile-raft interaction. International Journal for Numerical and Analytical Methods in Geomechanics, v. 18, n. 2: 73–92.

POULOS, H.G. (2001). Methods of analysis of piled raft foundations: A report prepared on behalf of technical committee TC18 on piled foundations. International Society of Soil Mechanics and Geotechnical Engineering, n. July, 46.

POULOS, H G. (1991). Foundation economy via piled raft systems . Keynote Paper of Pile

talk International, v. 91: 97–106.

POULOS, H.G. (1993). Piled raft in swelling or consolidating soils. Journal of Geotechnical Engineering, Vol. 119, No. 2: 374-380.

POULOS, H.G. & DAVIS, E.H. (1980). Pile Foundations Analysis and Design. John Wiley and Sons, New York. EEUU, 40.

PRAKASH, S.; SHARMA, H.D. (1990). Pile foundations in engineering practice. John Wiley & Sons, New York, EEUU, 736.

PRICE, G; WARDLE, I F. & BRE. (1986). Queen Elizabeth II Conference Centre: monitoring of load sharing between piles and raft. Proceedings of the Institution of Civil Engineers, v. 80, n. 6:1505–1518.

RANDOLPH, M. F.; WROTH, C. P. (1978.). Analysis of deformation of vertically loaded piles. Journal of Geotechnical and Geoenvironmental Engineering, v. 104, n. ASCE 14262.

RANDOLPH, M F. (1994). Design methods for pile groups and piled rafts. 13th International Conference on Soil Mechanics and Foundation Engineering, 5:61-82.

RESÉNDIZ, D. & AUVINET, G. (1973). Analysis of pile foundations in consolidating soils, Proc. 8th International Conference on Soil Mechanics and Foundation Engineering, Moscow, 2:211-218.

REUL, O. (2002). Study of the influence of the consolidation process on the calculated bearing behavior of a piled raft. Proc. 5th Eur. Conf. on Num. Methods in Geotechnical Engineering (NUMGE 2002), Paris, France, 383-388.

RINCÓN, C.L. & RODRÍGUEZ, E. (2001). Centrifuge Physical Modeling of a Wall without Anchors in a Soft Clay (In Spanish). Tesis de Maestría en Geotecnia, Facultad de Ingeniería, Universidad de Los Andes. Bogotá D. C. Colombia, 129.

RINCON, E., HORMAZA, B. & REBOLLEDO, J. (2021) Comparative analysis of Piled Raft Foundation System (PRFS) settlements placed on soft soils via geotechnical centrifuge. Soils and Rocks, v. 44.

RODRÍGUEZ, E. (2016). Experimental analysis of piled raft systems in consolidating soft soils (In Portuguese). Dissertação de Doutorado em Geotecnia. Universidade de Brasília, Brasília, Brasil, 261.

RODRIGUEZ, J.F. (2001). Use of Rigid Inclusions to Settlement Soft Soil Control (In Spanish). Tesis de Maestría en Ingeniería, Universidad Nacional Autónoma de México – UNAM, México D. F., México, 154 .

RODRÍGUEZ-REBOLLEDO, J. F. (2011). Modeling Behavior of Piles and Inclusions Under Regional Consolidation in the Lake Area of Mexico City. (In Spanish). Tesis de Doctorado en Ingeniería, Universidad Nacional Autónoma de México – UNAM, México D.F., México, 244.

RODRÍGUEZ-REBOLLEDO, J. F.; LEÓN, R. F. & CAMAPUM DE CARVALHO, J. (2019). Obtaining the Mechanical Parameters for the Hardening Soil Model of Tropical Soils

in the City of Brasília. Soils and Rocks, v. 42, n. 1:61–74.

RODRÍGUEZ-REBOLLEDO, J. F. ; AUVINET-GUICHARD, G. & MARTÍNEZ-CARVAJAL, H. E. (2015). Settlement analysis of friction piles in consolidating soft soils. DYNA, v 82, 192: 211-220.

RODRÍGUEZ-RINCÓN, E; CUNHA, R. P. D & CAICEDO HORMAZA, B. (2020). Analysis of settlements in piled raft systems founded in soft soil under consolidation process. Canadian Geotechnical Journal, v. 57, n. 4: 537–548.

ROSCOE, K. H.; SCHOFIELD, A. N. & WROTH, C. P. (1958). On the yielding of soils. Geotechnique, 8: 22-53.

ROSCOE, K. H.; BURLAND, J. B. (1968). On the generalised stress-strain behaviour of wet clays.

ROY, S., CHATTOPADHYAY, B. C, & SAHU, R. B. (2011). Piled-Raft foundation behavior on consolidating soft soil. Proceedings of Indian Geotechnical Conference, Kochi, India: 879-882.

RUSSO, G. (1998). Numerical analysis of piled rafts. International Journal for Numerical and Analytical Methods in Geomechanics, v. 22, n. 6: 477–493.

SALES, M. M., CUNHA, R. P., CARVALHO, J. C., & SILVA, C. M. (2002). Behavior predictions of a piled raft in the Federal District (In Portugues). In Anais do XII Congresso Brasileiro de Mecânica de Solos e Engenharia Geotécnica (COBRAMSEG), 1-8.

SANCTIS, L., & MANDOLINI, A. (2006). Bearing capacity of piled rafts on soft clay soils. Journal of Geotechnical and Geoenvironmental Engineering, ASCE, 132: 1600-1610.

SANCTIS, L., MANDOLINI, A., RUSSO, G., & VIGGIANI, C. (2002). Some remarks on the optimum design of piled raft. International Deep Foundations Congress 2002, ASCE, Orlando, Florida: 405-425.

SANTOYO, (2013). History and current events of the regional collapse of Mexico City.

SCHANZ, T; VERMEER, P A; BONNIER, P G. (1999). The hardening soil model: formulation and verification. Beyond 2000 in computational geotechnics, 281–296.

SCHOFIELD, A.N. & WROTH, P. (1968). Critical state soil mechanics. McGraw-hill, 310.

SHEN, R. F., LEUNG, C. F. & CHOW, Y. K. (2006). Negative skin friction on end-bearing piles. Proceedings of the 6th International Conference on Physical Modelling in Geotechnics, ICPMG, Taylor & Francis, London, UK, 875–880.

SHIBATA, T.; SEKIGUCHI, H. & YUKITOMO, H. (1982). Model test and analysis of negative friction acting of piles. Soils and Foundations, v. 22, n. 2: 29–39.

SINHA, A. & M. HANNA, A. (2016). 3D Numerical Model for Piled Raft Foundation. International Journal of Geomechanics. 17.

SOMMER, H; WITTMANN, P; RIPPER, P. (1985). Piled raft foundation of a tall building in Frankfurt clay. In: Proc. 11th Int. Conf. on SMFE, 2253–2257.

SURARAK, CH., LIKITLERSUANG, S., WANATOWSKI, D.; BALASUBRAMANIAM, A., OH, E. & GUAN, H. (2012). Stiffness and strength parameters for hardening soil model of soft and stiff Bangkok clays. Soils and Foundations, 52(4): 682-697.

TANG, Y., REN, X., CHEN, B., SONG, S., WANG, J. & YANG, P. (2012). Study on land subsidence under different plot ratios through centrifuge model test in soft-soil territory. Environmental Earth Sciences. 66(7): 1809-1816.

TAYLOR, R. N. (1995). Centrifuges in modelling: principles and scale effects. Geotechnical centrifuge technology, R.N. Taylor (Ed), Blackie Academic & Professional, London, UK, 19-33.

TEH, C. I., & WONG, K. S. (1995). Analysis of downdrag on pile groups. Geotechnique, 45(2), 191-207.

THAHER, M. JESSBERGER, H. L. (1991). The behavior of pile-raft foundations investigated in centrifuge model tests. Centrifuge 91, ISMFE, Rotterdam, Germany, 225-234.

TRAN, T. V., KIMURA, M., & BOONYATEE, T. (2012a). 3D FE Analysis of effect of ground subsidence and piled spacing on ultimate bearing capacity of piled raft and axial force of piles in piled raft. Open Journal of Civil Engineering, 2:206–213.

TRAN, T. V., TERAMOTO, S., KIMURA, M., BOONYATEE, T., & VINH, L. B. (2012b). *Effect of ground subsidence on load sharing and settlement of raft and piled raft foundations*. World Academy of Science, Engineering and Technology, International Journal of Civil, Environmental, Structural, Construction and Architectural Engineering, 6(2): 120-127.

VAN IMPE, W F. (1996). Sixth International Conference and Exhibition on Piling and Deep Foundations, Bombay, India.

VIGGIANI, C., MANDOLINI, A. & RUSSO, G.(2014). Piles and Pile Foundations.

VON SOOS, P. (2001). Properties of soil and rock (in German). Grundbau-Taschenbuch, Teil 1: Geotechnische 655 Grundlagen, 1: 117. John Wiley & Sons.

WANG, J., HUANG, T. & SUI, D. (2013). A Case Study on Stratified Settlement and Rebound Characteristics due to Dewatering in Shanghai Subway Station. The Scientific World Journal. V. 2013.

WATCHARASAWE, K., KITIYODOM, P. & JONGPRADIST, P. (2015). Numerical Analyses of Piled Raft Foundation in Soft Soil Using 3D-FEM. Geotechnical Engineering. 46. 109-116.

WATCHARASAWE, K., JONGPRADIST, P., KITIYODOM, P., & MATSUMOTO, T. (2021). Measurements and analysis of load sharing between piles and raft in a pile foundation in clay. Geomech. Eng, 24(6), 559-572.

WHITAKER, T. (1957). Experiments with model piles in groups. Geotechnique, 7(4), 147-167 p.

WIESNER, T. J; BROWN, P. T. (1980) Laboratory tests on model piled raft foundations. Journal of Geotechnical and Geoenvironmental Engineering, v. 106 (7):767-783.

XIE, Y., & CHI, S. (2020). Optimization method of reducing the differential settlements of piled raft foundations based on pile-to-pile interaction theory. Advances in Civil Engineering, 2020.

YANG, Q., KE, Y., ZHANG, D., CHEN, B., GONG, H., LV, M., ZHU, L. & LI, X. (2018). Multi-Scale Analysis of the Relationship between Land Subsidence and Buildings: A Case Study in an Eastern Beijing Urban Area Using the PS-InSAR Technique. Remote Sensing. v 10(7): 1006.

ZEEVAERT, L. (1957a). Compensated friction-pile foundation to reduce the settlement of buildings on the highly compressible volcanic clay of Mexico City. In: Proc. 4th Int. Conf. on SMFE. 1: 81-86.

ZEEVAERT, L.(1957b) Foundation Design and Behaviour of Tower Latino Americana in Mexico City. Géotechnique, v. 7, n. 3:115–133.

ZEEVAERT, L. (1983). Foundation engineering for difficult subsoil conditions. 624.

ZEEVAERT, Leonardo. Foundation problems related to ground surface subsidence in Mexico City. ZEEVAERT, L. (1963). Foundation problems related to ground surface subsidence in Mexico City. ASTM (STP), v 322:57-66.

ZHANG, L., & LIU, H. (2017). Seismic response of clay-pile-raft-superstructure systems subjected to far-field ground motions. Soil Dynamics and Earthquake Engineering. 101. 209-224. 10.1016/j.soildyn.2017.08.004.

ZHANG, L., GOH, S-H. & LIU, H. (2017). Seismic response of pile-raft-clay system subjected to a long-duration earthquake: centrifuge test and finite element analysis. Soil Dynamics and Earthquake Engineering. 92. 488-502.

ZHEMOCHKIN, B N; SINITSYN, A P. (1962). Practical methods of designing foundation beams and slabs resting on an elastic foundation. State Publishing House for Lit. on Struct., Archit. and Struct. Matl., Moscow.

ZHENYUE, S. & GA, Z. (2008). Centrifuge modeling of ground settlement due to groundwater pumping. China Civil Engineering Journal, 41(4):67-72.

ZHU, L., GONG, H., LI, X., WANG, R., CHEN, B., DAI, Z., & TEATINI, P. (2015). Land subsidence due to groundwater withdrawal in the northern Beijing plain, China. Engineering Geology, 193, 243-255.

APPENDICES

Appendix A: Laboratory test

CONSOLIDATION TEST						

Sample	Kaolin	Type	Manufactured		L1	
Project			Research		Data	30/1/2019

Specific gravity	Gs	2.61		Initial moisture		69.27	%
Initial soil moisture	wo	71.96	%	Initial saturation	So	100.36	%
Final soil moisture	wf	-98.37	%	Initial height of voids	Hvo	16.35	mm
Sample initial height	Ho	25.09	mm	Initial void index	eo	1.87	
Sample initial area	Ao	31.19225	cm^2	Strain gauge initial reading	Lo	-0.07	mm
Sample initial weight	Wo	122.33	gr	Strain gauge final reading	Lf	8.69	mm
Initial solid weight	Wso	71.14	gr	Sample variation	DH	8.62	mm
Initial water weight	Wwo	51.19	gr	final height of voids	Hvf	7.73	mm
Initial height of solids	Hso	8.74	mm	Final void ratio	ef	0.88	
Initial height of water	Hwo	16.41	mm	Final saturation	Sf	100	
Air height	Hao	-0.06	mm				

Load	L def	DH	Hv	e	ε	Cv
(kg/cm^2)	(mm)		(mm)			(cm^2/min)
0	0	0.00	16.35	1.87	0.00	
Swell	0.066	0.07	16.42	1.88	0.00	
0.25	0.792	0.79	15.56	1.78	0.03	0.1137
0.5	1.468	1.47	14.88	1.70	0.06	0.1137
1	2.592	2.59	13.76	1.57	0.10	0.1182
2	4.257	4.26	12.09	1.38	0.17	0.1230
4	6.162	6.16	10.19	1.17	0.25	0.1392
8	8.096	8.10	8.26	0.94	0.32	0.0308
4	7.869	7.87	8.48	0.97	0.31	0.5000
2	7.412	7.41	8.94	1.02	0.30	0.3844
4	7.685	7.69	8.67	0.99	0.31	0.4549
8	8.317	8.32	8.03	0.92	0.33	0.4549
16	9.918	9.92	6.43	0.74	0.40	0.2246
8	9.632	9.63	6.72	0.77	0.38	0.7688
4	9.193	9.19	7.16	0.82	0.37	0.2824
2	8.689	8.69	7.66	0.88	0.35	0.1155

Compressibility Parameters	
Cc	-0.730
Cs	-0.342
Cr	-0.172

Figure A.1. Consolidation test for layer L1.

CONSOLIDATION TEST

Sample	Kaolin	Type	Manufactured		L2		

Project			Research		Data	30/1/2019	

Specific gravity	Gs	2.61		Initial moisture			63.78	%
Initial soil moisture	wo	65.44	%	Initial saturation	So		100.56	%
Final soil moisture	wf	44.55	%	Initial height of voids	Hvo		15.85	mm
Sample initial height	Ho	25.18	mm	Initial void index	eo		1.70	
Sample initial area	Ao	31.509826	cm²	Strain gauge initial reading	Lo		-1.40	mm
Sample initial weight	Wo	126.96	gr	Strain gauge final reading	Lf		188.80	mm
Initial solid weight	Wso	76.74	gr	Sample variation	DH		-190.20	mm
Initial water weight	Wwo	50.22	gr	final height of voids	Hvf		206.04	mm
Initial height of solids	Hso	9.33	mm	Final void ratio	ef		22.08	
Initial height of water	Hwo	15.94	mm	Final saturation	Sf		100	
Air height	Hao	-0.09	mm					

Load	L def	Lec def	DH	Hv	e	ε	Cv
(kg/cm²)	(mm)			(mm)			(cm²/min)
0	0	0.00	0.00	15.85	1.70	0.00	
Swell	0.053	1.35	0.05	15.90	1.70	0.00	
0.25	0.446	11.33	0.45	15.40	1.65	0.02	0.1182
0.5	0.936	23.77	0.94	14.91	1.60	0.04	0.1055
1	1.752	44.50	1.75	14.10	1.51	0.07	0.1137
2	3.057	77.65	3.06	12.79	1.37	0.12	0.1146
4	4.82	122.43	4.82	11.03	1.18	0.19	0.1335
8	6.713	170.51	6.71	9.14	0.98	0.27	0.1961
4	6.499	165.07	6.50	9.35	1.00	0.26	0.4843
2	6.059	153.90	6.06	9.79	1.05	0.24	0.2175
4	6.317	160.45	6.32	9.53	1.02	0.25	0.4346
8	6.937	176.20	6.94	8.91	0.96	0.28	0.4282
16	8.548	217.12	8.55	7.30	0.78	0.34	0.1250
8	8.354	212.19	8.35	7.49	0.80	0.33	0.4920
4	7.933	201.50	7.93	7.92	0.85	0.32	0.2373
2	7.433	188.80	7.43	8.42	0.90	0.30	0.1055

Compressibility Parameters	
Cc	-0.651
Cs	-0.232
Cr	-0.397

Figure A.2. Consolidation test for layer L2.

154

CONSOLIDATION TEST

Sample	Kaolin	Type	Manufactured		L3	

Project			Research		Data	30/1/2019

Specific gravity	Gs	2.61		Initial moisture		59.04 %
Initial soil moisture	wo	44.13 %		Initial saturation	So	70.96 %
Final soil moisture	wf	-150.72 %		Initial height of voids	Hvo	15.62 mm
Sample initial height	Ho	25.25 mm		Initial void index	eo	1.62
Sample initial area	Ao	31.94912 cm²		Strain gauge initial reading	Lo	-0.03 mm
Sample initial weight	Wo	115.69 gr		Strain gauge final reading	Lf	6.94 mm
Initial solid weight	Wso	80.27 gr		Sample variation	DH	6.91 mm
Initial water weight	Wwo	35.42 gr		final height of voids	Hvf	8.71 mm
Initial height of solids	Hso	9.63 mm		Final void ratio	ef	0.91
Initial height of water	Hwo	11.09 mm		Final saturation	Sf	100
Air height	Hao	4.54 mm				

Load	L def	DH	Hv	e	ε	Cv
(kg/cm²)	(in)	(mm)	(mm)			(cm²/min)
0	0.004	0.00	15.62	1.62	0.00	
Swell	0.031	0.03	15.65	1.63	0.00	
0.25	0.36	0.36	15.27	1.59	0.01	0.1335
0.5	0.739	0.74	14.89	1.55	0.03	0.2660
1	1.32	1.32	14.31	1.49	0.05	0.1663
2	2.181	2.18	13.45	1.40	0.09	0.1453
4	3.737	3.73	11.89	1.24	0.15	0.1428
8	5.814	5.81	9.81	1.02	0.23	0.2086
4	5.653	5.65	9.97	1.04	0.22	0.4549
2	5.26	5.26	10.37	1.08	0.21	0.9492
4	5.464	5.46	10.16	1.06	0.22	0.5339
8	6.038	6.03	9.59	1.00	0.24	0.5000
16	7.937	7.93	7.69	0.80	0.31	0.2246
8	7.782	7.78	7.85	0.82	0.31	0.4693
4	7.401	7.40	8.23	0.85	0.29	0.4693
2	6.943	6.94	8.68	0.90	0.27	0.0706

Compressibility Parameters	
Cc	-0.627
Cs	-0.166
Cr	-0.427

Figure A.3. Consolidation test for layer L3.

155

TRIAXIAL TEST - CID						
Sample	Kaolin	Type	Manufactured			
Project		Doctoral Research			Data	4/2/2019

Sample identification		SAMPLE L1-1		SAMPLE L1-2		SAMPLE L1-3
Test type		CID		CID		CID
Sample type		Manufactured		Manufactured		Manufactured
Diameter	(mm)	51.2		50.89		51.64
		51.25		51.43		51.67
		51.06	51.17 mm	50.91	51.070 mm	51.69	51.667 mm
Initial height	(mm)	101.6		102.89		100.95
		101.89		102.89		101.2
		101.57	101.68 mm	102.76	102.850 mm	101.01	101.053 mm
Head displa.	Δh		5.280 mm		7.740 mm		11.210 mm
Capsule No			5		37		1
W capsule			6.080 gr		6.080 gr		6.090 gr
W initial wet soil			328.710 gr		324.660 gr		318.800 gr
W final wet soil			295.150 gr		283.770 gr		272.270 gr
W dry soil			191.110 gr		188.480 gr		186.620 gr
Volumetric chamber area			40.97 cm3		40.97 cm3		40.97 cm3
Failure speed			0.003 mm/min		0.003 mm/min		0.003 mm/min
Specific gravity of solids			2.61		2.61		2.61
Deviator stress applied			1.00 kg/cm2		2.00 kg/cm2		3.00 kg/cm2
Chamber pressure for consolidation			3.95 kg/cm2		4.95 kg/cm2		5.95 kg/cm2

Figure A.4. Triaxial test CID for layer L1.

TRIAXIAL TEST - CID						

Sample	Kaolin	Type	Manufactured			
Project		Doctoral Research			Data	6/2/2019

		SAMPLE L2-1		SAMPLE L2-2		SAMPLE L2-3
Sample identification						
Test type		CID		CID		CID
Sample type		Manufactured		Manufactured		Manufactured
Diameter	(mm)	50.34		50.45		50.08
		50.45		50.94		50.39
		50.42	50.40 mm	50.12	50.503 mm	50.07	50.180 mm
Initial height	(mm)	100.33		99.27		99.85
		100.26		99.33		99.87
		99.94	100.18 mm	98.58	99.060 mm	99.8	101.053 mm
Head displa.	Δh		4.830 mm		6.960 mm		9.280 mm
Capsule No			10		5		1
W capsule			5.940 gr		5.340 gr		6.780 gr
W initial wet soil			328.710 gr		327.650 gr		327.930 gr
W final wet soil			295.150 gr		294.450 gr		293.970 gr
W dry soil			191.110 gr		190.170 gr		191.640 gr
Volumetric chamber area			40.97 cm3		40.97 cm3		40.97 cm3
Failure speed			0.003 mm/min		0.003 mm/min		0.003 mm/min
Specific gravity of solids			2.61		2.61		2.61

Deviator stress applied	1.00 kg/cm2	2.00 kg/cm2	3.00 kg/cm
Chamber pressure for consolidation	3.95 kg/cm2	4.95 kg/cm2	5.95 kg/cm

Figure A.5. Triaxial test CID for layer L2.

157

	TRIAXIAL TEST - CID					

Sample	Kaolin	Type	Manufactured			
Project		Doctoral Research			Data	7/2/2019

		SAMPLE L3-1		SAMPLE L3-2		SAMPLE L3-3
Sample identification						
Test type		CID		CID		CID
Sample type		Manufactured		Manufactured		Manufacture
Diameter	(mm)	50.52		51.16		50.76
		50.79		50.98		50.5
		50.17	50.49 mm	50.89	50.935 mm	50.42	50.580 mm
Initial height	(mm)	101.58		102.76		102.75
		101.25		102.85		102.81
		102.08	101.64 mm	102.86	102.823 mm	102.56	102.707 mm
Head displa.	Δh		4.110 mm		8.310 mm		11.630 mm
Capsule No			8		5		1
W capsule			6.010 gr		5.980 gr		6.560 gr
W initial wet soil			336.500 gr		340.680 gr		335.190 gr
W final wet soil			321.940 gr		307.960 gr		309.590 gr
W dry soil			209.320 gr		211.450 gr		207.150 gr
Volumetric chamber area			40.97 cm3		40.97 cm3		40.97 cm3
Failure speed			0.003 mm/min		0.003 mm/min		0.003 mm/mi
Specific gravity of solids			2.61		2.61		2.61
Deviator stress applied			2.00 kg/cm2		3.00 kg/cm2		5.00 kg/c
Chamber pressure for consolidation			4.95 kg/cm2		5.95 kg/cm2		7.95 kg/c

Figure A.6. Triaxial test CID for layer L3.

Appendix B: Instrumentation calibration

a)

b)

Figure B.1. a) Cell 1 and b) Cell 2 Flexiforce load cells calibration

The graph in a) shows Load (N) versus Voltage (mV) with equation $y = 7917.8x^2 + 417.23x$

The graph in b) shows Load (N) versus Voltage (mV) with equation $y = 8020.2x^2 + 339.43x$

a)

b)

Figure B.2. a) Cell 1 and b) Cell 2 LCM200 FUTEK load cells calibration

Figure B.3. LCM300 FUTEK load cells calibration
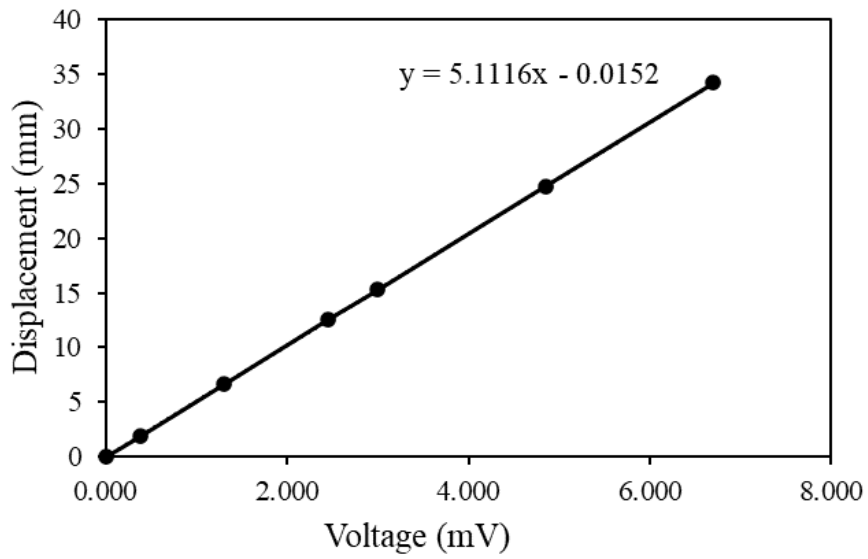
Figure B.4. LVDT calibration

162

Appendix C: Load-settlement curves for C2, C3, and C4
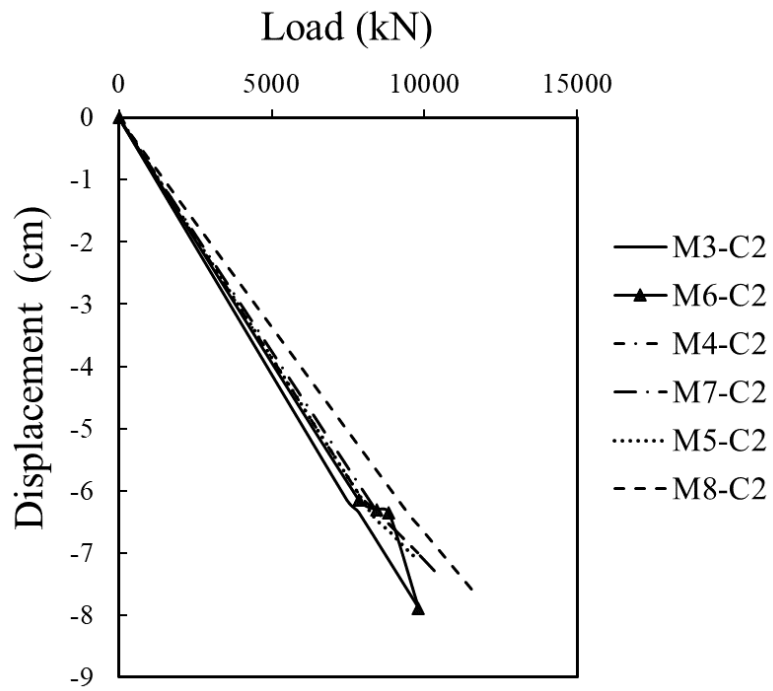
Figure C.1. Load-settlement curves for configurations M3 to M8 simulated with condition C2.
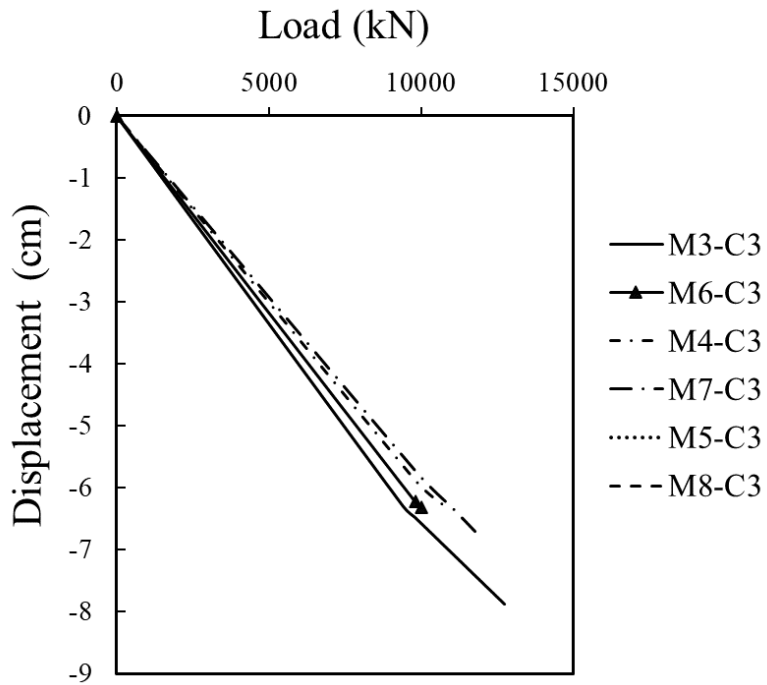
Figure C.2. Load-settlement curves for configurations M3 to M8 simulated with condition C3.
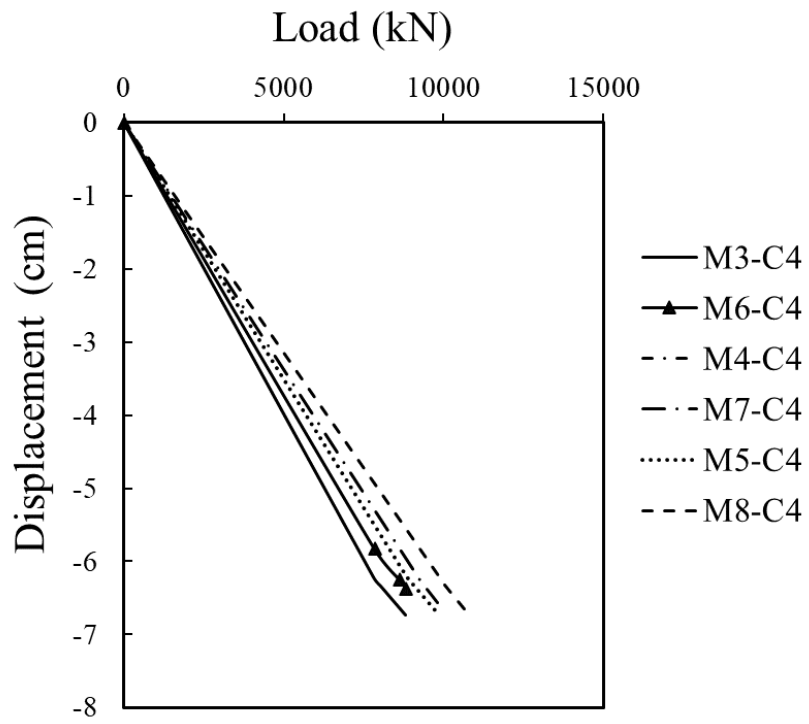
Figure C.3. Load-settlement curves for configurations M3 to M8 simulated with condition C4**.**

Appendix D: Distribution Loads

	Raft	Piles	Raft	Piles	Raft	Piles	Raft	Piles	Raft	Piles	Raft	Piles
	M3 3x3 C		M6 3x3 T		M4 4x4 C		M7 4x4 T		M5 5x5 C		M8 5x5 T	
Load-Stage 2 (%)	83	17	70	30	68	32	50	50	59	41	35	65
Load-Stage 3 (%)	52	48	39	61	28	72	23	77	15	85	16	84

C2

	Raft	Piles	Raft	Piles	Raft	Piles	Raft	Piles	Raft	Piles	Raft	Piles
	M3 3x3 C		M6 3x3 T		M4 4x4 C		M7 4x4 T		M5 5x5 C		M8 5x5 T	
Load-Stage 2 (%)	73	27	68	32	60	40	45	55	47	53	27	73
Load-Stage 3 (%)	28	72	89	11	0	100	1	99	6	94	0	100

167

Appendix E: Displacements
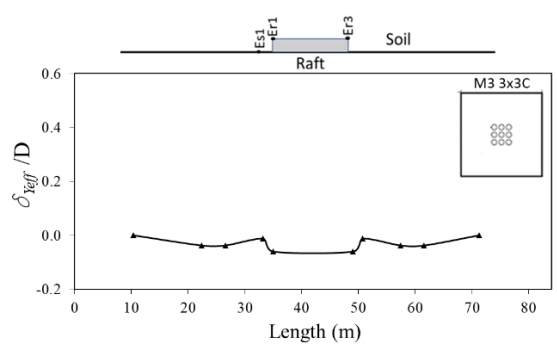
a)
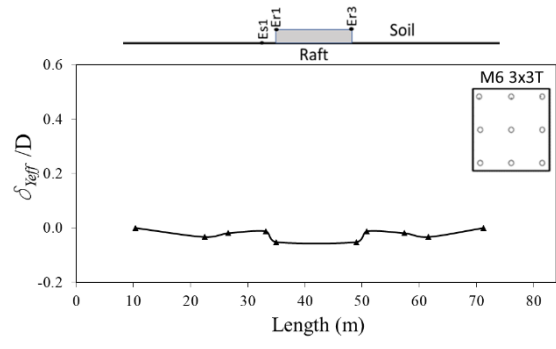
b)
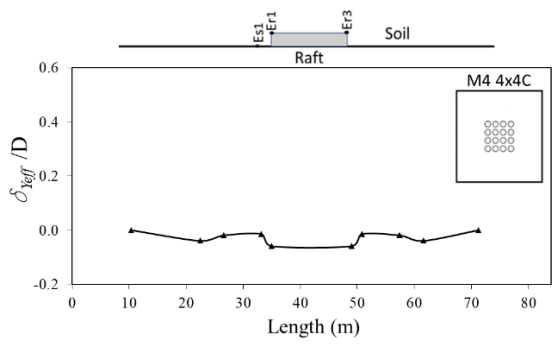
c)
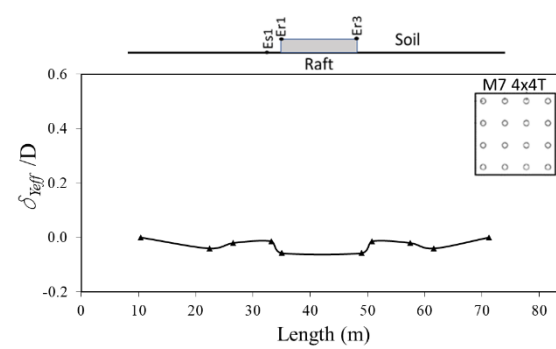
d)
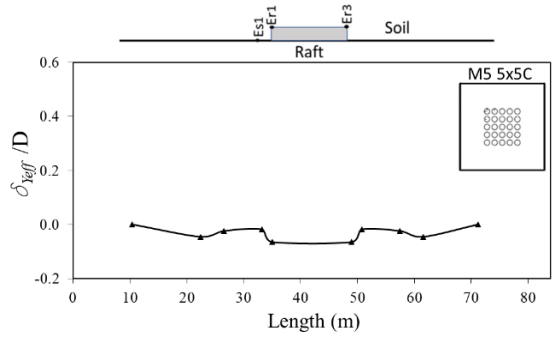
e)
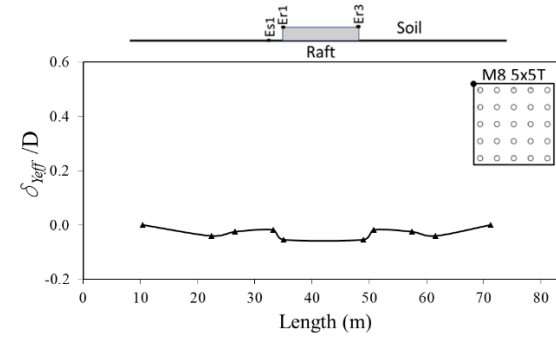
f)

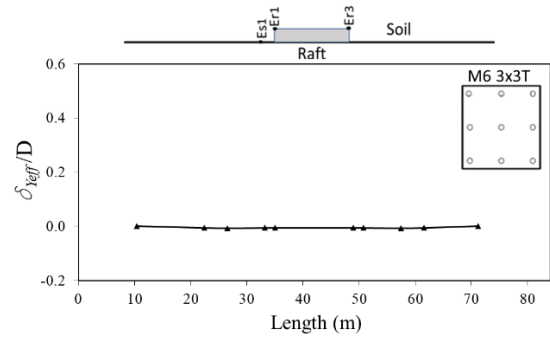**Figure E.1.** C2 Stage 2
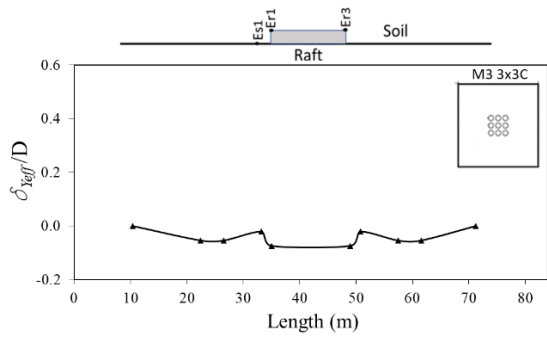
a)
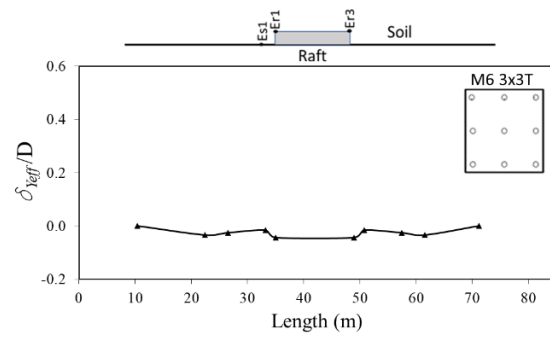
b)
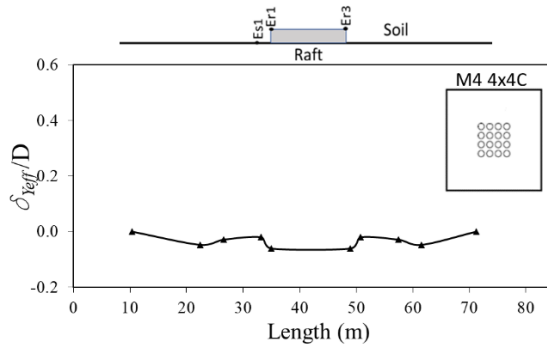
c)
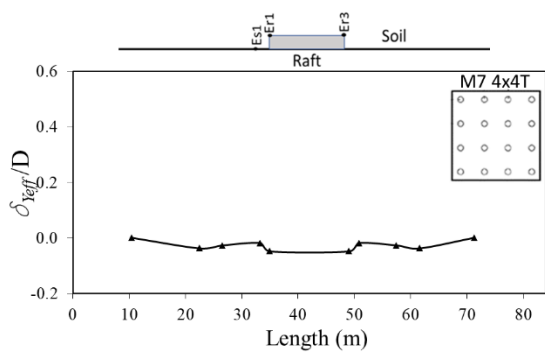
d)
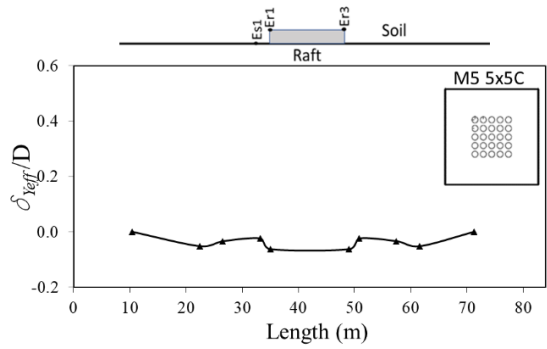
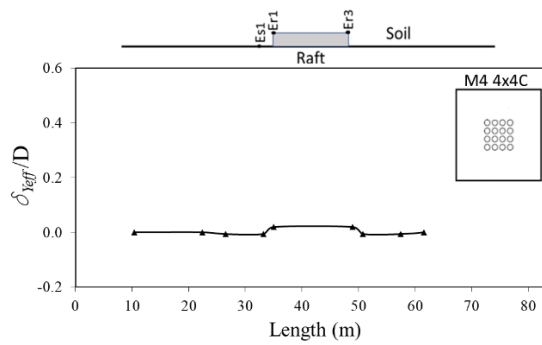e)
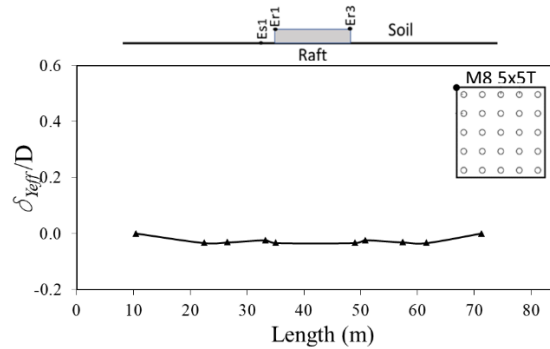
f)

Figure E.2. C2 Stage 3
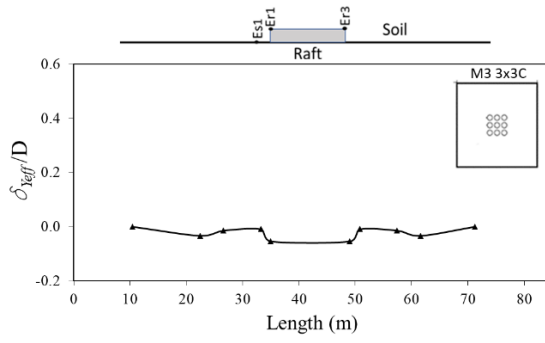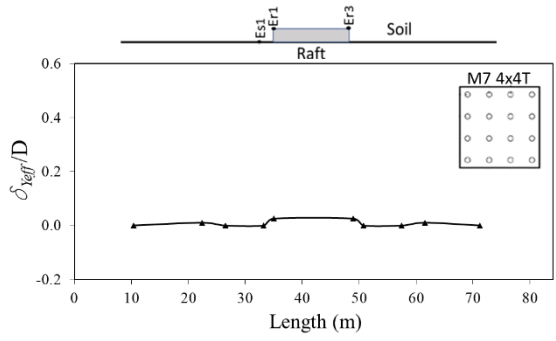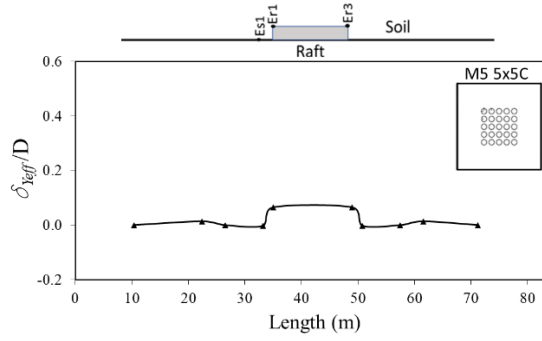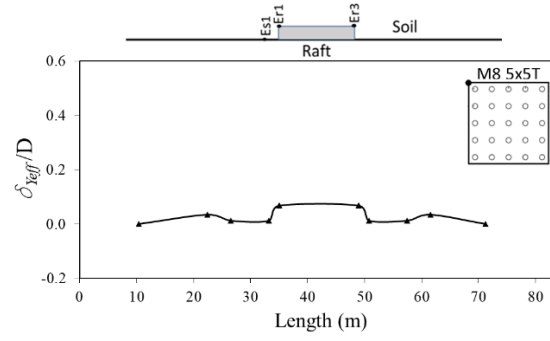
a)
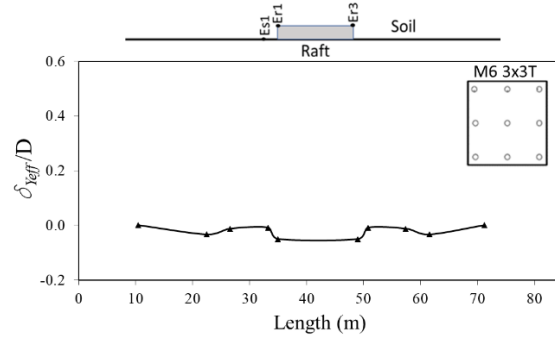
b)
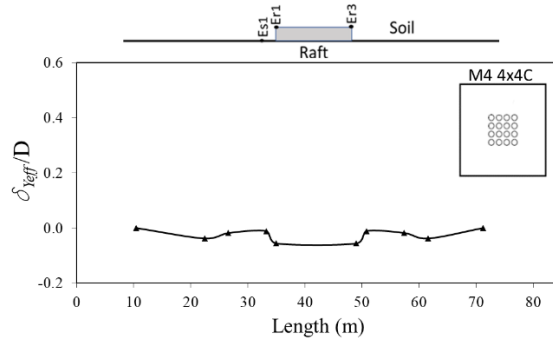
c)
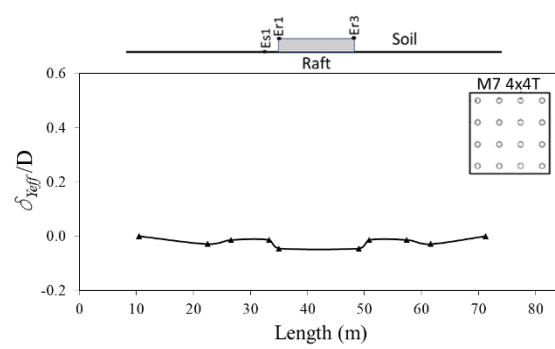
d)
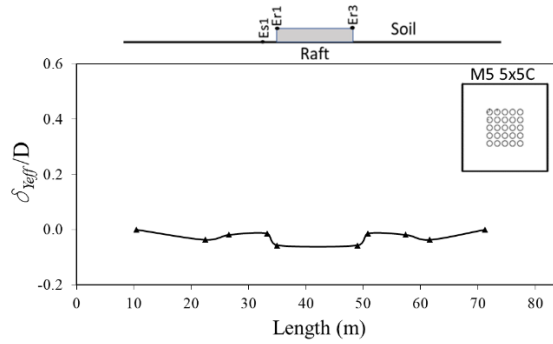
e)
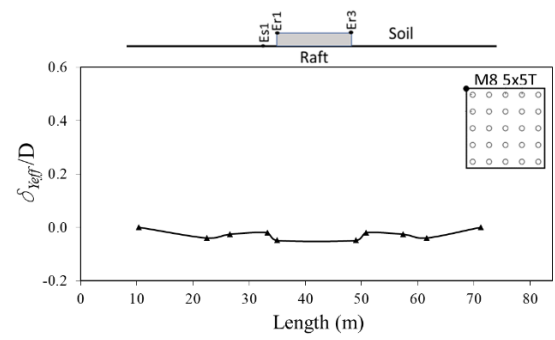
f)

Figure E.3. C3 Stage 2
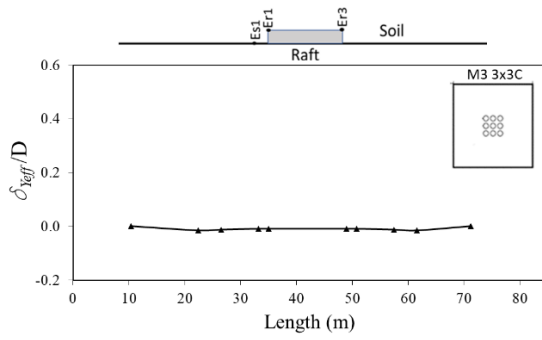
a)

b)

c)

d)

e)

f)

Figure E.4. C3 Stage 3